



**The Abdus Salam
International Centre for Theoretical Physics**



2272-2

**Joint ICTP-IAEA School on Synchrotron Applications in Cultural Heritage and
Environmental Sciences and Multidisciplinary Aspects of Imaging Techniques**

21 - 25 November 2011

**Use of selected analytical techniques for high-resolution imaging and elemental
mapping of cultural heritage objects and in environmental sciences**

Jozef Kaiser
*Brno University of Technology
Czech Republic*

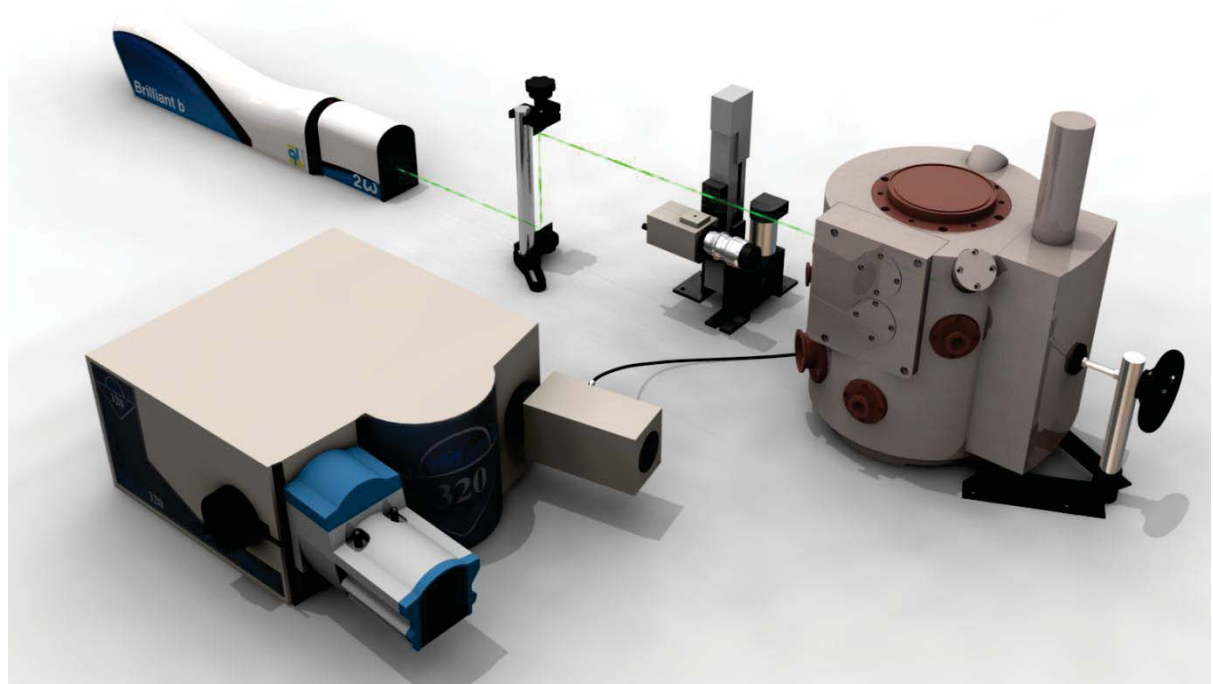


Use of selected analytical techniques for high-resolution imaging and elemental mapping of cultural heritage objects and in environmental sciences

Jozef Kaiser

kaiser@fme.vutbr.cz

<http://libs.fme.vutbr.cz/>

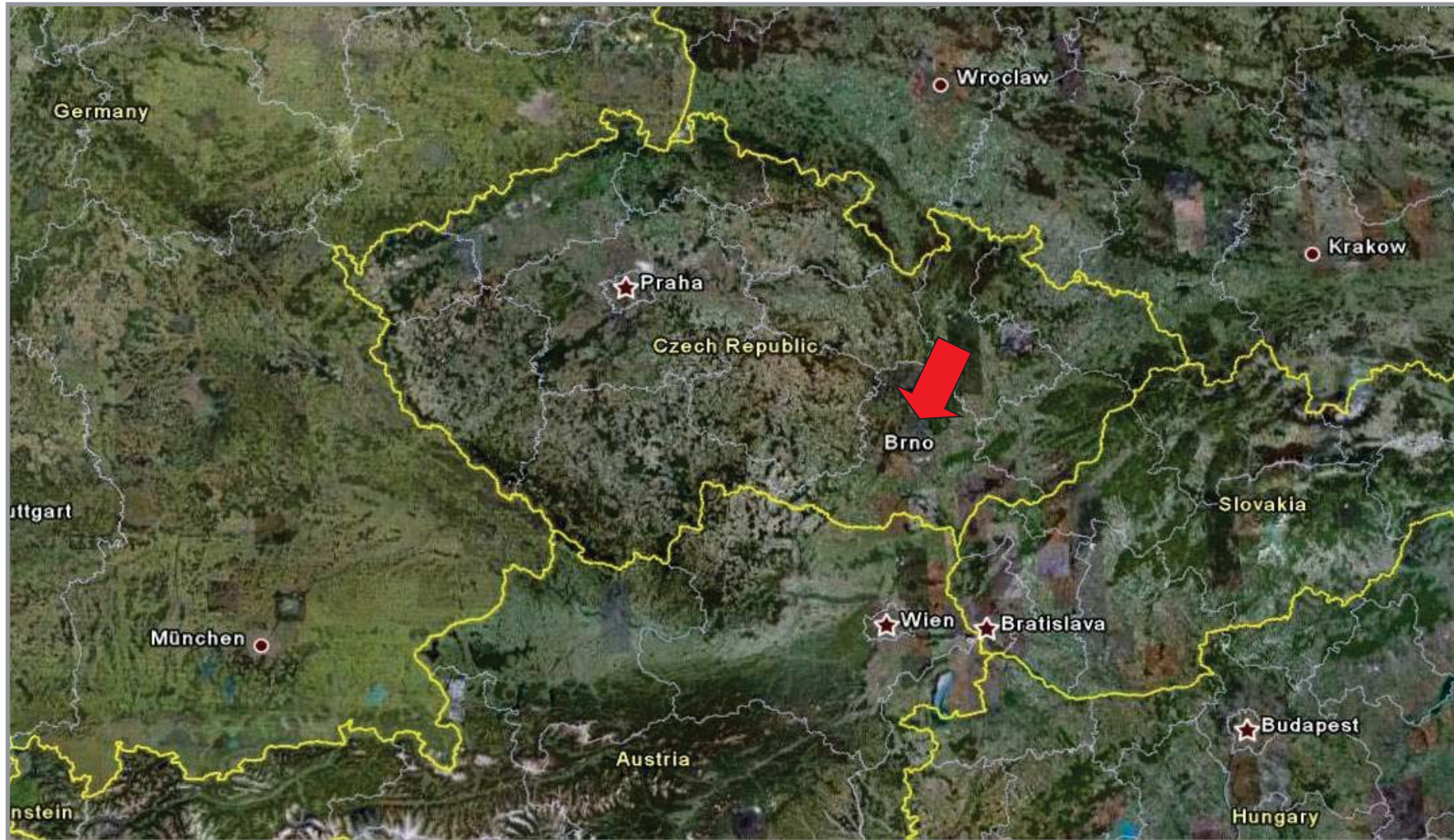


Outline



- 1) Introduction of Institutes
- 2) Experimental techniques
 - μ radiography and μ tomography (μ CT)
 - dual-energy μ CT
 - lab-based sources
 - Laser Induced Breakdown Spectroscopy – LIBS
- 3) Applications
 - LIBS, LA-ICP-MS mapping
 - combination of μ CT and LIBS (LA-ICP-MS) mapping
 - LIBS in phytoremediation

Location



Brno – the capital city of Moravia



- Brno 366 000 inhabitants
- Second largest city in Czech Republic
- Average year temperature 9.6°C
- Altitude 190-425 m above sea level



The University



Brno University of Technology

- Founded in 1899
- Second-largest Technical University in the Czech Republic
- 8 faculties
- 21 000 students
- 170 study branches

Faculty of Mechanical Engineering

- Founded in 1900
- 15 institutes
- About 4600 students

The University - MU



Masaryk University

- Founded in 1919
- The second-largest public university in the Czech Republic
- 9 faculties
- 43 000 students
- more than 200 study branches

Faculty of Science

- Founded in 1919
- 13 Departments
- About 4 400 students



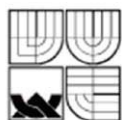
Establishment of a **Centre of Excellence**
conducting research in the area
of **QUALITY OF LIFE** and **HUMAN HEALTH**.



CEITEC



Masaryk University
www.muni.cz



Brno University of
Technology
www.vutbr.cz



Mendelova
univerzita
v Brně
Mendel University
in Brno
www.mendelu.cz



University of Veterinary
and Pharmaceutical
Sciences Brno
www.vfu.cz



Institute of Physics
of Materials, Academy
of Sciences of the Czech
Republic
www.ipm.cz



Veterinary Research
Institute
www.vri.cz

- 6 partners
- 557 researchers (2015)
- 7 research programmes
- 64 research groups
- 25,000 m² of new laboratories
- 10 core facilities
- Planned budget of EUR 210 mil.
- Start of research activities: Q1 2011
- Project completion: Q4 2015

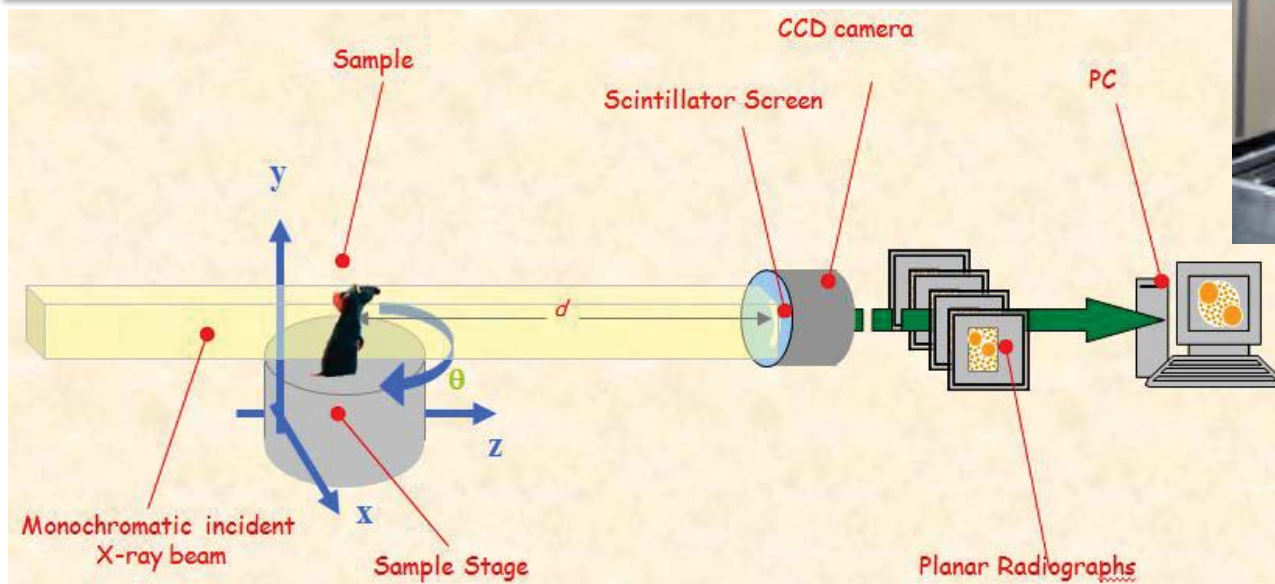
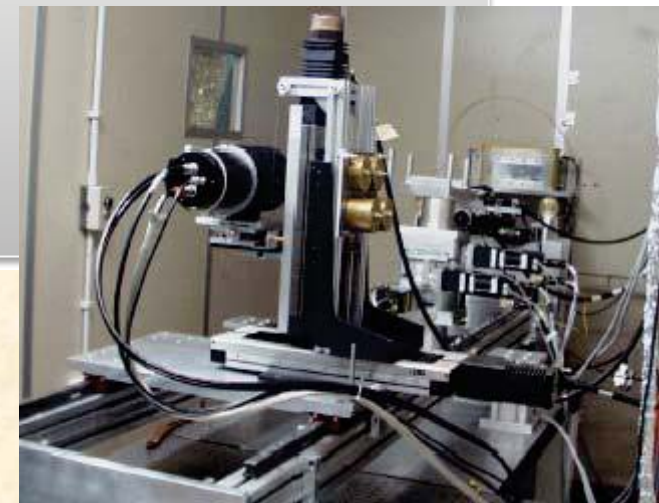
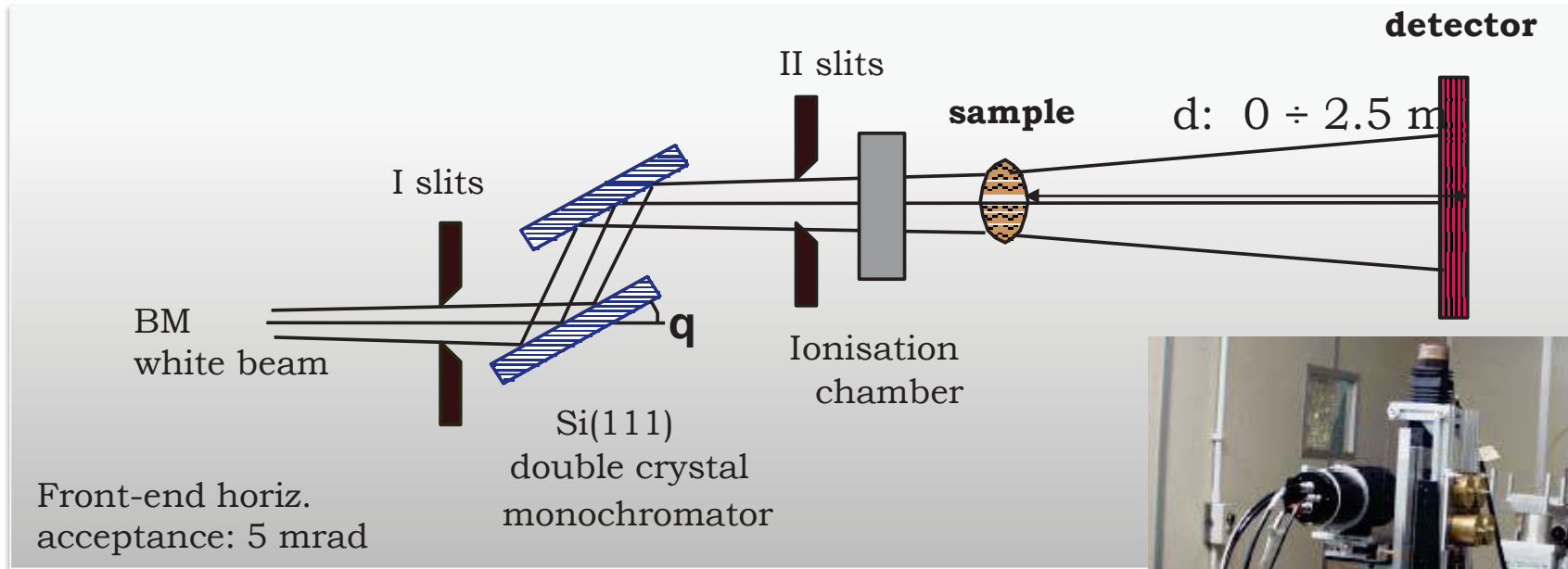
<http://www.ceitec.cz/>

GOALS



- Development and application of CT techniques for visualization of entire 3D structure of different samples with high spatial resolution.
- Development of laser-ablation based analytical techniques for 2D and 3D high-resolution elemental mapping.
- Combination of these two techniques.
- Key partners:
 - Department of Chemistry, MU, Brno, Czech Rep. (Dr. K. Novotný),
 - Synchrotron Elettra, Trieste, Italy (Dr. G. Tromba),
 - Oak Ridge National Lab., Oak Ridge, TN, USA (Dr. M. Martin),
 - Shenyang Institute of Automation, Chinese Academy of Sciences, Shenyang City, China (Dr. L. Sun).

μ CT – the SYRMEP beamline @ ELETTRA



Source: G. Tromba and the SYRMEP team @ ELETTRA



Advantages of SR for hard X-ray imaging

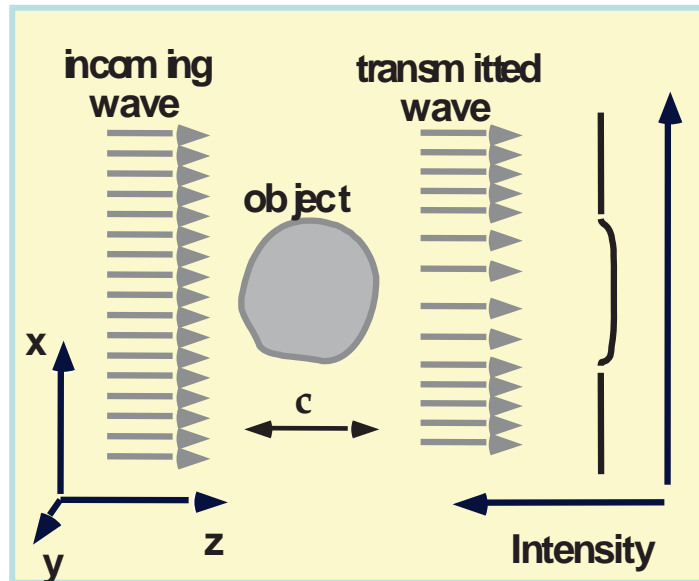
Characteristics	Advantages
Monochromaticity	no beam hardening k and L edge imaging quantitative CT evaluations optimization of X-ray energy (dose reduction)
Collimation	parallel beams, scatter reduction
Spatial coherence	phase sensitive techniques
Intensity	reduction of exposure time

μCT – the SYRMEP beamline @ ELETTRA

Source: G. Tromba and the SYRMEP team @ ELETTRA



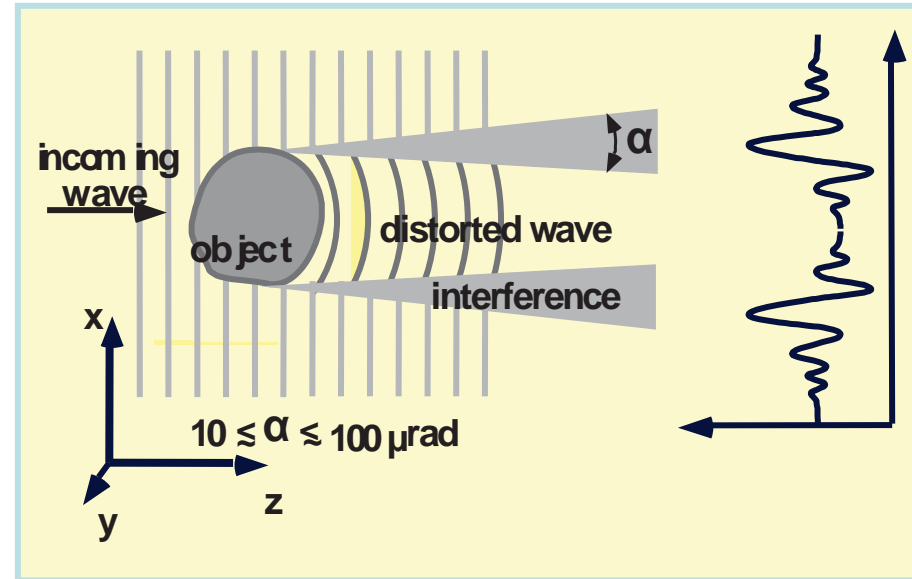
Phase-Contrast (PHC) imaging - the technique exploits the high spatial coherence of the X-ray source



Conventional radiology

$$(\Delta I/I)_{\text{abs}} = e^{-c \Delta \mu}$$

$$\Delta \Phi = 2\pi c \Delta \delta / \lambda$$



$\mathbf{n} = 1 - \delta - i\beta$: refraction index

$\mu = 4\pi \beta / \lambda$: linear absorption coeff.

c : object size // to beam direction

PHC

In conventional radiology image formation is based on differences in X-ray absorption properties of the samples. The image contrast is generated by density, composition or thickness variation of the sample. Main limitation: **poor contrast in soft tissue differentiation**.

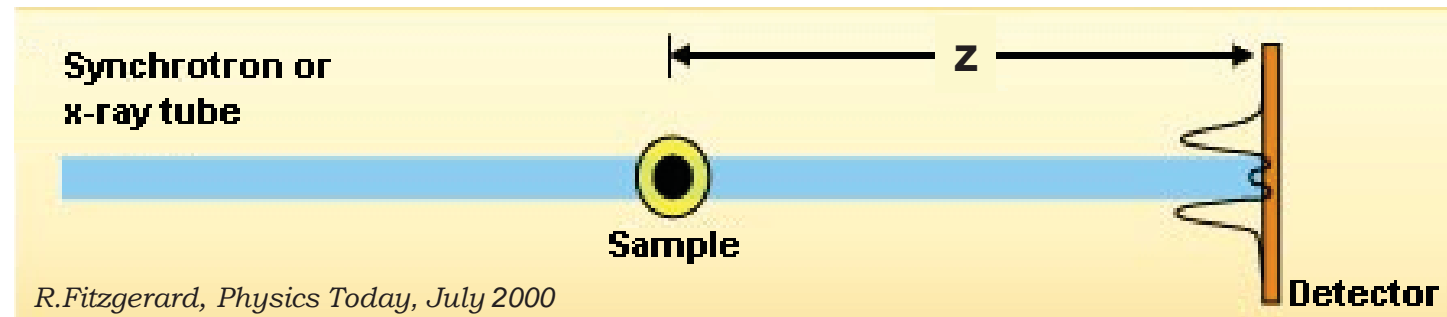
Phase sensitive techniques are based on the observation of the *phase shifts* produced by the object on the incoming wave. Contrast arises from interference among parts of the wave front differently deviated (or phase shifted) by the sample. Edge enhancement effects.

μ CT – the SYRMEP beamline @ ELETTRA

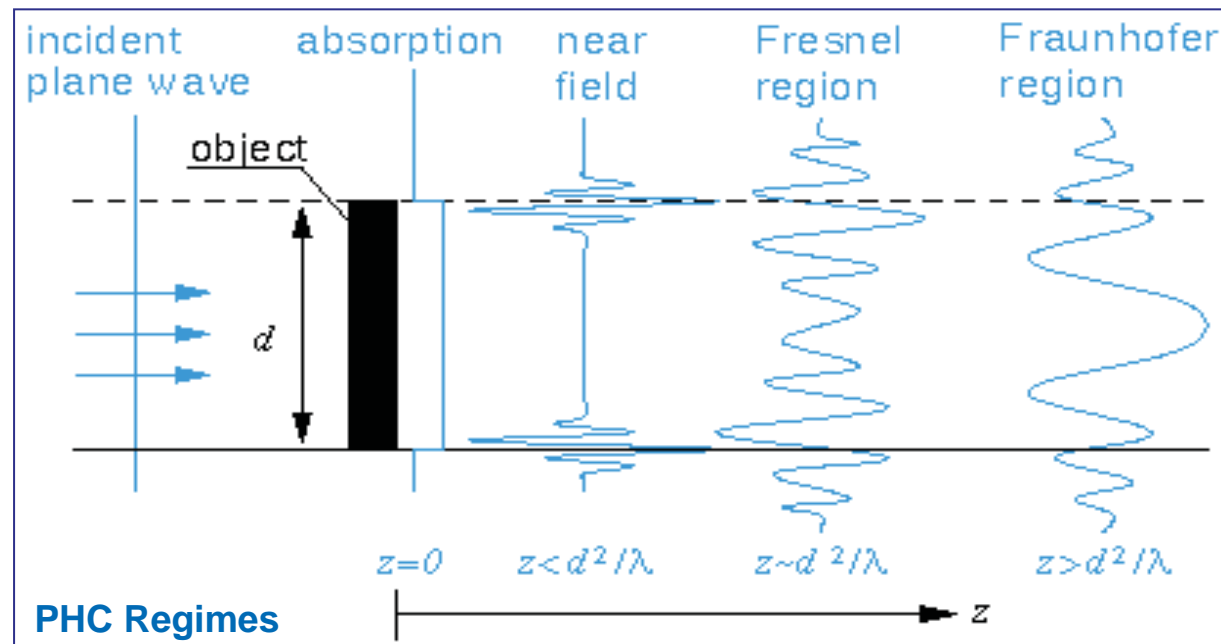
Source: G. Tromba and the SYRMEP team @ ELETTRA



PHC imaging setup



- $z = 0$ -> absorption image
- For $z > 0$ -> interference between diffracted and un-diffracted wave produces edge and contrast enhancement. A variation of δ , producing a phase shift, can be detected
- Measure of $\nabla^2\Phi(x,y)$



μ CT – the SYRMEP beamline @ ELETTRA

Application Examples



PHC and L, K-edge imaging: Mapping of the metal intake in plants by X-ray μ -radiography and μ -CT

- Accumulation of metals, such as Cu, Zn, As, Cd, Pb, Hg, in the environment is a high health risk because of the possibility for these elements to be transferred to living organisms through fresh water or vegetables.
- Among the different solutions, a very promising method is phytoremediation: it consists in the removal of contaminants by means of their absorption and accumulation in roots and leaves of plants, specially cultivated for this purpose and then harvested. Recently, also transgenic plants have been obtained, with higher accumulation properties.
- To study these problems: detection of contaminants, comparison of accumulation properties of the various plants, mapping of possible biological structures accumulating specific metals within a tissue.
- We used dual-energy micro-radiography taking advantage of the highly-monochromatic, large-field synchrotron radiation to detect the heavy-metal accumulation in 2D and 3D biological samples.

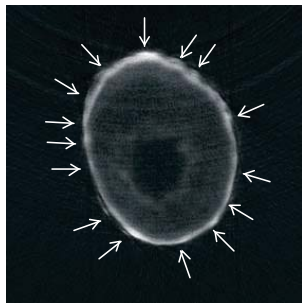
μ CT – the SYRMEP beamline @ ELETTRA

Application Examples



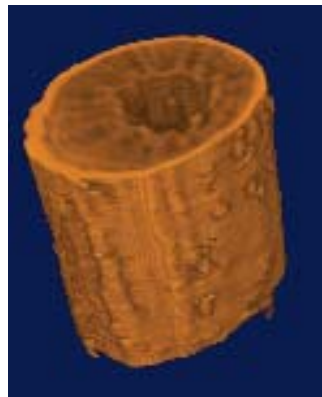
Mapping of the metal intake in plants by X-ray μ -radiography and μ -CT

Dyplotaxis erucoides root grown in 2% CuSO_4 solution

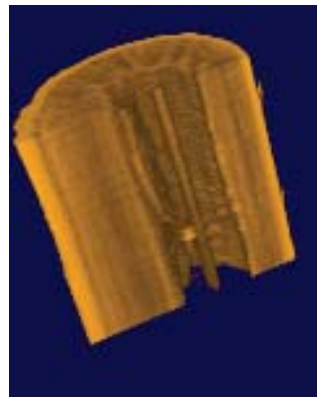


difference

$E = 9.05$ and 8.90 keV



$h = 1$ mm
 \varnothing ca. 3 mm

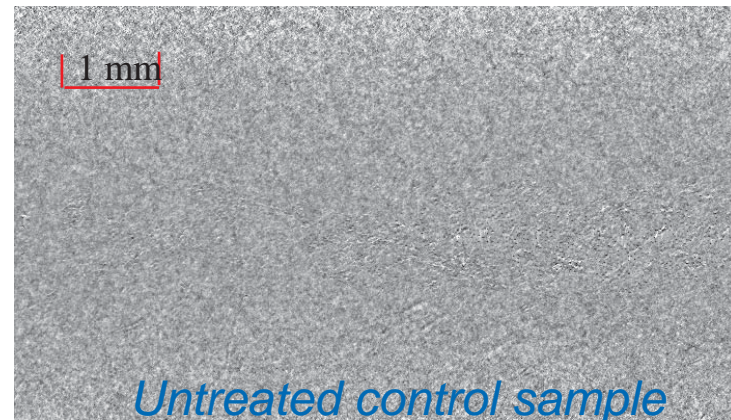


3D rendering

Helianthus annuus leaf treated in a 10 mM PbSO_4 solution



$E = 13.150$ and 12.975 keV



Untreated control sample

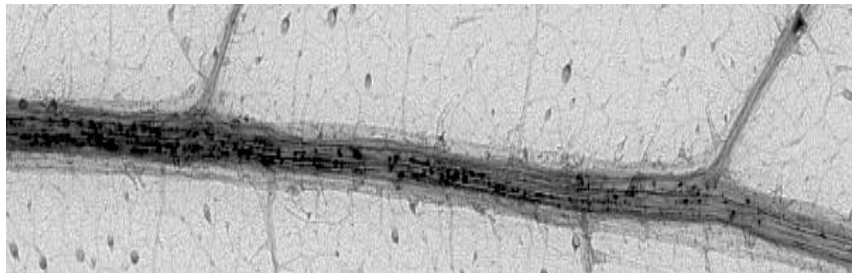
μ CT – the SYRMEP beamline @ ELETTRA

Application Examples

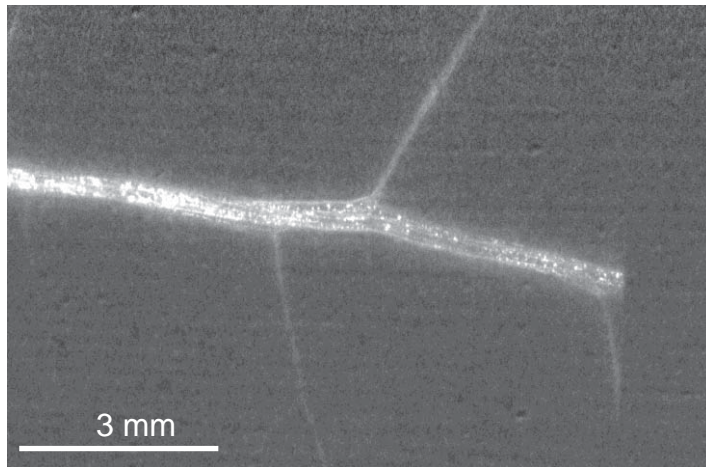


Mapping of the metal intake in plants by X-ray μ -radiography and μ -CT

Helianthus annuus leaf treated in a 10 mM PbSO_4 solution

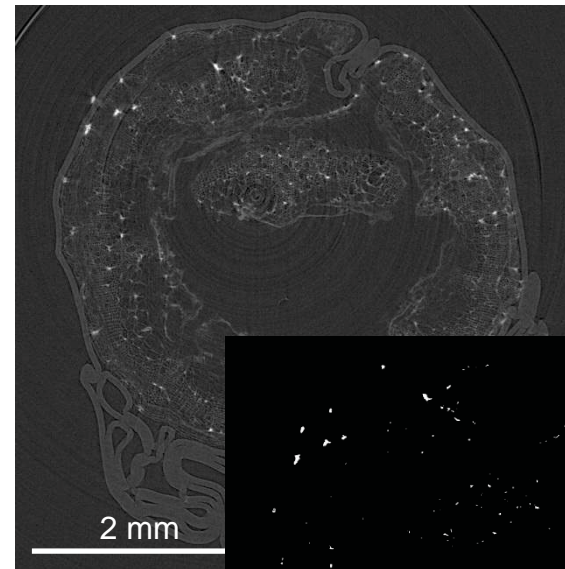


$E=13.150$ keV, planar radiograph



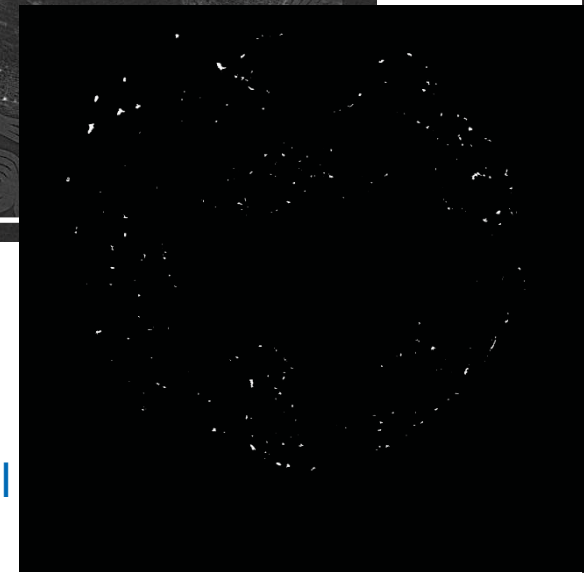
difference $E = 13.150$ and 12.975 keV

Helianthus annuus root treated in a 10 mM PbSO_4 solution



μ CT slice

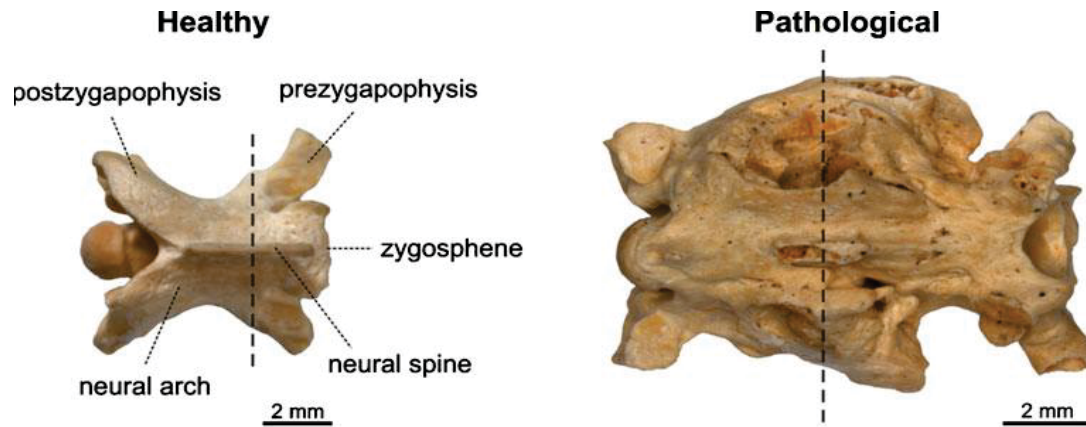
Differential μ CT slice



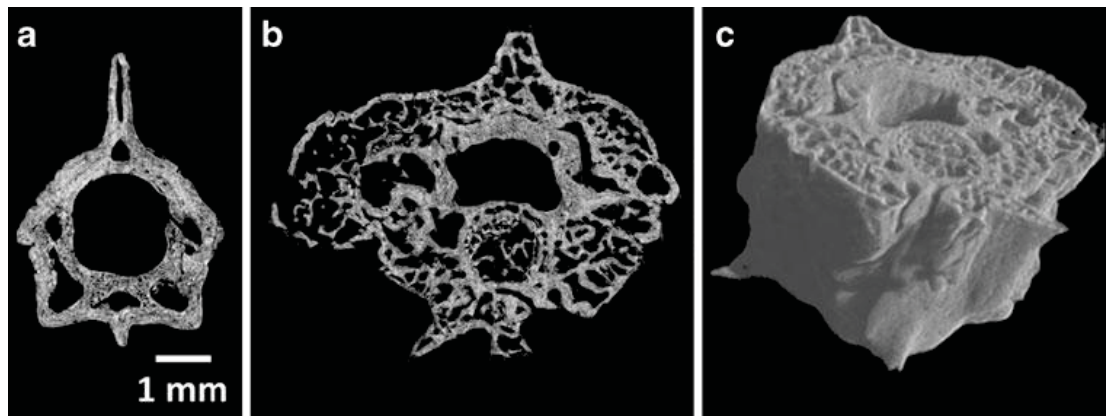
μ CT – the SYRMEP beamline @ ELETTRA Application Examples



μ -CT of fossil samples



(~ 1 Ma years old) snake vertebra



SR- μ CT slices of **a** healthy and **b** pathological fossil snake vertebra together with **c** the 3D rendering of the investigated fossil snake vertebra segment.

μ CT – TOMOLAB @ Elettra



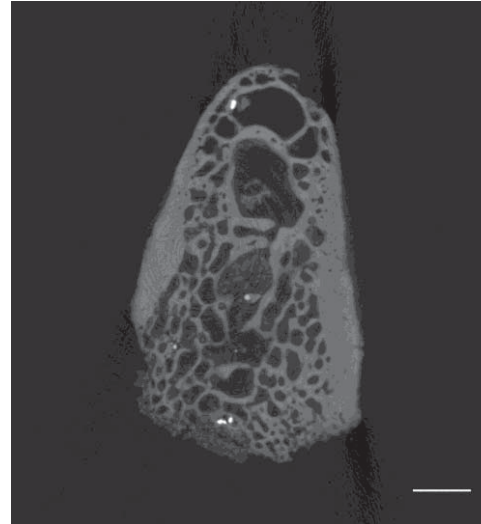
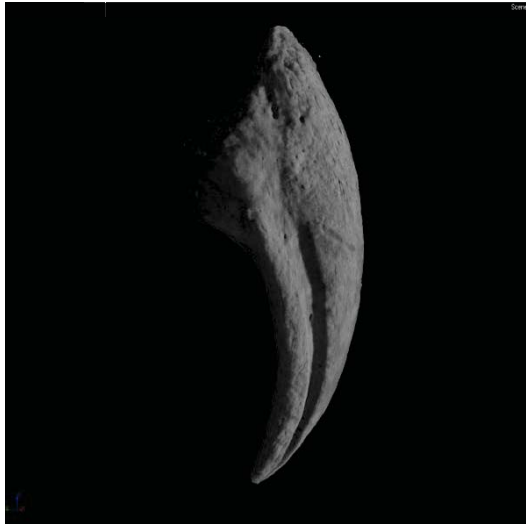
<http://www.elettra.trieste.it/Labs/TOMOLAB/>

- TOMOLAB is a cone-beam μ CT system equipped with a sealed microfocus X-ray tube, which guarantees a focal spot size of 5 microns, in an energy range from 40 up to 130 kV, and a maximum current of 300 μ A.
- A water cooled CCD camera providing a good combination between a large field of view (49.9 mm \times 33.2 mm) and a small pixel size (12.5 \times 12.5 microns²) is used as detector. Due to the cone-beam geometry it is possible to achieve a spatial resolution close to the focal spot size.
- Maximum allowed sample size is \varnothing 4.5 centimeters (the horizontal field of view of the CCD camera is \sim 5 centimeters and the sample has to fit it all during the scan).

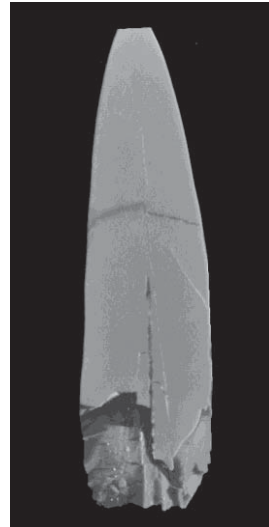
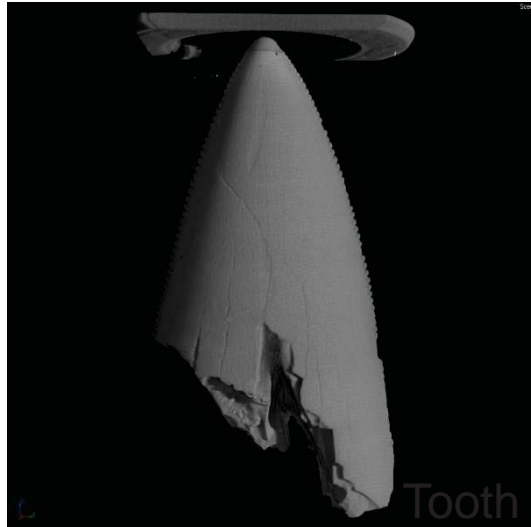
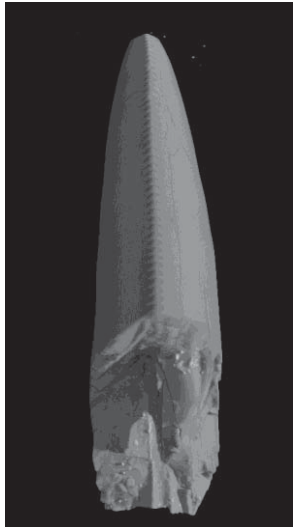
μ CT – TOMOLAB @ Elettra Application examples



μ -CT of fossil samples



Claw,
bar 5 mm



Tooth

Source:
M. Galiová, *et al.*, unpublished

GE v tome x I 240 @ CEITEC

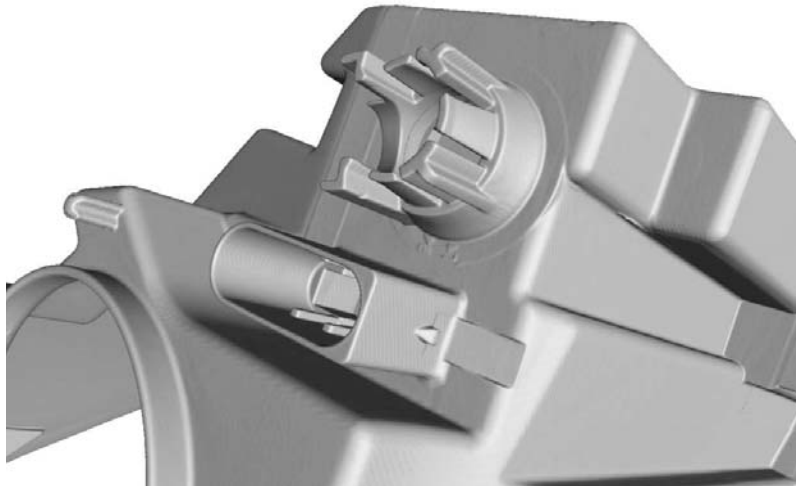
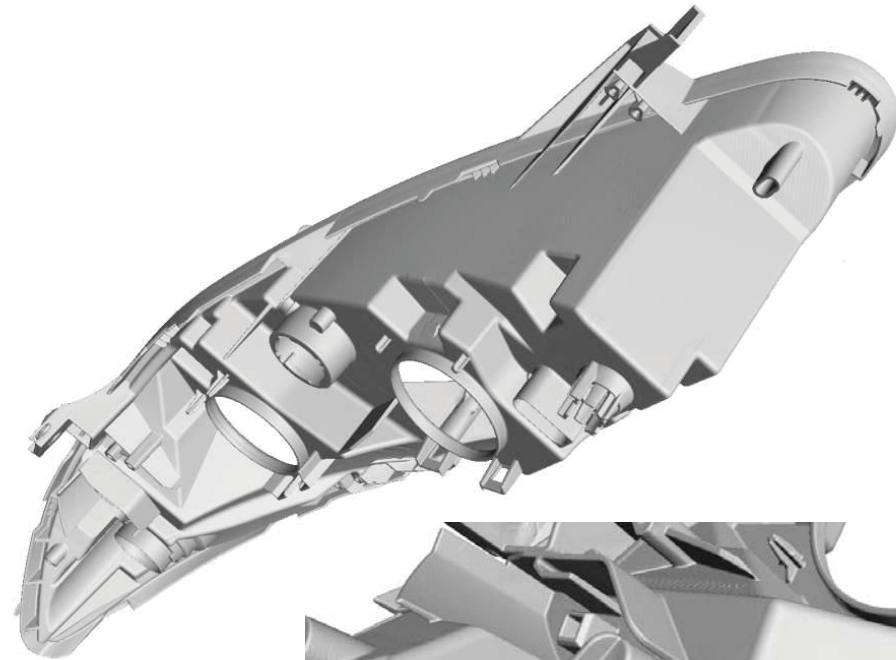


<http://www.ge-mcs.com/en/radiography-x-ray/ct-computed-tomography/vtomex-l-240.html>

- Source – 2 sources – microfocus (240 kV, 320 W, 3 -200 μm spot size) and nanofocus (up to 180 kV, 15 W, $< 0.9 \mu\text{m}$ spot size).
- Detector – DXR 250 (flat panel, 2048 x 2048 pixels, pixel size 200 μm x 200 μm , dynamic range 1:10000, up to 7.5 frames/s).

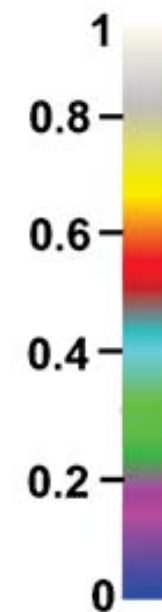
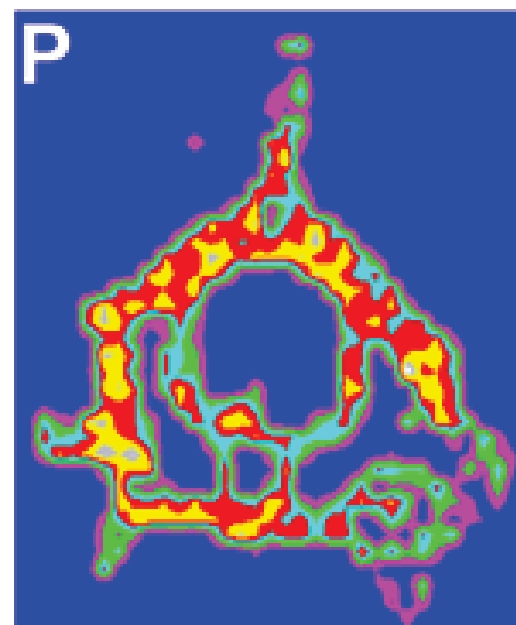
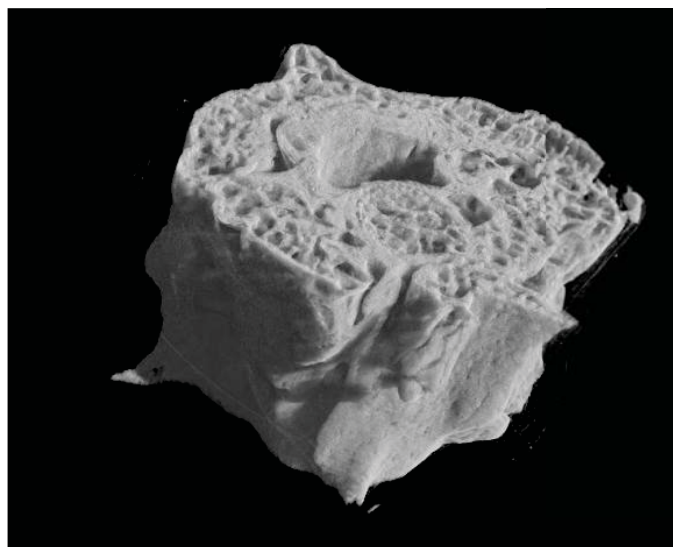
GE v tome x I 240 @ CEITEC

Application examples



J. Kaiser, *et al.*: unpublished

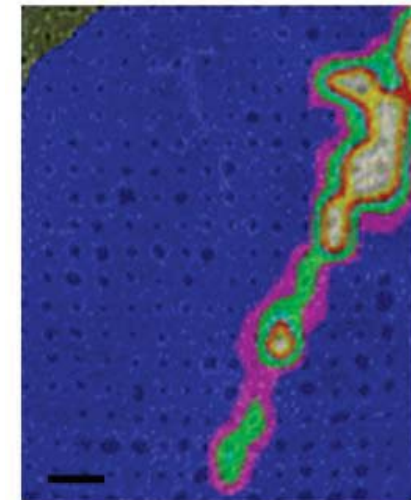
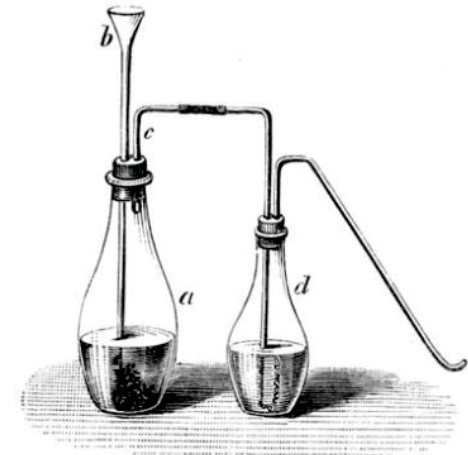
HR 3D imaging → Chemical mapping



Laser ablation for sampling



- The **total content** of trace or matrix elements (i.e. accumulated metals) in the samples (e.g. plant tissues) can be determined utilizing routine methods e.g. „wet analysis“ AAS or AES after the dissolution of the plant compartments.
- In order to investigate the trafficking, the **spatial distribution** of such metal ions in the tissues must be studied.



Laser ablation for sampling

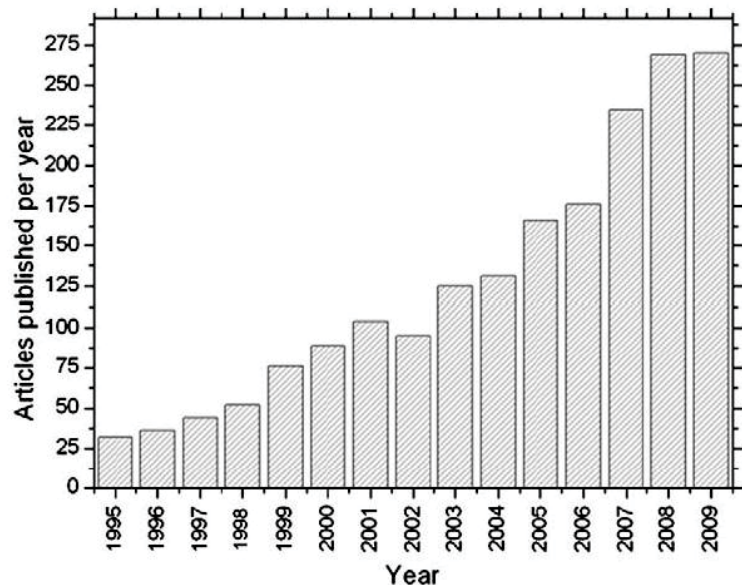


- Laser ablation is widely used for sampling of solid material into inductively coupled plasma mass/optical spectrometer (LA-ICP-MS/OES).
- LIBS as a type of atomic emission spectroscopy, which utilises a highly energetic laser pulse as the excitation source.
- LIBS is able to determine elemental composition of sample using radiation of this, laser-created plasma. Moreover, it is able to provide map of the elements of interest in different types of materials with high spatial resolution.

LIBS vs. LA-ICP-MS / LIBS is growing



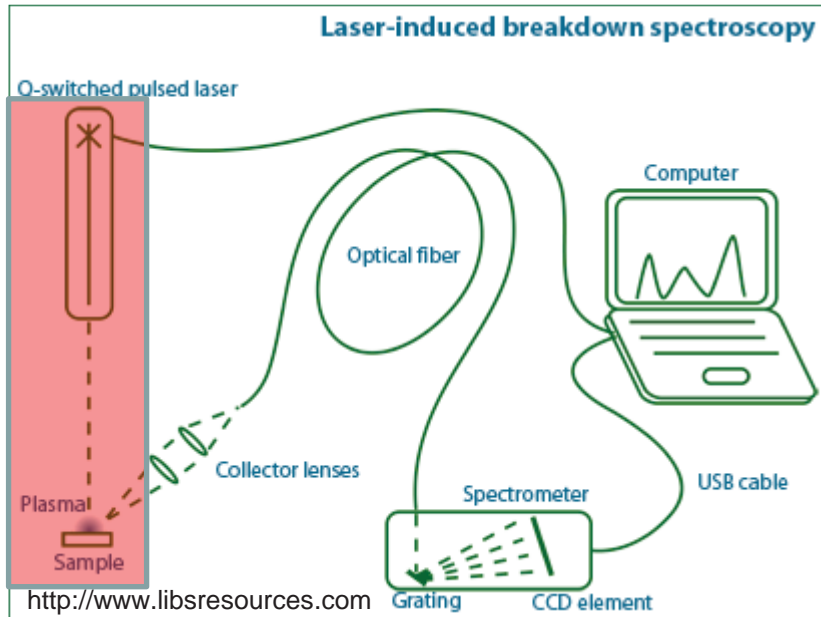
- LIBS setup is simpler, the experiments are most cost reliable.
- LIBS gives a instantaneous signal directly related to the location at which a single ablation event occurred.
- LA-ICP-MS, usually more experimental difficulties – this technique involves sample transport, so the signal produced in the mass spectrometer is not directly attributable to a specific location on the sample (without considerable care in the analysis).
- Detection limits: LA-ICP-MS – (in general) lower.



Articles published per year in LIBS since 1995.

Source: F.J. Fortres, J.J. Laserna, Spectrochim. Acta B 65 (2010) 975-990.

LIBS – the ablation source



Creating the LIBS plasma

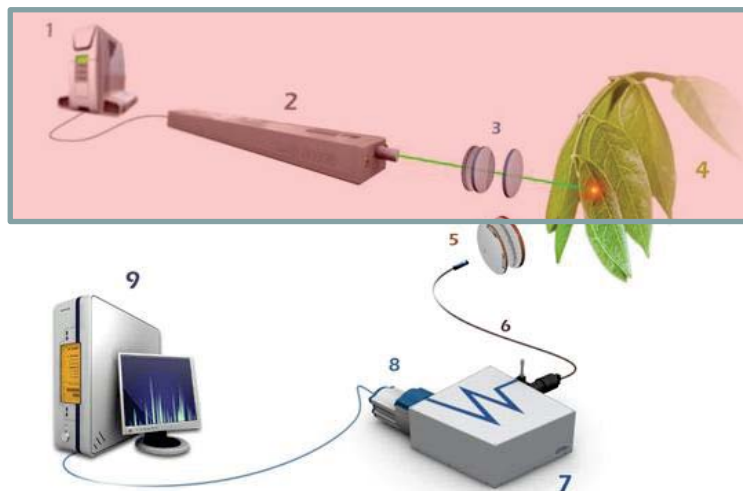
Plasma plume is created using an ablation laser.

Nowadays, the mostly used are nanosecond-pulsed solid state lasers, such as Q switched Nd:YAG. For increasing incident intensity and decreasing spot size the laser pulse is usually focused.

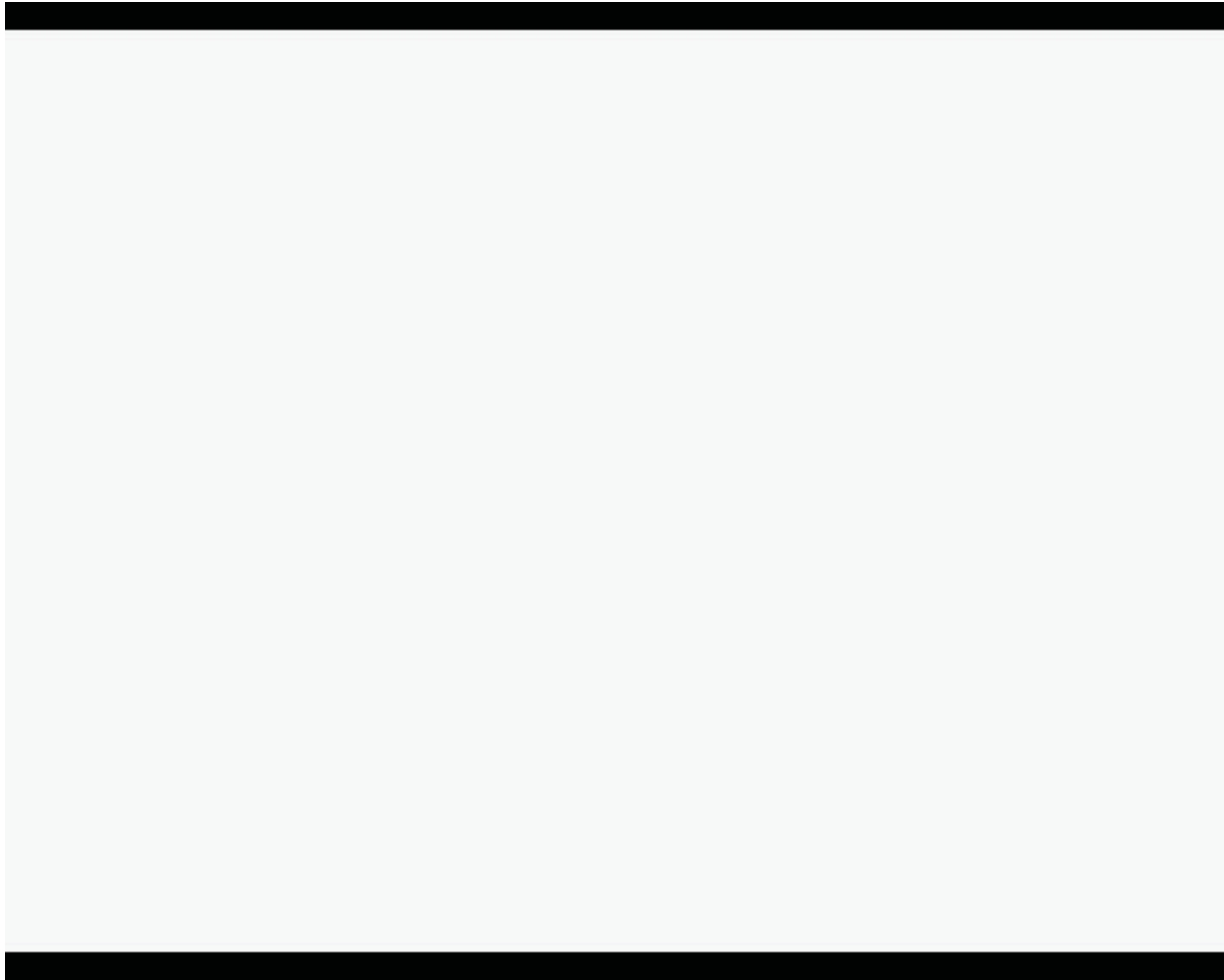
Typical fluxes on the surface then reaches orders of GW/cm^2 .

The ablation spot is heated with speed about 10^{10} K/s and small amount of sample (in order of nanograms) is vaporized.

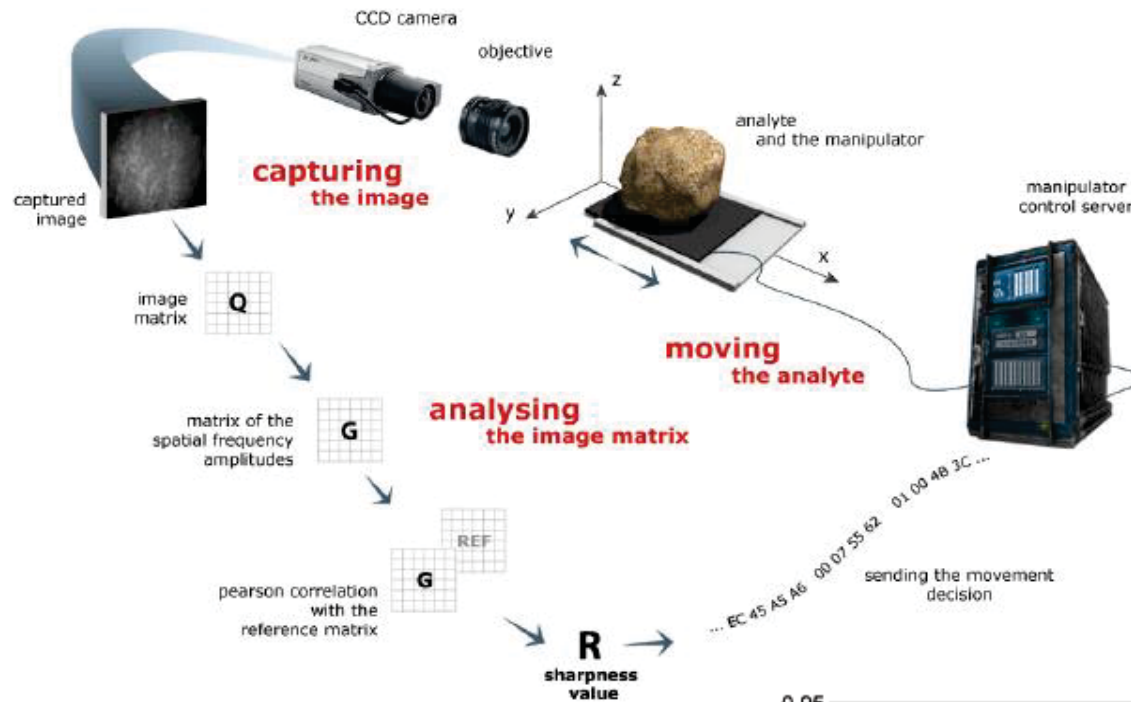
The plasma plume during the pulse duration expands with a speed about 10 km/s and creates an acoustic shock wave.



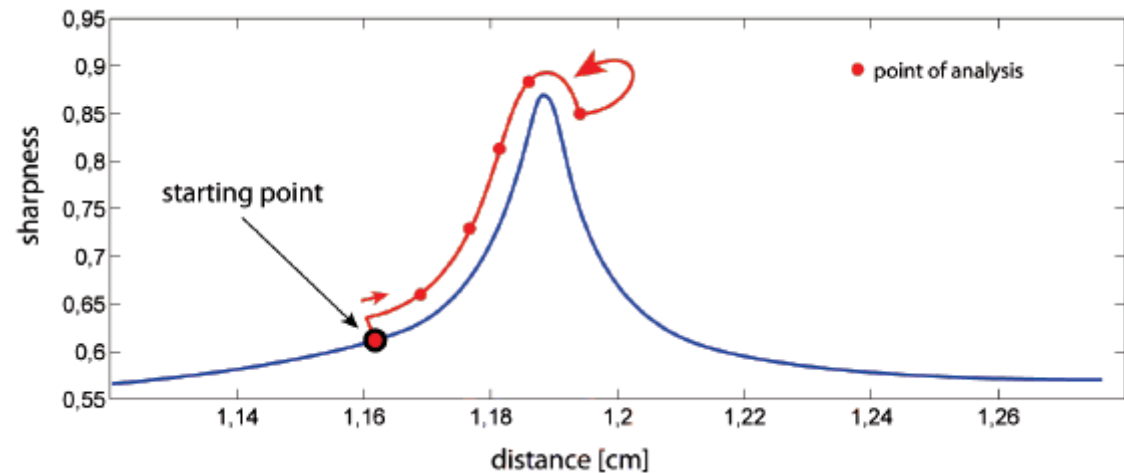
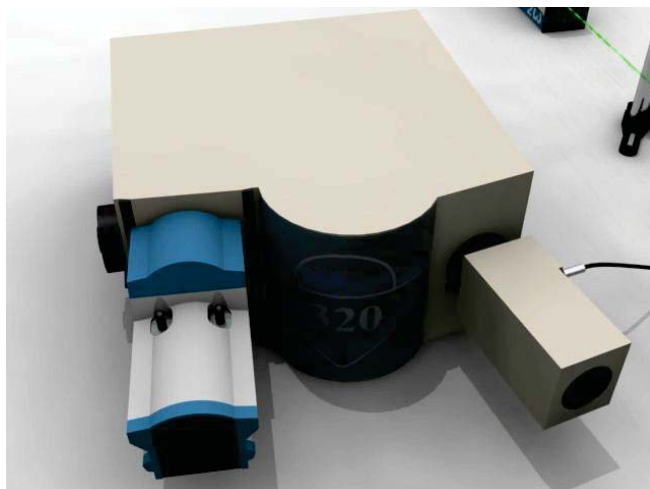
LIBS – the interaction chamber



The setup at BUT - autofocus



Schematic summary of the processes in the one cycle of the autofocus algorithm.

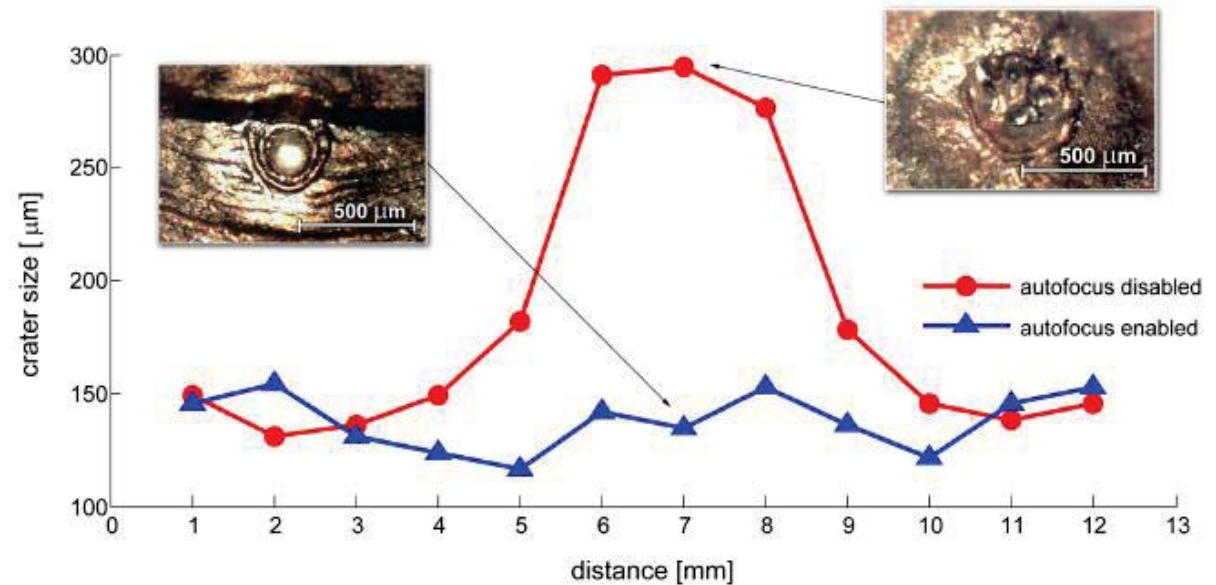


Schematic view of the algorithm convergence procedure.

The setup at BUT - autofocus



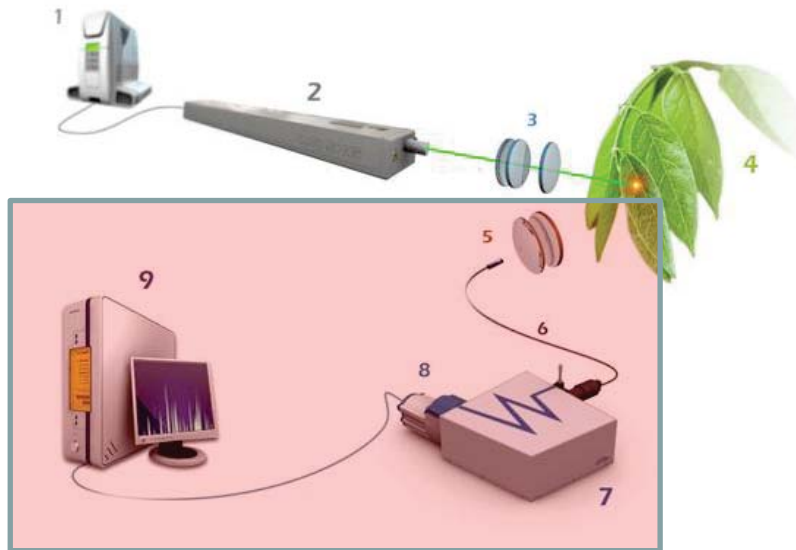
(a) A metal sample with welded bump (~ 1.5 mm height) .



Autofocus effect on ablation crater diameter.

More details in: J. Novotný *et al.*: Optical Engineering 48 (2009), 103604

LIBS – the plasma radiation



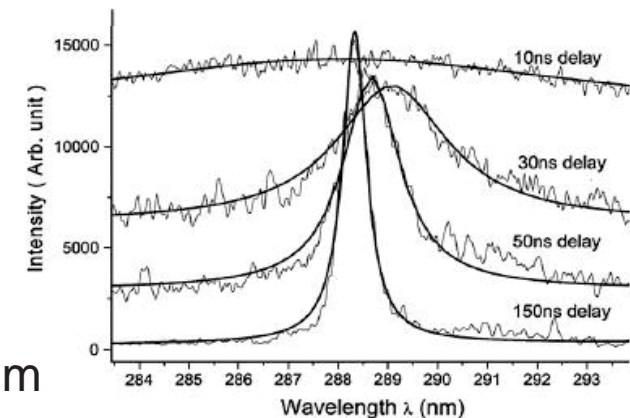
Collecting of the plasma radiation

Plasma radiation in the wavelength range *typically* 200-800 nm is collected and transported to the spectrometer (Czerny Turner or Echelle configurations are used usually) by an optical setup. There the light is dispersed by a system of mirrors, prisms and diffraction grating and illuminates an (I)CCD array in the camera. The signal in the form of relation between intensity and wavelength is then processed by a computer.

Plasma radiation

Just after the laser pulse the plasma plume starts to cool down.

Typically after a few microseconds that the laser pulse hits the target the best conditions for realizing LIBS measurements occur.



Si I 288.6 nm

Before this temporal interval the LIBS analysis cannot be performed due to the strong bremsstrahlung background caused by ion-ion or electron-ion interactions within the plasma.

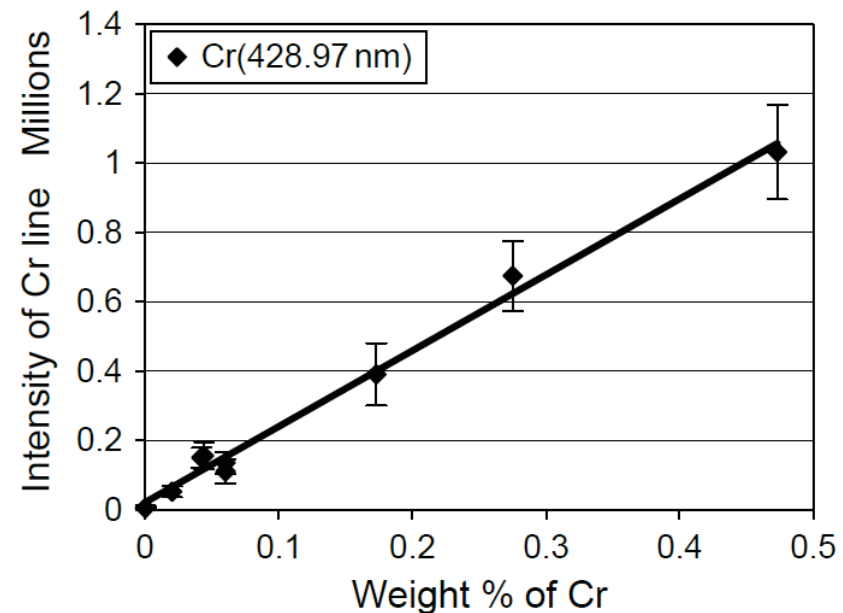
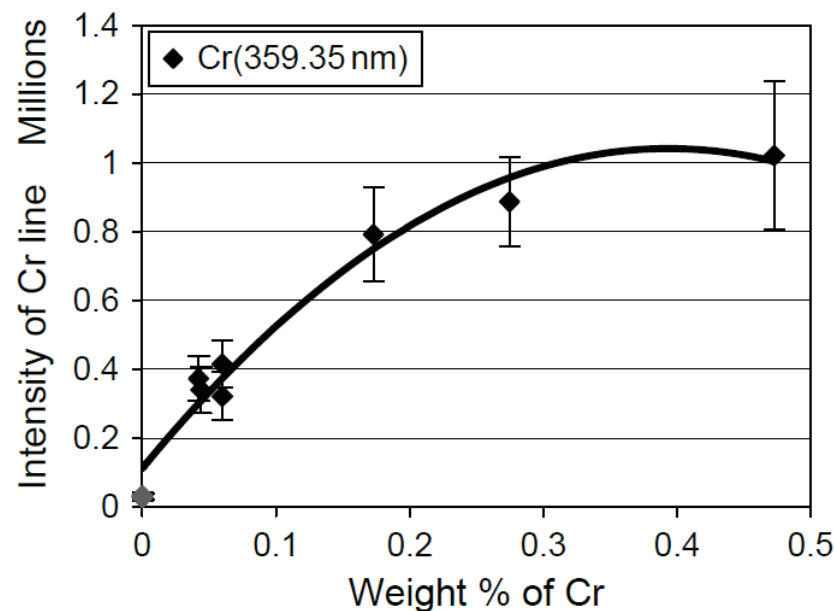
As the plasma is cooling down, this background intensity fades out and sharp emission lines (so called "elements' footprints") become visible.

LIBS – data processing



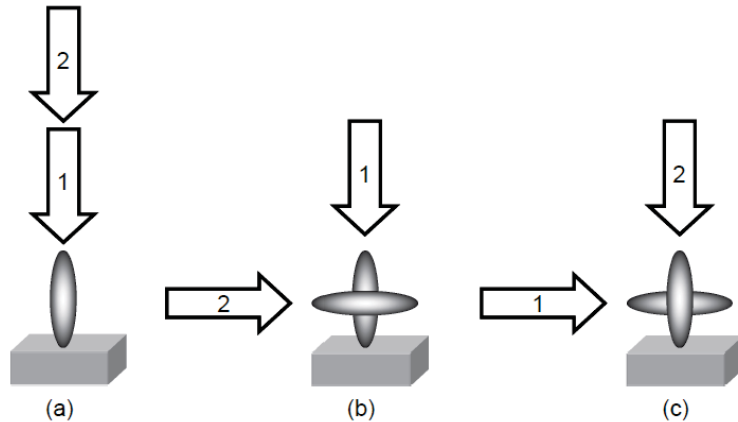
Data processing

Knowing the emission lines of ions, it is possible to determine chemical elements present in the sample (qualitative analysis). To determine their concentrations - to provide quantitative analysis - calibration must be performed in order to determine the relation between concentration and emission line intensity.



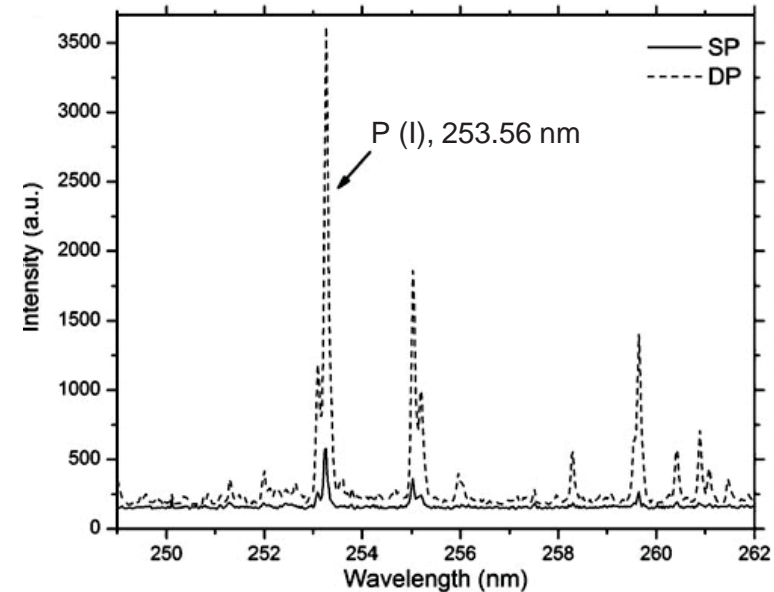
Left: calibration curve using absolute intensity of Cr (359.35 nm) line, Right: calibration curve using absolute intensity of Cr (428.97 nm) line.

LIBS – different experimental configurations

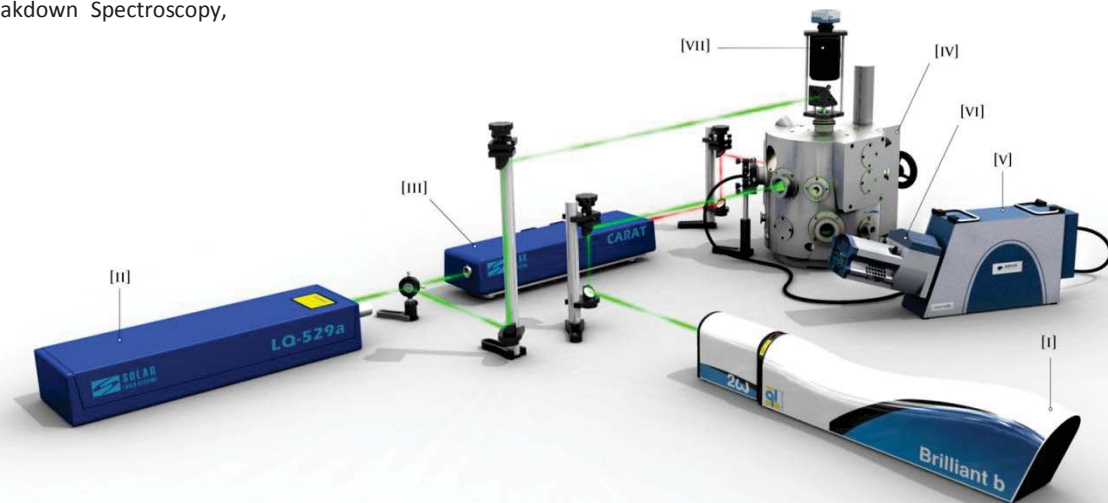


Common pulse configuration in Dual-Pulse (double pulse) LIBS. a) collinear, b) orthogonal reheating and c) orthogonal pre-ablative.

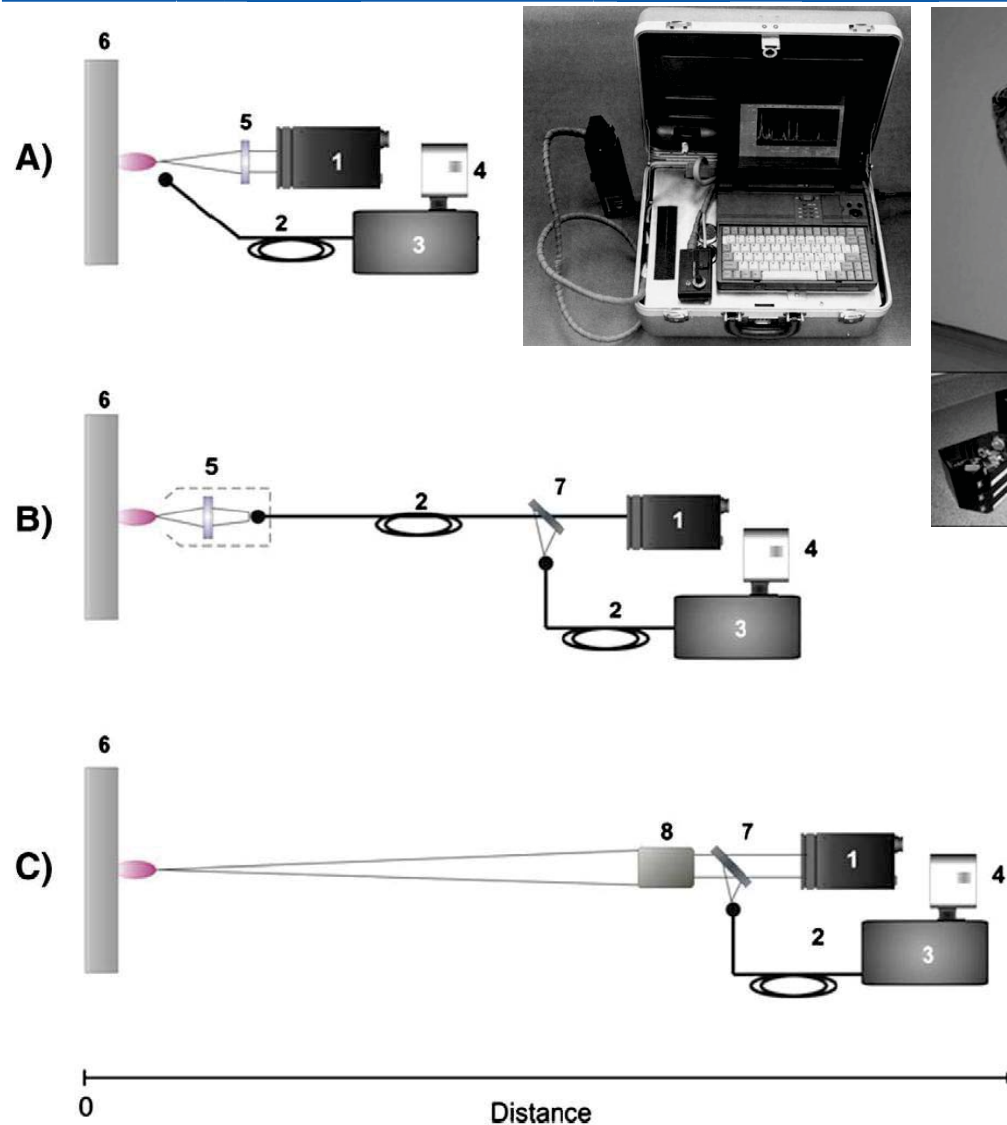
Source: J.P. Singh, S.N. Thakur, Laser-Induced Breakdown Spectroscopy, Amsterdam, 2007.



[I] LIBS ablation laser (Quantel, Brilliant B). [II] DP-LIBS ablation (or re-heating) laser and pump laser for Ti:Sa laser [III] Solar LS, LQ 529A. [III] Ti:Sa laser (Solar LS, Carat). [IV] Interaction chamber with 2 μm precision movements in x, y, z directions (Tescan s.r.o.). [V, VI] detection system, [VII] CCD



LIBS – Fieldable LIBS



Alternative configurations for an experimental set-up based on LIBS: A) (man) portable system, B) remote system and C) stand-off system.

1. Laser head, 2. Optical fiber, 3. Spectrometer, 4. Detector, 5. Focusing lens, 6. Sample, 7. Dichroic mirror and 8. Telescope.

LIBS – detection limits/comparison



Detection limits

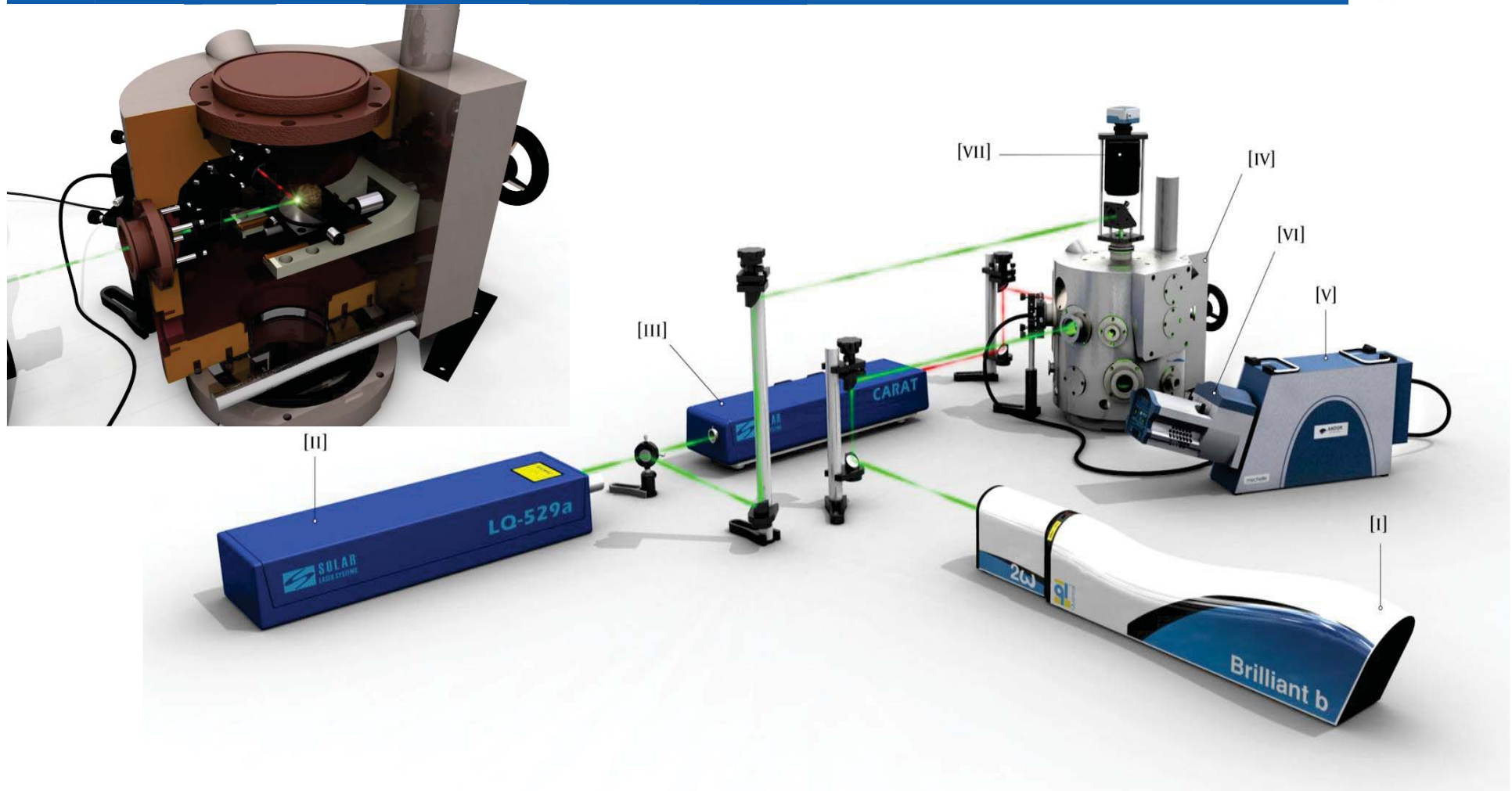
Typical detection limits of elements are from ppm, however, this varies a lot among different elements, sample types and experimental conditions, such as pressure or laser wavelength. Some elements can be detected even at concentration below 1 ppm, however some can be detected only qualitatively or have not been LIBS detected yet.

	Analytical techniques				
	GC-MS	LIBS	Raman	IMS	XRF
<i>Analytical capabilities</i>					
Selectivity	*****	***	****	**	***
Detection power	*****	**	***	**	***
Absolute analysis	*****	**	*****	**	**
Analytical information	Molecular	Atomic	Molecular	Molecular	Atomic
<i>Operational featuring</i>					
Sample preparation	*****	*****	*****	*****	*****
Sample size	*****	*****	*****	*****	*****
Lateral resolution	-	****	***	-	**
Depth resolution	-	*****	-	-	-
Speed	*****	*****	****	***	***
Simplicity of analysis	****	****	****	****	****
Solid sampling capability	-	*****	*****	-	*****
Instrumentation maturity	****	**	***	***	***
Scalability	**	****	*****	***	*****

GC-MS - gas chromatography–mass spectrometry,
 IMS – ion mobility spectrometry,
 XRF – X-ray fluorescence spectroscopy.

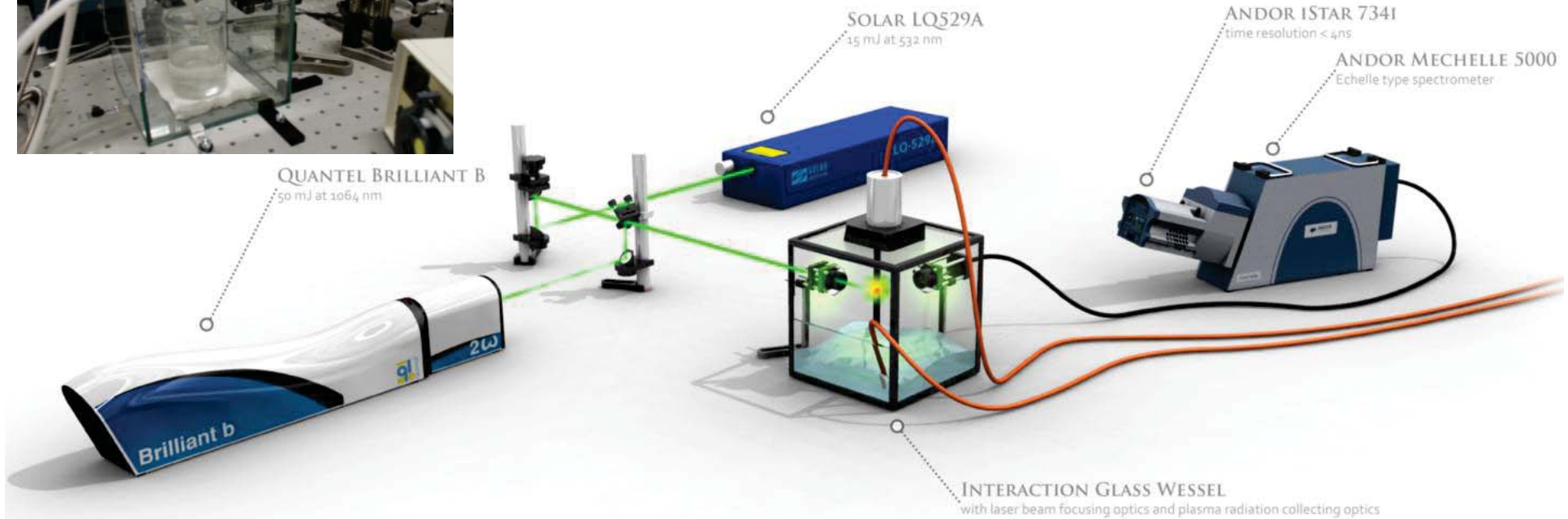
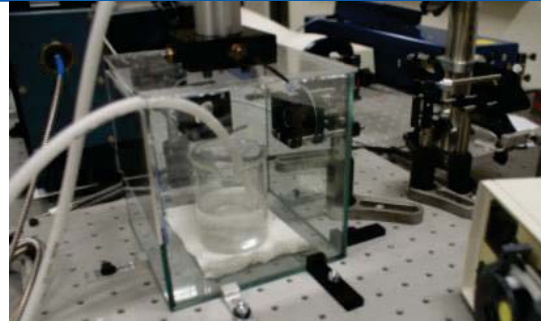
***** excellent; **** very good; *** good; ** medium; • poor.

The LIBS setups at BUT



[I] LIBS ablation laser (Quantel, Brilliant B). [II] DP-LIBS ablation (or re-heating) laser and pump laser for Ti:Sa laser [III] Solar LS, LQ 529A. [III] Ti:Sa laser (Solar LS, Carat). [IV] Interaction chamber with 2 μm precision movements in x, y, z directions (Tescan s.r.o.) [V + VI] Echelle spectrometer equipped with ICCD camera (ME5000, Mechelle, iStar, Andor), [VII] CCD camera. 35

The LIBS setups at BUT



LIQUID LIBS SETUP

Main field of application:

- Algal solution measurements, combination of LIBS (elemental analysis) with Raman spectrometry (algae iodine value from fatty acids).

Liquid LIBS –application example



ALGAL SOLUTIONS

- AN ALGAL SOLUTIONS (*TRACHYDISCUS MINUTUS* BOURRELLY) WITH VARIOUS METALS (Cu, Ca, Na, Mg) WERE USED IN THE FIRST LABORIOUS EXPERIMENTS.
- PHOTOSYNTHESIS: THE PLANTS CONVERT THE ENERGY OF SOLAR RADIATION INTO THE CHEMICAL ENERGY STORED IN PROTEINS, LIPIDS, CARBOHYDRATES, ETC.
- ALGAL LIPIDS ARE AMONG THE MOST PROMISING POTENTIAL PRODUCTS FOR BIOFUELS AS WELL AS FOR NUTRITION.

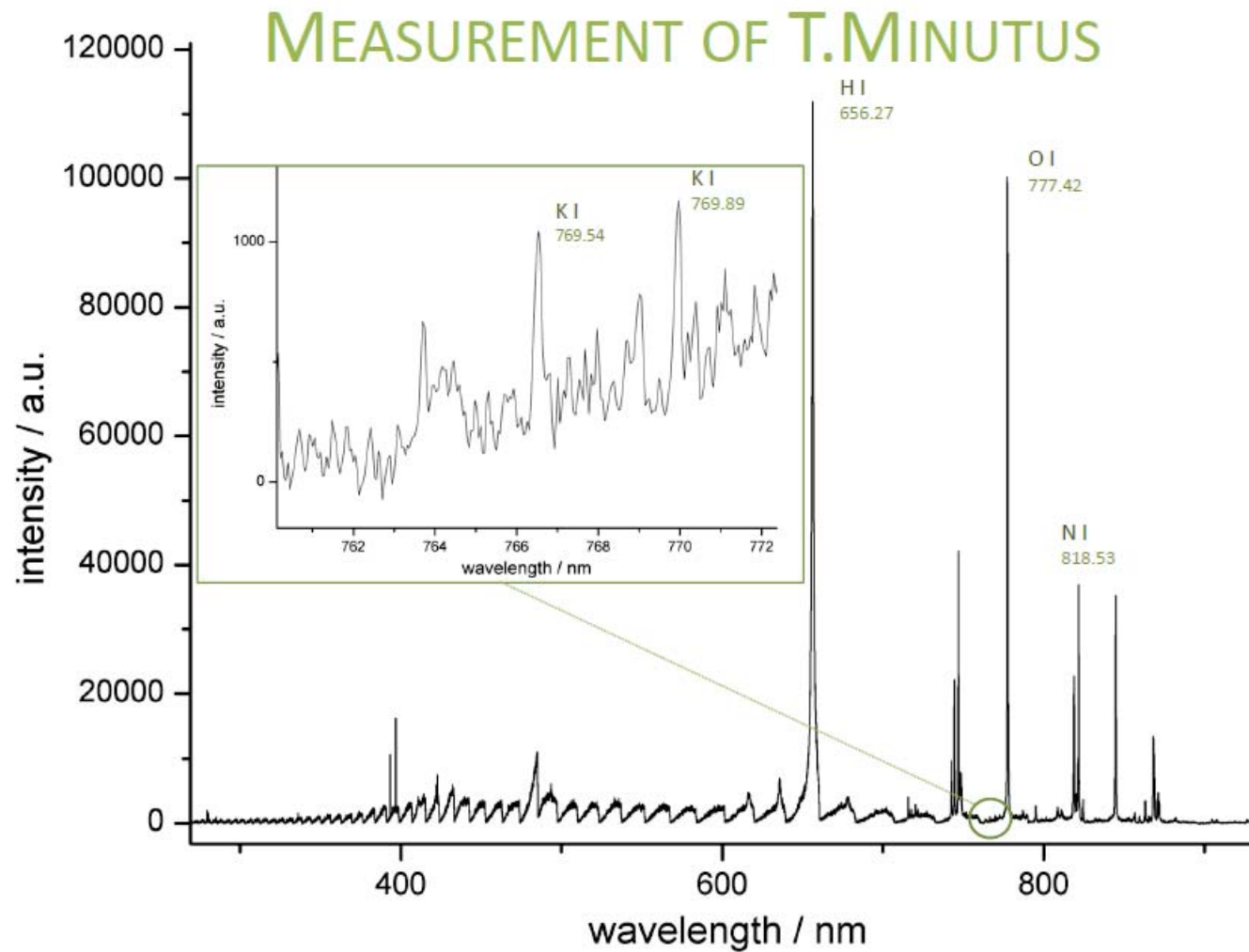


Trachydiscus Minutus

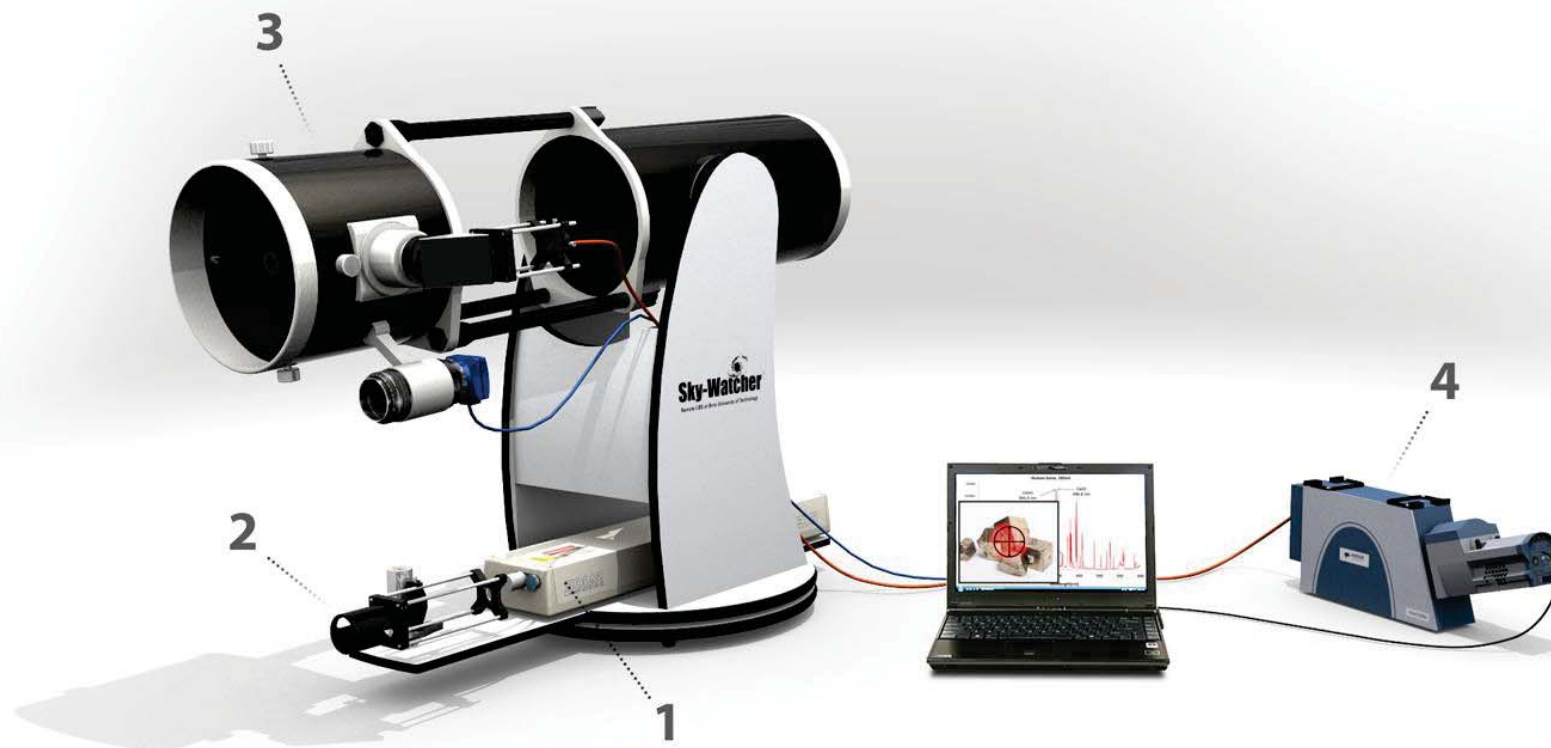
ARTICLE:

ILIEV, I. ET AL.: THE ALGA TRACHYDISCUS MINUTUS (PSEUDOSTRAURASTRUM MINUTUM): GROWTH AND COMPOSITION. GENERAL AND APPLIED PLANT PHYSIOLOGY, 23 APRIL 2010, VOLUME 36 (3-4), PP. 222 – 231.
SAMEK, O. ET AL.: RAMAN MICROSCOPY OF INDIVIDUAL ALGAL CELLS: SENSING UNSATURATION OF STORAGE LIPIDS IN VIVO. SENSORS, 17 SEPTEMBER 2010, VOLUME 10, PP. 8635 – 8651.

Liquid LIBS –application example



The LIBS setups at BUT

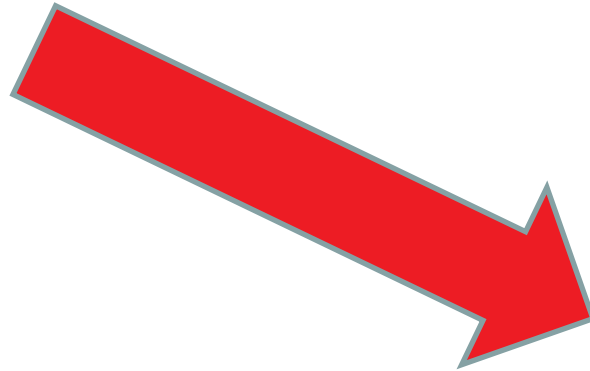


Standoff LIBS system

1 – Nd:YAG laser (Solar LQ 916) 2 – focusing optics 3 – collecting telescope (Sky-Watcher)
4 – detection system (Andor Mechelle 5000 + Andor Istar 734)

- Fast characterization and sorting of archaeological objects.

The LIBS setups at BUT

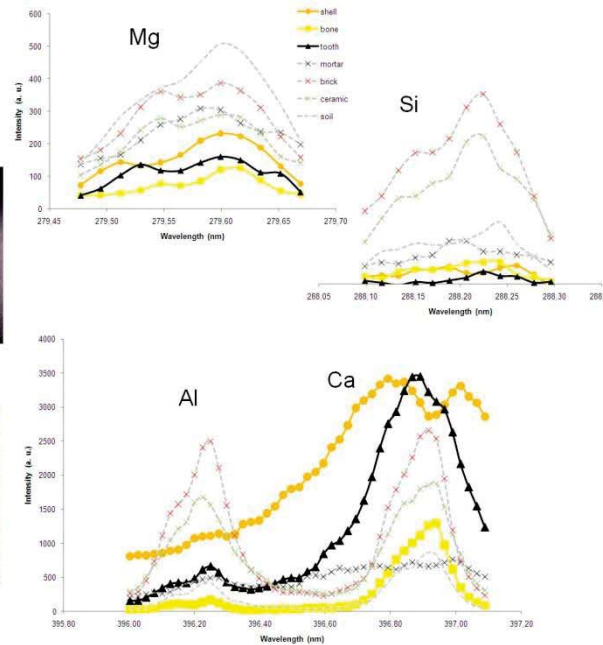
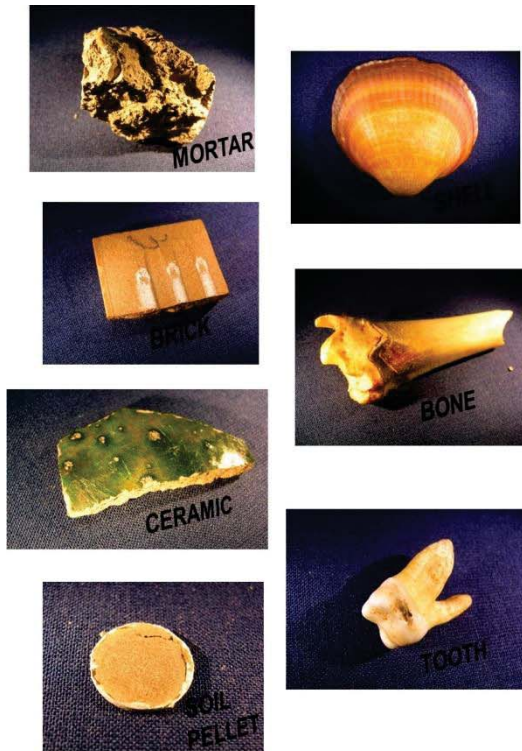


Standoff LIBS system

Ongoing work – remote LIBS



Artificial Neural Network (ANN) for the identification and classification of mineralized tissues and bio-mineral structures



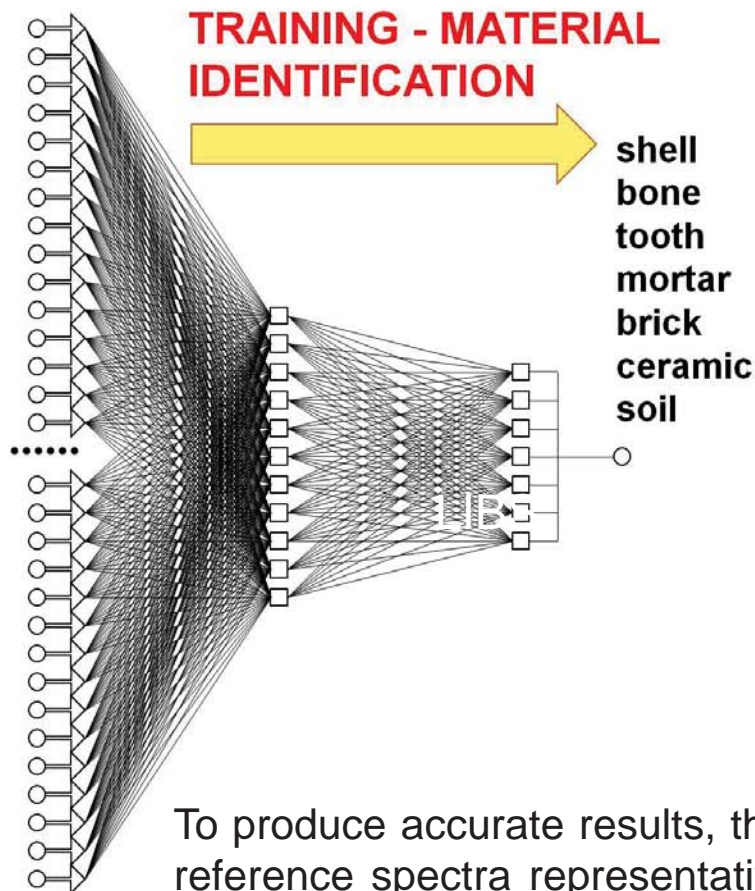
Three sets of spectra were recorded for 18 samples; the first training set of 98 spectra was used for the algorithm training. The training phase results in finding the best set of weights and bias values that would minimize the network output errors. This was done by using a backpropagation algorithm. The network optimization was carried out with the verification set of 21 spectra. To reduce of input data, we used only selected spectral intervals ($\Delta\lambda$) for lines detectable elements: Mg (279.55 nm), Si (288.16 nm), Al (396.15 nm), Ca (396.85 nm) and its combination_{4,1}

HRDLICKA, A., *et al.*: Development of a remote laser-induced breakdown spectroscopy system for investigation of calcified tissue samples. Applied Optics, May 2010, vol. 49, no. 13, p. C16-C20.

Ongoing work – remote LIBS



ANN for the identification and classification of mineralized tissues and bio-mineral structures



Input data (spectral intervals)

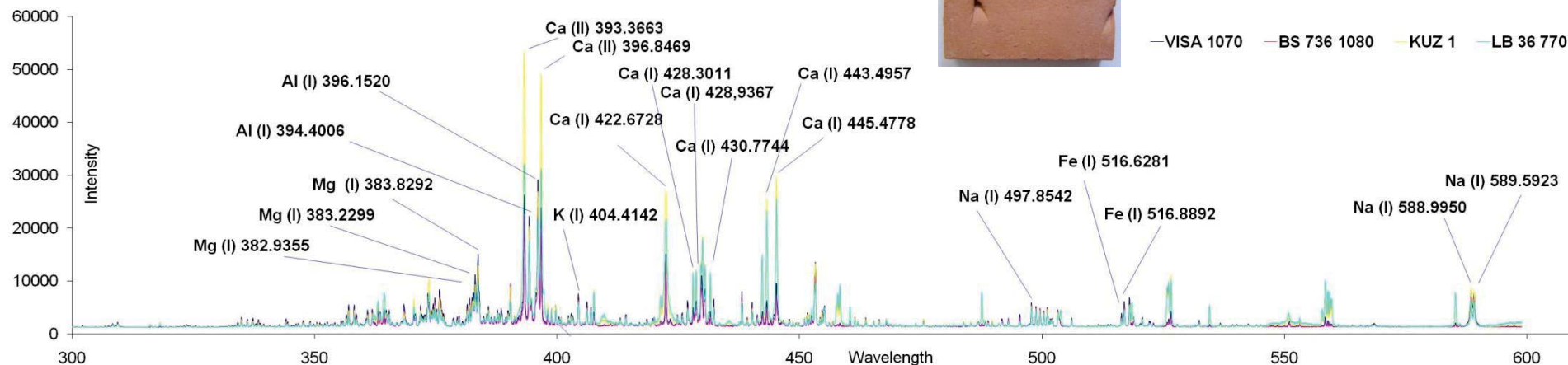
Test spectrum	Test sample	$\Delta\lambda$ [nm] Si (288.1-288.3)	$\Delta\lambda$ [nm] Si (288.1-288.3) Mg(278.4-278.6)	$\Delta\lambda$ [nm] Al+Ca (396.0-397.0)	$\Delta\lambda$ [nm] Si (288.1-288.3) Al+Ca (396.0-397.0)	$\Delta\lambda$ [nm] Si (288.1-288.3) Mg(278.4-278.6) Al+Ca (396.0-397.0)
No. 34	tooth	✗ ? ✗	Right ✓	Right ✓	Right ✓	Right ✓
No. 49	tooth	Right ✓	Right ✓	✗ ? ✗	Right ✓	Right ✓
No. 50	tooth	✗ ? ✗	Right ✓	Right ✓	Right ✓	Right ✓
No. 71	bone	Right ✓	Right ✓	Right ✓	Right ✓	Right ✓
No. 77	shell	✗ ? ✗	✗ ? ✗	✗ ? ✗	Right ✓	Right ✓
No. 82	shell	Wrong ✗	Wrong ✗	Right ✓	Right ✓	Right ✓
No. 101	bone	Right ✓	Right ✓	Right ✓	Right ✓	Right ✓
No. 110	bone	Right ✓	Right ✓	Right ✓	Right ✓	Right ✓
No. 126	tooth	Right ✓	✗ ? ✗	✗ ? ✗	Right ✓	Right ✓
No. 135	tooth	Wrong ✗	Right ✓	✗ ? ✗	Right ✓	Right ✓

To produce accurate results, the algorithm needs to be trained (i.e. calibrated) with a set of reference spectra representative of the targets to be analyzed (in our case, shell, mortar, soil, ceramic, tooth or bone). The first of all, the spectral emission of the plasma was measured for “known” set of materials for the identification of “unknown” samples. The obtained spectra were used to train ANN and the output was defined as 7 types of material (i.e. shell, mortar, brick, soil, ceramic, tooth or bone).

Ongoing work – remote LIBS



ANN for the comparison of brick samples



—VISA 1070 —BS 736 1080 —KUZ 1 —LB 36 770

brick sample	VISA 1070	LB 36 770	KUZ 1	BS 736 1080	HRS 6950	HRG 73 1050	HRG 75 1050	SL 345	SL 367 910	SL 367 950	SL 370 950	predicted	SLD 74 950	TA 26 950	TA 25 1050	predicted	TA 795 1060	TA 795 1100		
Na ₂ O [%]	1.4	0.23	0.44	0.61	0.80	0.52	0.59	0.63	0.71	0.75	1.1	1.1	0.84	0.59	0.59	0.55	0.75	0.56	0.62	
K ₂ O [%]	2.6	2.2	1.7	2.1	3.2	2.3	2.7	1.9	2.4	2.8	2.4	3.5	2.6	4.0	4.5	4.2	4.0	4.3	4.4	
SiO ₂ [%]	68	45	68	76	59	73	74	73	62	61	65	-	63	74	64	59	-	63	60	60
MnO [%]	0.13	0.03	0.04	0.08	0.06	0.09	0.05	0.16	0.06	0.06	0.08	0.11	0.08	0.07	0.08	0.08	0.07	0.08	0.08	
Fe ₂ O ₃ [%]	5.9	4.4	3.3	5.1	8.9	6.1	4.4	6.5	5.1	4.7	4.0	3.8	5.2	5.6	6.9	6.0	6.2	6.8	6.6	
MgO [%]	1.8	1.7	1.5	1.1	2.5	1.7	1.3	1.1	3.2	2.8	2.6	3.1	2.7	1.0	2.9	3.7	3.4	3.4	3.6	
Al ₂ O ₃ [%]	16	15	8.3	12	22	14	12	15	13	13	11	9.3	13	14	14	16	14	16	15	
TiO ₂ [%]	1.1	1.2	0.66	0.81	1.1	0.75	0.64	1.0	0.68	0.67	0.79	0.83	0.89	0.72	0.82	-	0.80	0.81	0.83	
CaO [%]	2.1	19	13	1.0	0.77	1.2	3.5	0.75	11	11	10	5.2	12	1.0	7.1	7.9	7.0	15	7.7	
P ₂ O ₅ [%]	0.15	0.14	0.04	0.10	0.21	0.05	0.09	0.07	0.06	0.10	0.11	-	0.08	0.12	0.17	-	0.08	0.16	0.13	
SO ₂ [%]	0.00	1.2	0.50	0.02	0.17	0.02	0.16	0.01	1.3	0.84	0.10	-	0.05	0.01	0.06	0.12	-	0.06	0.02	

Simultaneous prediction for 7 elements

Inputs: 32 (intensities of selected emission lines)
 Outputs: 7 (contents of 7 elements)
 Training: 15
 Test: 1
 Multilayer Perceptron (three layer)
 Iterations: 100
 Train - 100 epochs

Inputs:
 Na(I) 588.995, Na(I) 589.592, K(I) 404.414, Mn(I) 403.075,
 Mn(I) 403.306, Mn(I) 403.448, Fe(I) 516.6281, Fe(I) 516.889
 Mg(I) 382.934, Mg(I) 383.230, Mg(I) 383.829, Mg(I) 457.110,
 Al(I) 308.215, Al(I) 309.271, Al(I) 309.284, Al(I) 343.935,
 Al(I) 344.486, Al(I) 345.2658, Al(I) 394.401, Al(I) 396.152,
 Ca(I) 393.366, Ca(I) 396.847, Ca(I) 422.673, Ca(I) 428.301,
 Ca(I) 428.937, Ca(I) 430.253, Ca(I) 443.496, Ca(I) 445.478,
 Ca(I) 558.875, Ca(I) 559.446

Prediction element by element

Inputs: (spectral intervals)
 Outputs: 1 (content of selected element)
 Training: 45
 Test: 1
 Multilayer Perceptron (three layer)
 Iterations: 100
 Train: 100 epochs

Inputs:
 Na 588.0 - 590.0 nm (107 pixels)
 K 404.0 - 406.0 nm (103 pixels)
 Fe 516.0 - 518.0 nm (103 pixels)
 Mg 382.0 - 384.0 nm (100 pixels)
 Al 308.0 - 310.0 nm (100 pixels)
 Ti 340.0 - 342.0 nm (104 pixels)
 Ca 442.0 - 444.0 nm (104 pixels)
 P 312.0 - 314.0 nm (106 pixels)
 S 230.0 - 232.0 nm (104 pixels)

- prediction of brick chemical composition by artificial neural networks based on spectra obtained by remote LIBS.
- for major elements, good results were obtained in both cases, simultaneous prediction and prediction element by element
- for minor elements (P and S), results are very poor due to weak signal. On the other hand, next improvement can be reached in future by extension of spectra database.
- this approach can be useful for fast in-situ monitoring brick masonry of historical buildings. On the frame of ongoing work the spectral database will be expanded with data obtained from real (archeological) samples and the spreadsheet for ANN calculations will be optimized.

DP LIBS setup at the MU



- laser wavelengths 266 nm + 1064 nm
- grating 2400 g/mm
- interpulse delay 500 ns
- energy 10 mJ/pulse + 90 mJ/pulse
- delay 1 μ s , integration time 10 μ s,
- entrance slit 50 μ m
- distance of ablation craters 150 μ m (x, y)

1 – Ablation laser (New Wave, MACRO 266 nm), 2 – Re-heating laser (Quantel Brilliant, 1064 nm), 3 – Sample holder and precision movements, 4 – Delay Generators (Stanford RS), 5 – Spectrometer and ICCD camera (Jobin Yvon, Triax).

LA-ICP-MS setup at the MU



LA-ICP-MS

Nd:YAG laser (New Wave Research (UP 213))

ICP-MS spectrometer (Agilent 7500)

laser fluence: 9.5 J/cm^2

carrier gas: helium (flow 0.6 l/min)

laser repetition rate: 20 Hz

laser pulse width: 4.2 ns

volume of ablation cell: 20 cm^3

RF power: 1350 W

Applications - MAPPING



- LIBS of (bio)minerals

Samples of cultural heritage

- LIBS (LA-ICP-MS) of fossil bear tooth
- LIBS (LA-ICP-MS and μ CT) of fossil snake vertebra

Environmental studies

- LIBS of plant compartments

LIBS - geological samples (granite)



200 μm

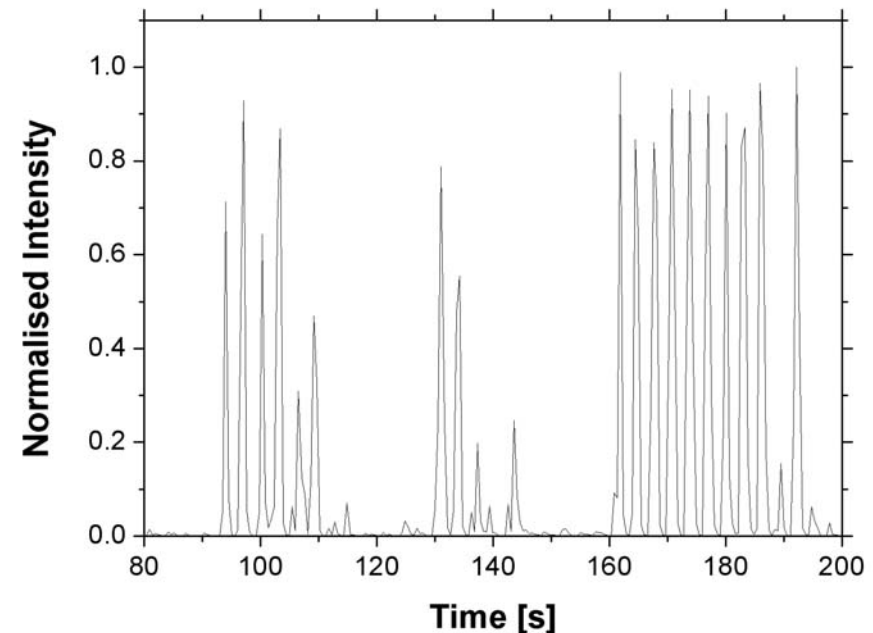
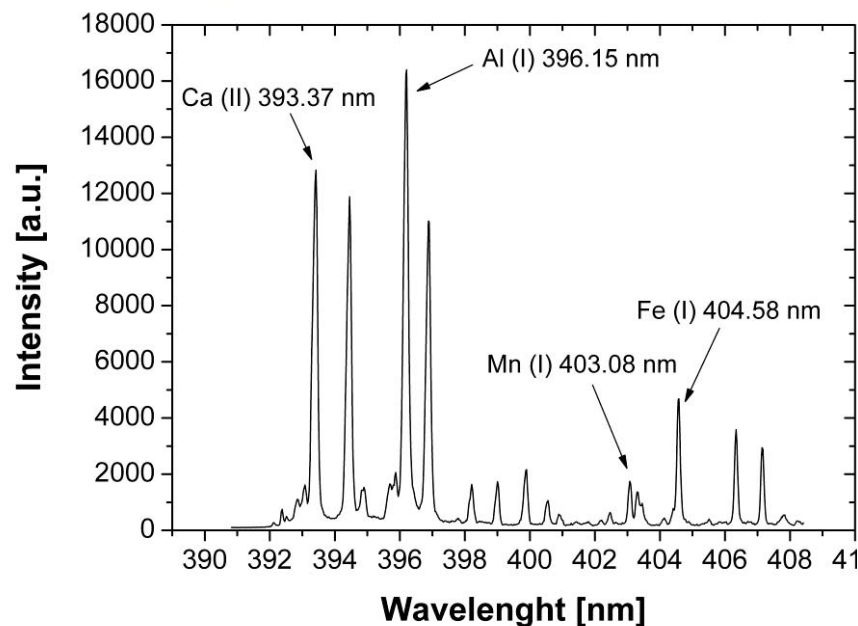
LIBS

120 μm laser spot diameter, 2 laser pulses per sample point

LA-ICP-MS

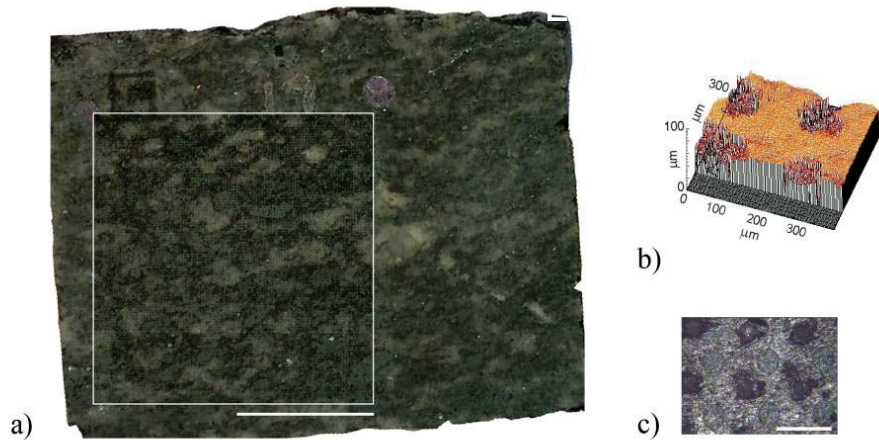
hole drilling mode, 110 μm laser spot diameter, 20 laser pulses per sample point, distance between individual laser spots was 200 μm

^{42}Ca , ^{27}Al , ^{56}Fe , ^{55}Mn

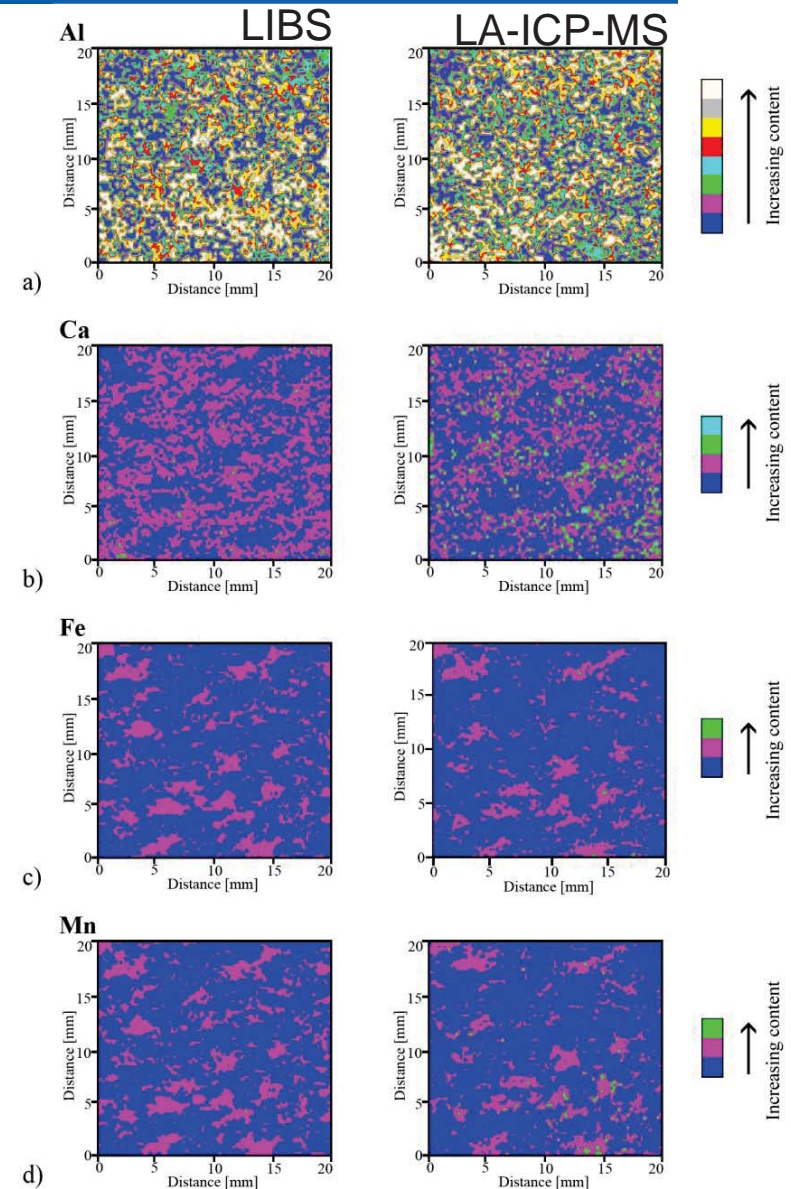


K. Novotný, J. Kaiser, M. Galiová, et al.: Mapping of different structures on large area of granite sample using laser-ablation based analytical techniques, an exploratory study, *Spectrochimica Acta Part B* 63 (2008) 1139–1144.

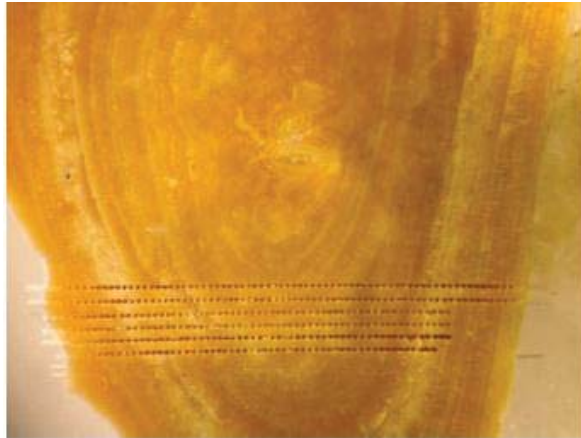
LIBS - geological samples



LIBS and LA-ICP-MS were used for a multi-element (Ca, Al, Fe, Mn) mappings of a granite sample surface. The sample was scanned with 100 x 100 individual sample points to map an area of 20 x 20 mm². The normalized signals were used for construct of contour plots which were colored according local distribution of the selected elements. The results of these two laser-based methods were compared and found to be similar.



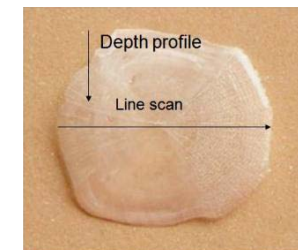
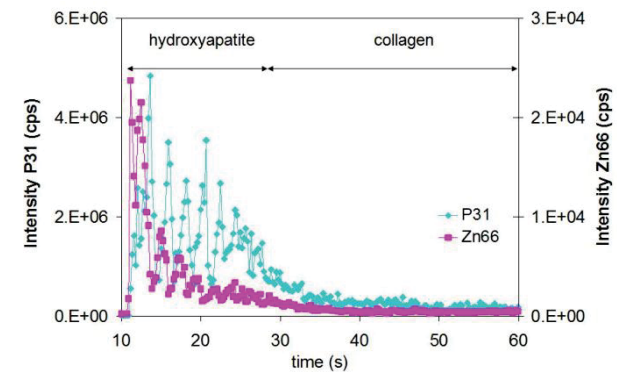
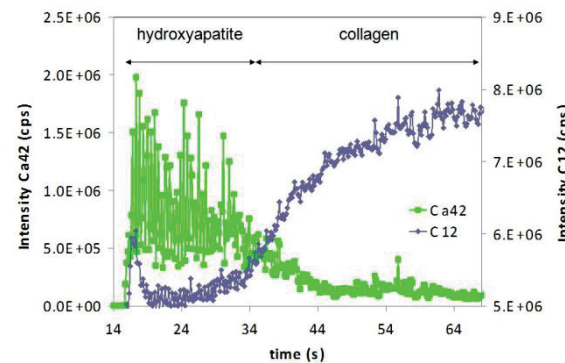
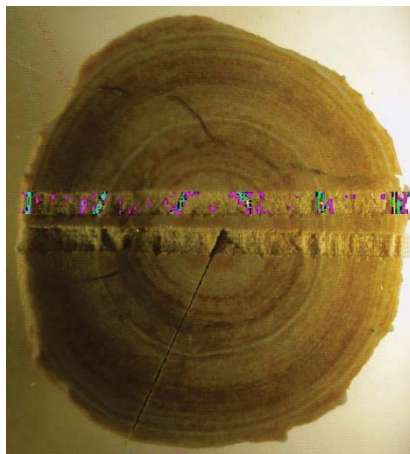
LIBS on Biominerals



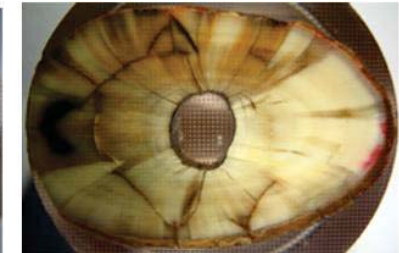
Example of the (cut) urolithic concrement (left) and fish scale sample (right) with the visible LIBS and LA-ICP-MS ablation patterns, respectively.

Source: M. Holá *et al.* - unpublished

P I (213.60 nm)

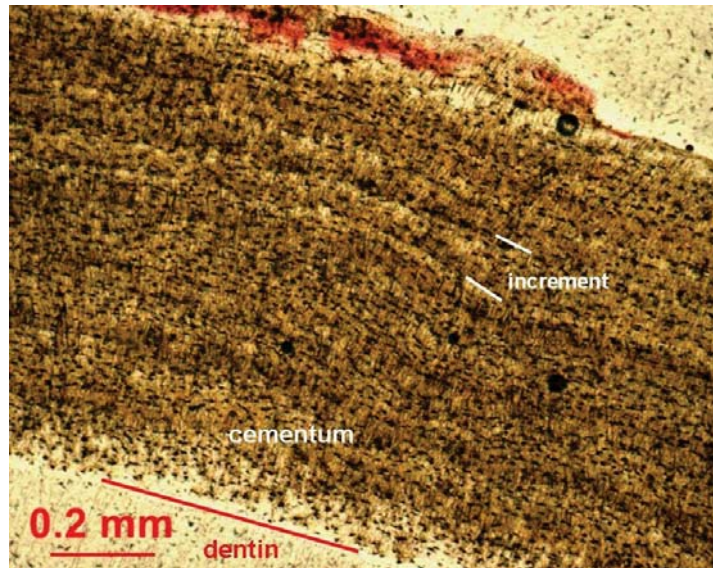


LIBS - fossil bear tooth



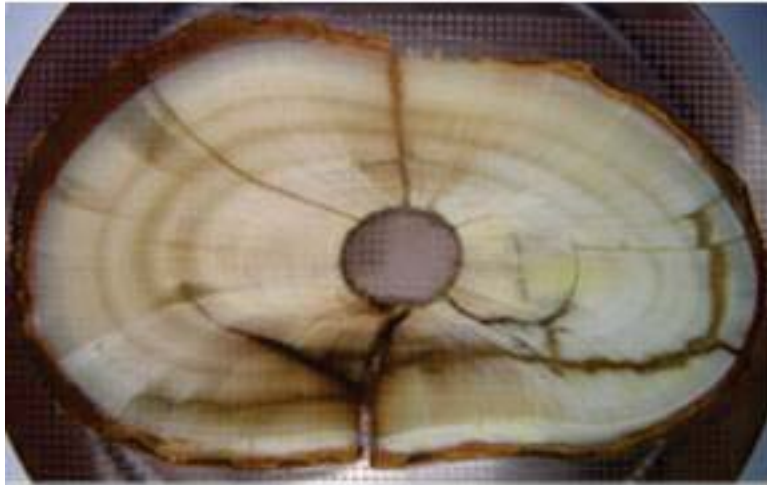
- ❖ The investigated tooth (canine-C₁) of fossil brown bear (*Ursus arctos*) was excavated at Dolní Věstonice II-Western Slope, South Moravia, Czech Republic.
- ❖ The locality is dated to $26\,640 \pm 110$ BP (uncalibrated ¹⁴C data) and belongs to Gravettian.

LIBS - fossil bear tooth

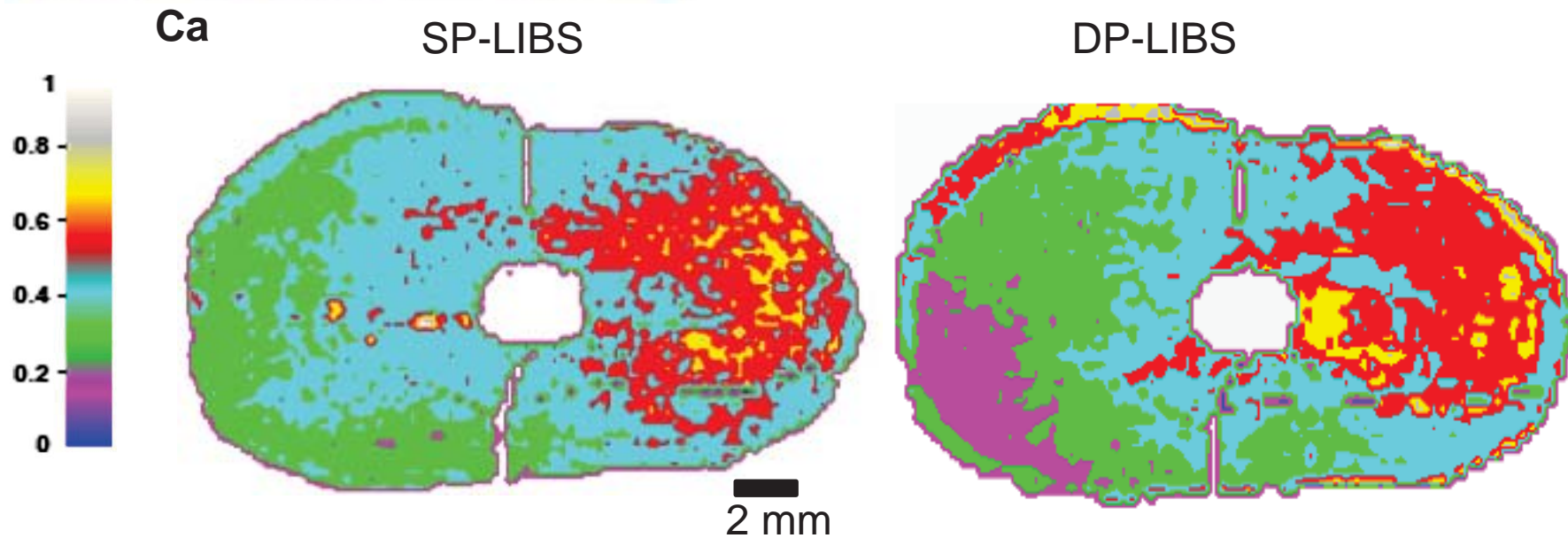


- Abrasion of tooth's occlusal area and increments of cementum of tooth's root were studied in order to determine the age and seasonality.
- This bear died at the age of 14 years and it is possible to appoint the term of death from unfinished summer increment and absence of winter increment in between summer and autumn season (August to October).

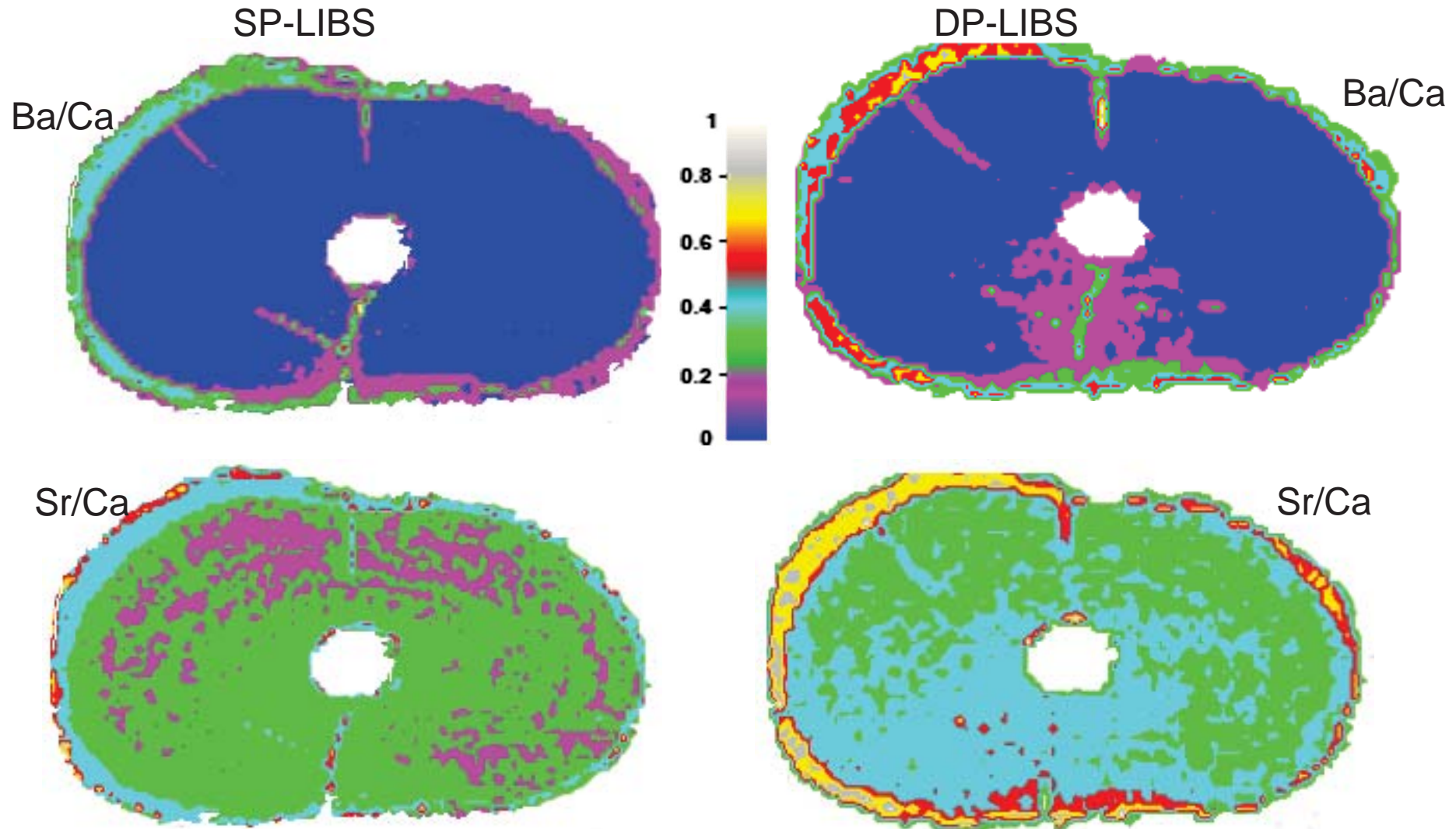
LIBS - fossil bear tooth



Comparison of calcium distribution within the investigated cross section of canine tooth root.

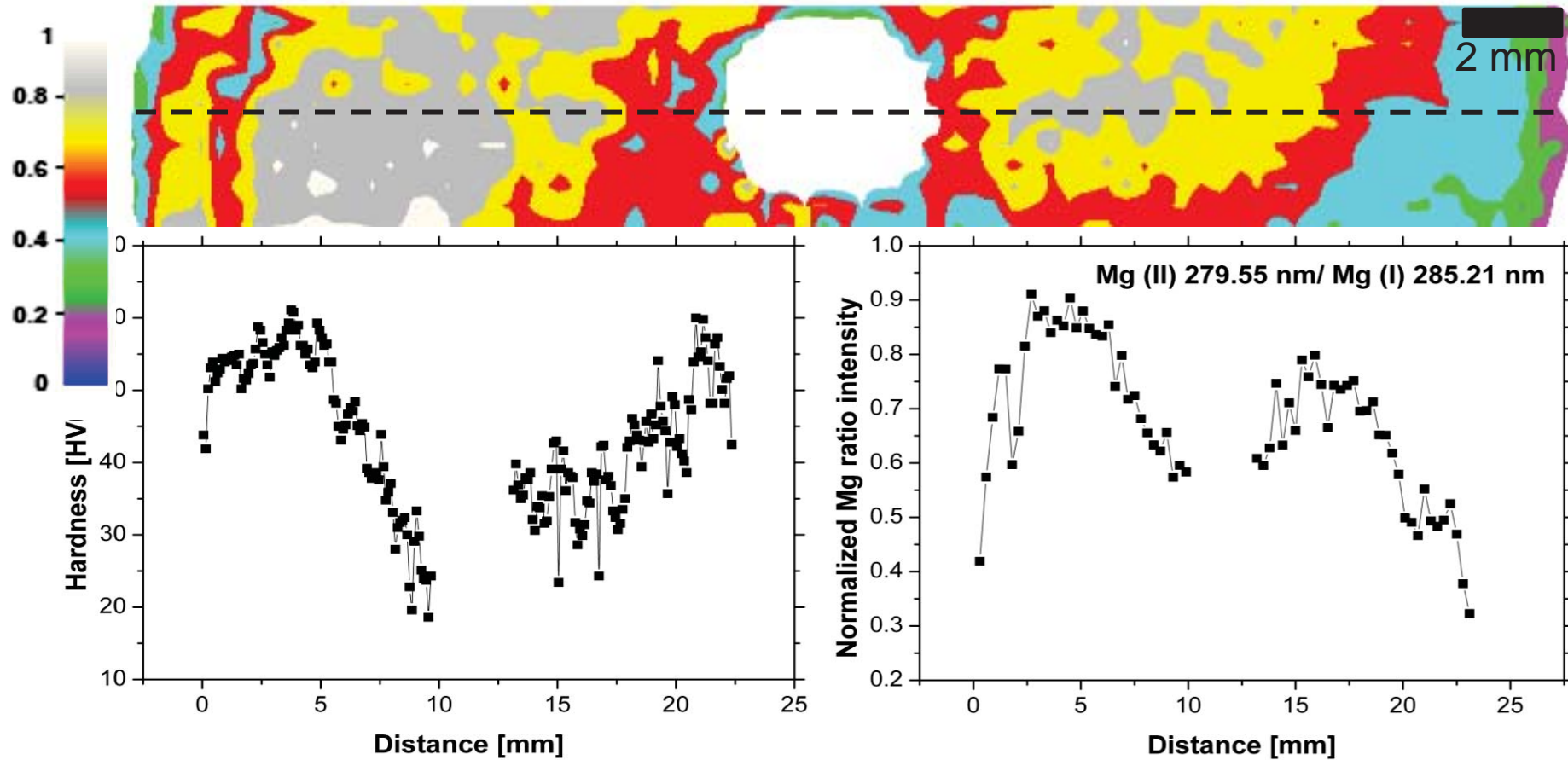


LIBS - fossil bear tooth



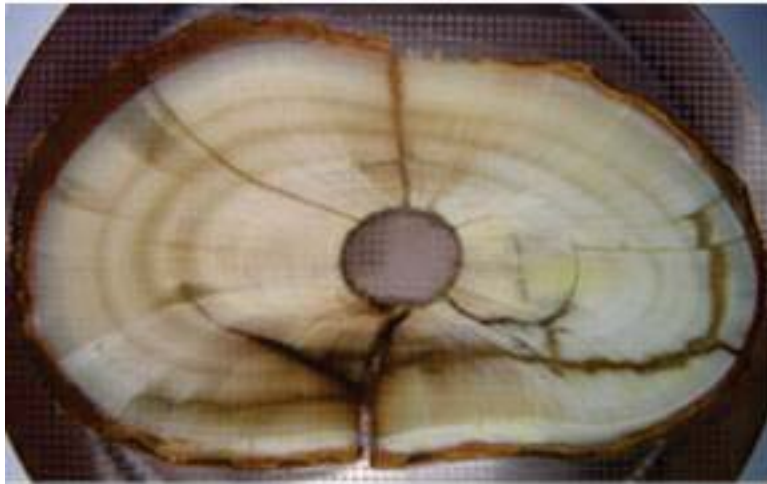
M. Galiová, J. Kaiser, F. Fortres, K. Novotný *et al.*: Multielemental analysis of prehistoric animal teeth by laser-induced breakdown spectroscopy and laser ablation inductively coupled plasma mass spectrometry. *Applied Optics* 49 (2010) C191-C199.

THE HARDNESS OF THE SAMPLE (CANINE TOOTH ROOT)

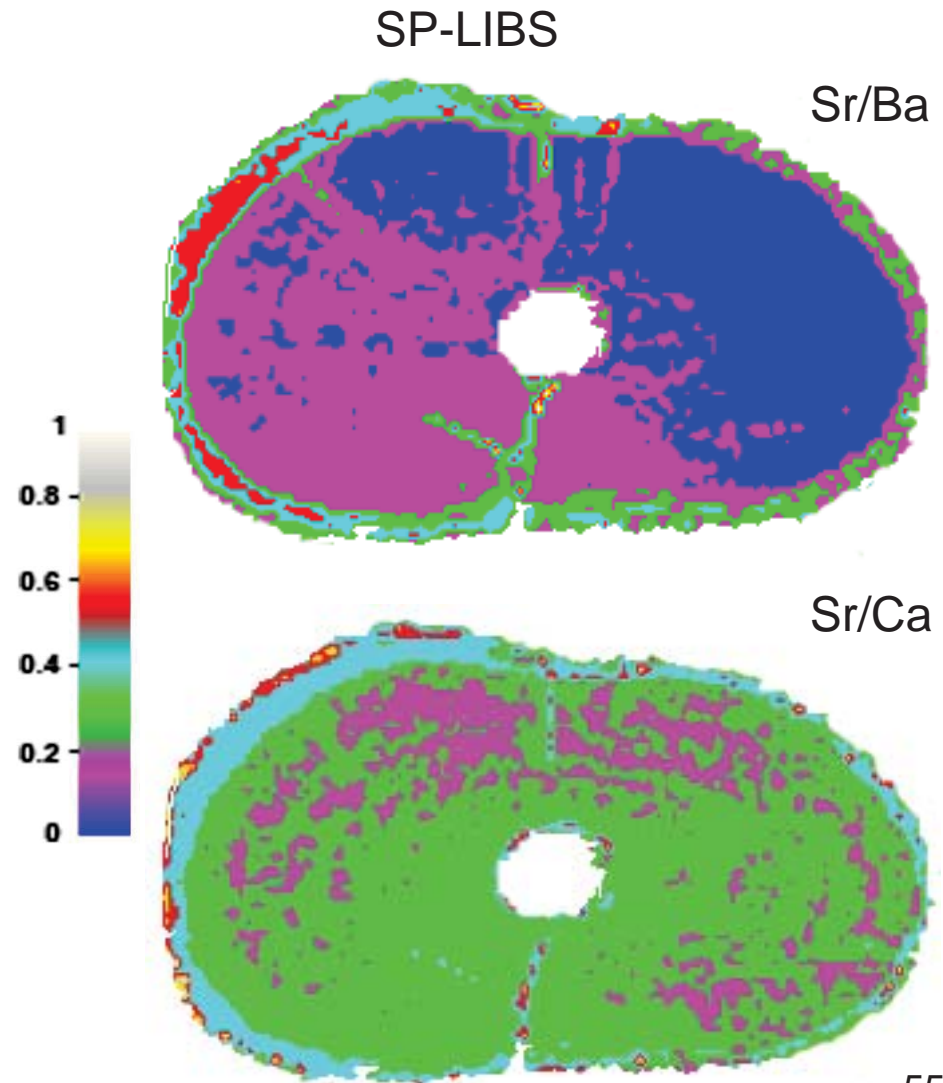


- ☛ The estimation of the sample hardness via magnesium ionic to atomic line intensity ratios is shown.
- ☛ The estimated hardness characteristic was proved by microhardness measurements.
- ☛ The Vickers test pattern was placed nearby the LIBS ablation craters for Mg detection.

LIBS - fossil bear tooth



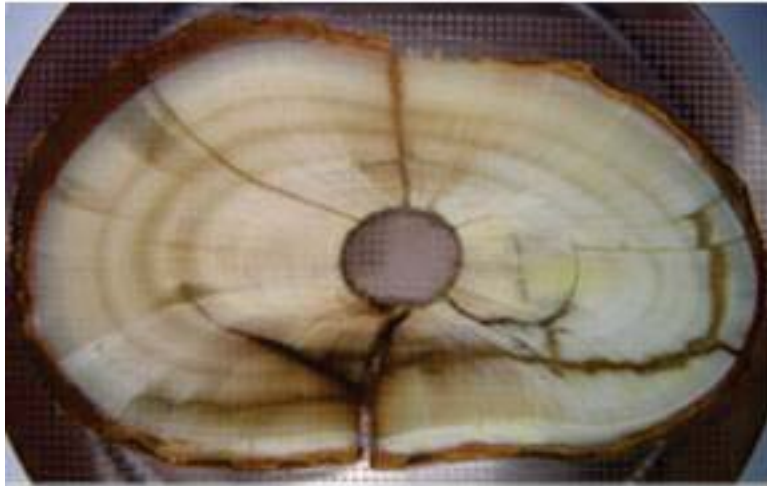
The seasonal fluctuations of the Sr/Ca and Sr/Ba detected by utilized laser-ablation based techniques (SP and DP LIBS and LA-ICP-MS) evidenced the migration of this bear between his hibernaculum's location and the place where the fossils were found.



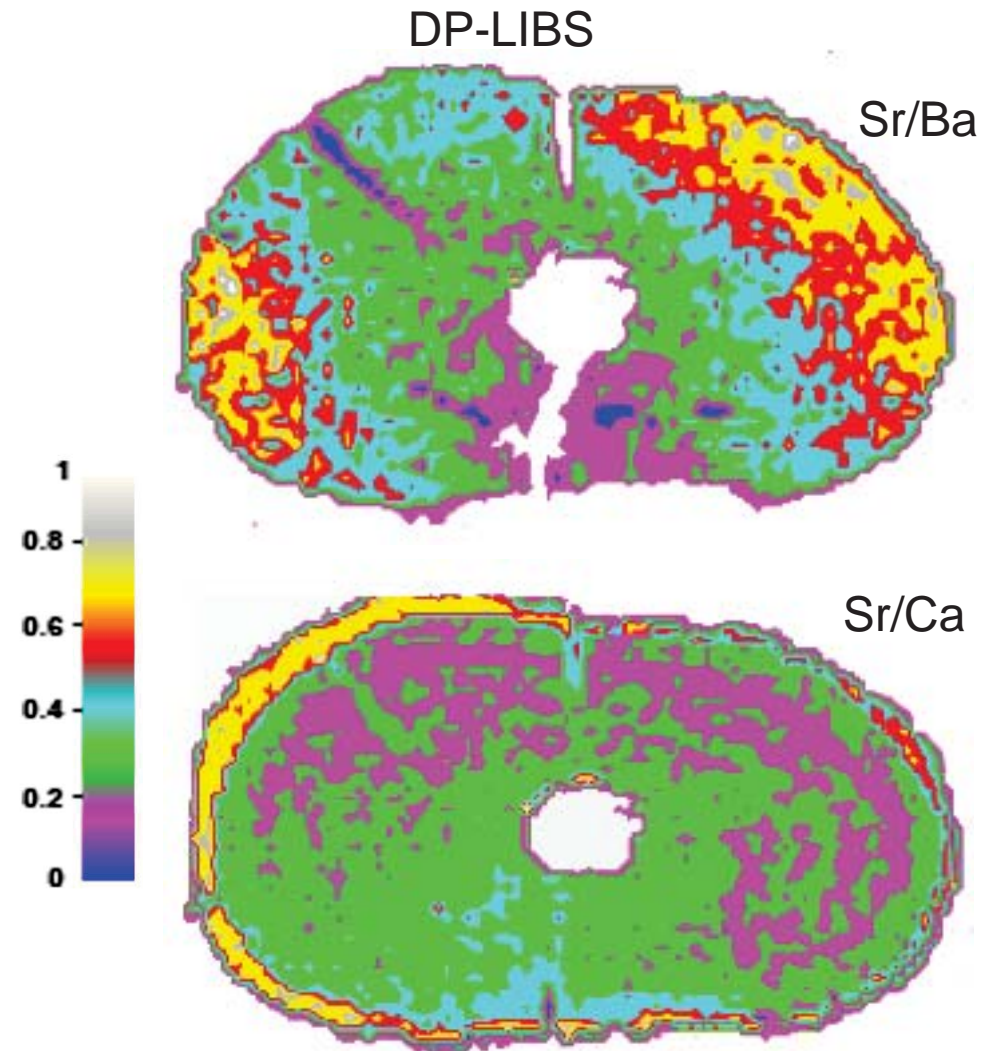
55

55

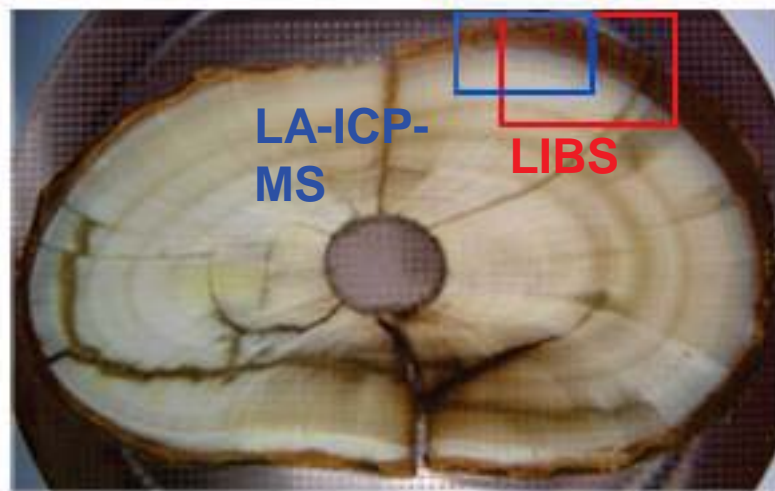
LIBS - fossil bear tooth



The dark areas on the sample are well correlated with the lower Sr/Ba Sr/Ca ratio in the map. They are rather related to the narrow winter strips.

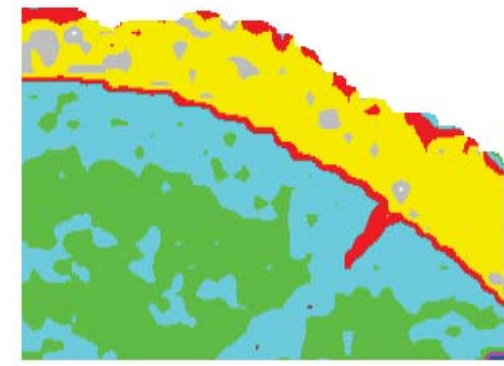
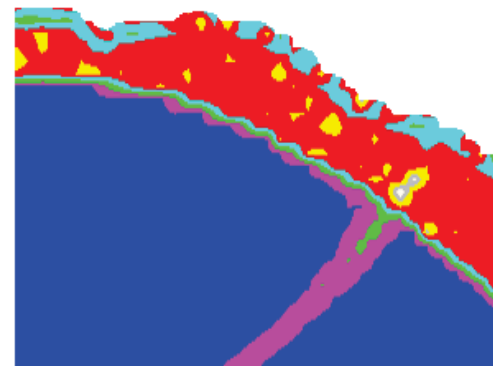


COMPARISON OF LIBS AND LA-ICP-MS MAPPING

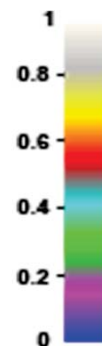


Ba/Ca

Sr/Ca

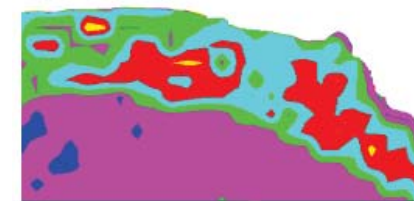


1 mm



$^{135}\text{Ba}/^{43}\text{Ca}$

$^{86}\text{Sr}/^{43}\text{Ca}$



100 μm

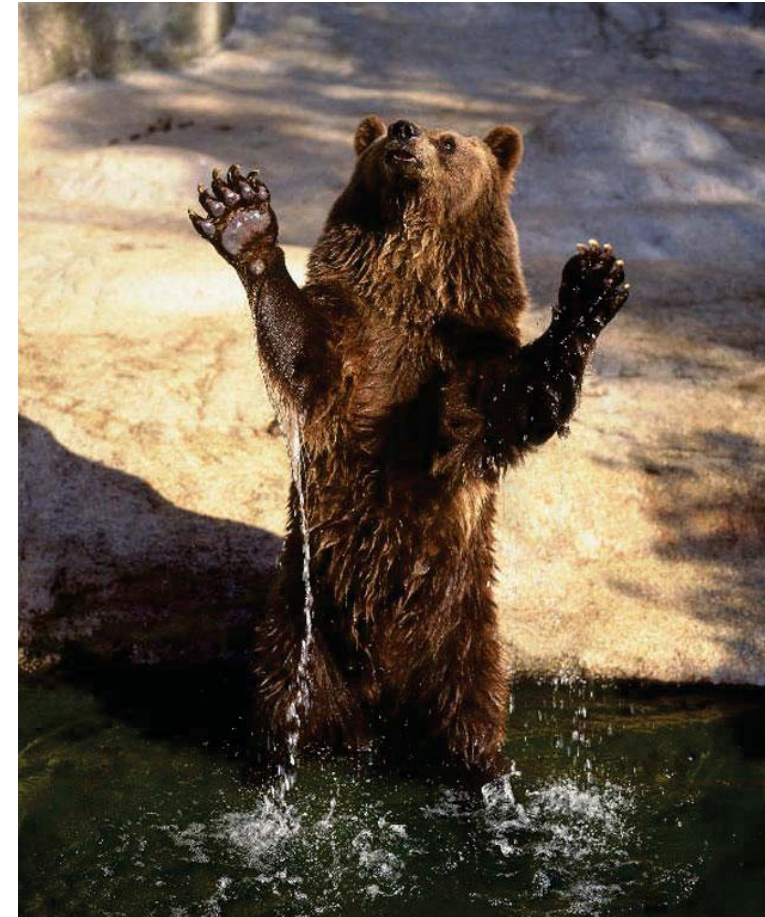
close to areas in the sample mapped by DP-LIBS and LA-ICP-MS comparable diameters of the ablation craters and spatial resolution

LIBS - fossil bear tooth, RESULTS

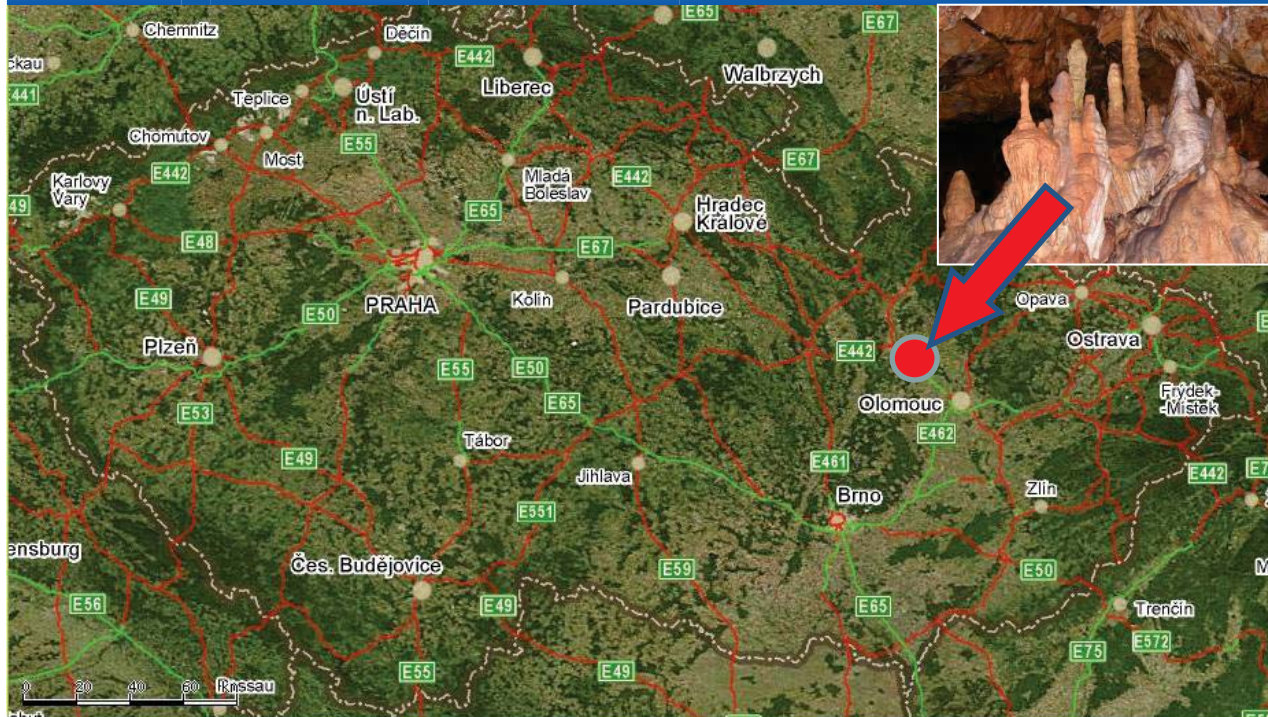


If the tooth is not very affected by diagenesis from the LIBS and LA-ICP-MS measurements it can be concluded that




- ❖ the bear consumed a plant food mainly in the hot seasons by the Sr/Ca increased ratio visible mainly in the LIBS scans,
- ❖ the bears migration is characteristic not only for the years seasons but also for different years which is visible by comparison of the Sr/Ba ratios in the particular wide strips from the outer to the inner part of the dentine in the LA-ICP-MS maps and by the Sr/Ba decrease observable in the LIBS scan,
- ❖ the bear probably changed its living territory in one direction.



LIBS - fossil snake vertebra

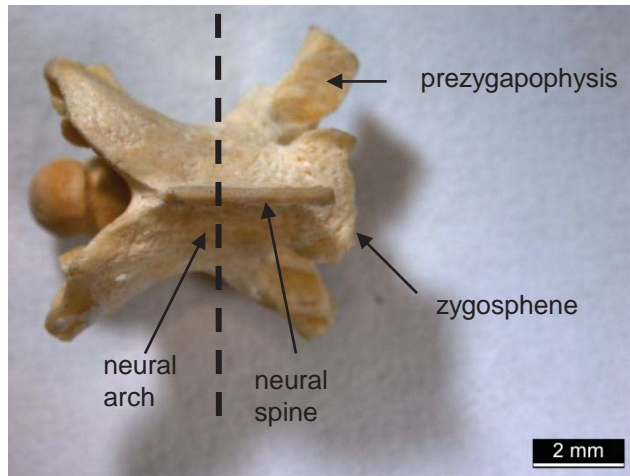


~ 1 Ma

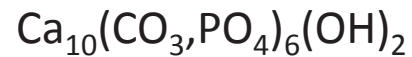
-  Material of fossil snakes comes from the Mladeč Caves site near the Olomouc city.
-  Samples come from the deposits of the talus cone in the „Dóm mrtvých“ being excavated in 1958-1959 (excavation no. II).
-  The palaeontological research documents the Early Pleistocene (Early Biharian) age of the vertebrate assemblage. Snake fauna shows on the warm interglacial environment. Deposits of the excavation no. II are correlated with waalian interglacial, possibly the end of the waalian interglacial (Ivanov 1993, 2007).

59

LIBS - fossil snake vertebra



Mineral component of the bone: carbonised hydroxy-apatite



The Ca/P ratio is 2:1 in normal bone.

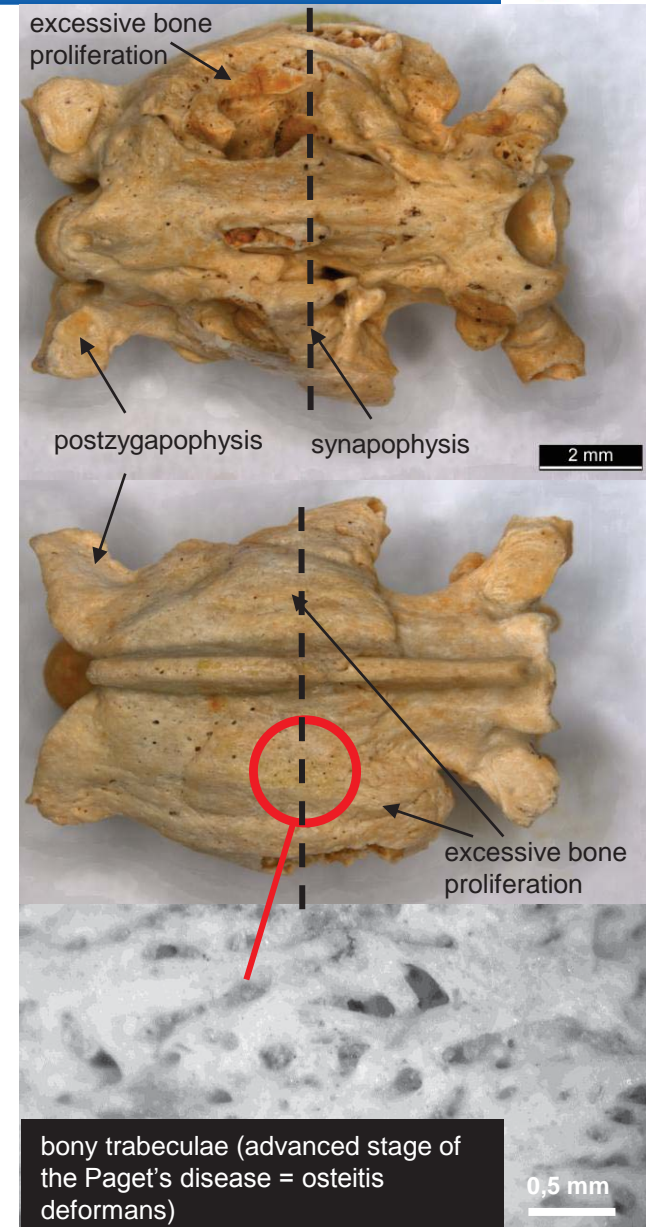
Natrix natrix specimen from the Mladeč Caves, Ealpy Pleistocene (Early Biharian).

Healthy vertebra:

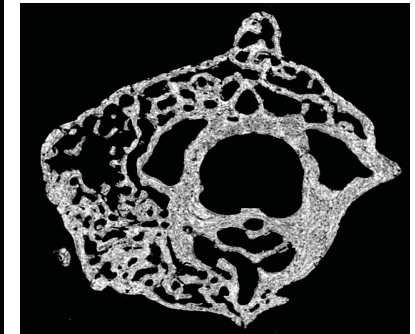
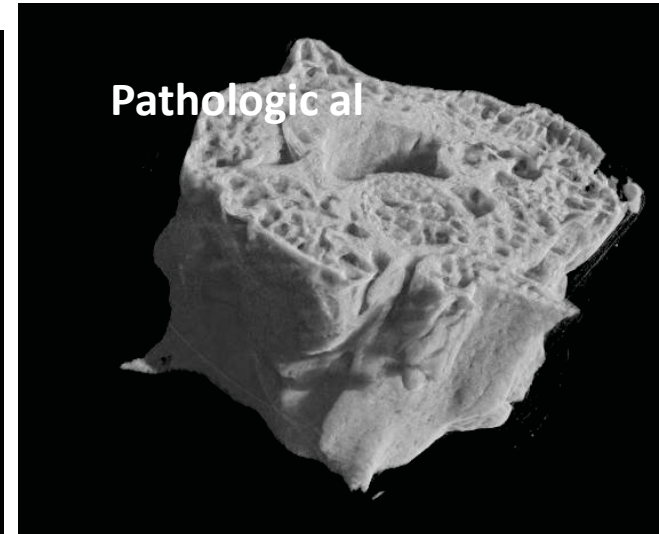
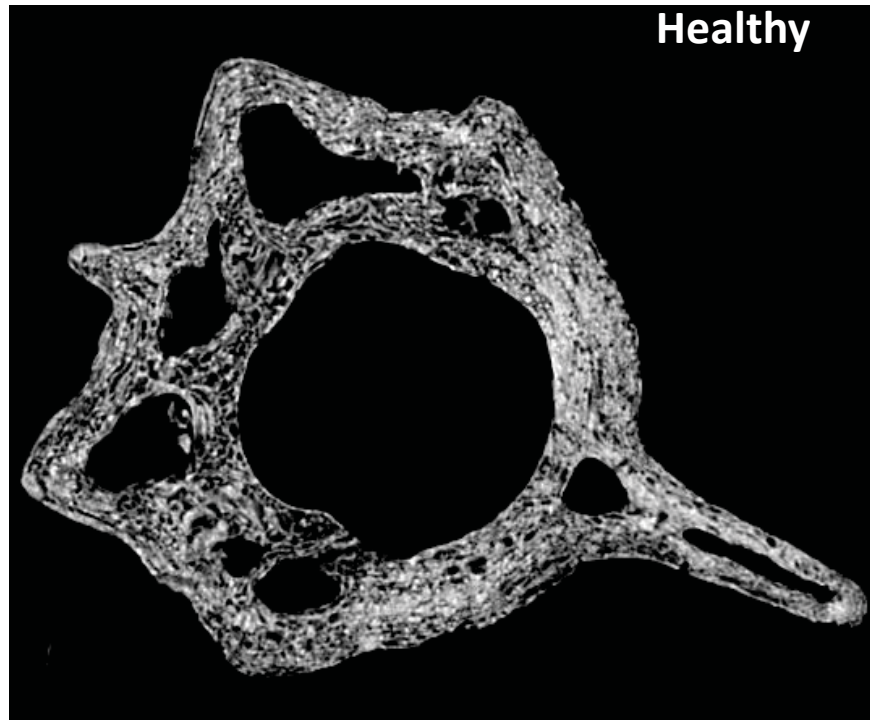
A middle trunk vertebra. A section cuts the vertebra through the anterior portion of the neural arch, zygosphene and prezygapophyses. In ventro-lateral direction the section cuts the area of synapophyses.

Pathological vertebra:

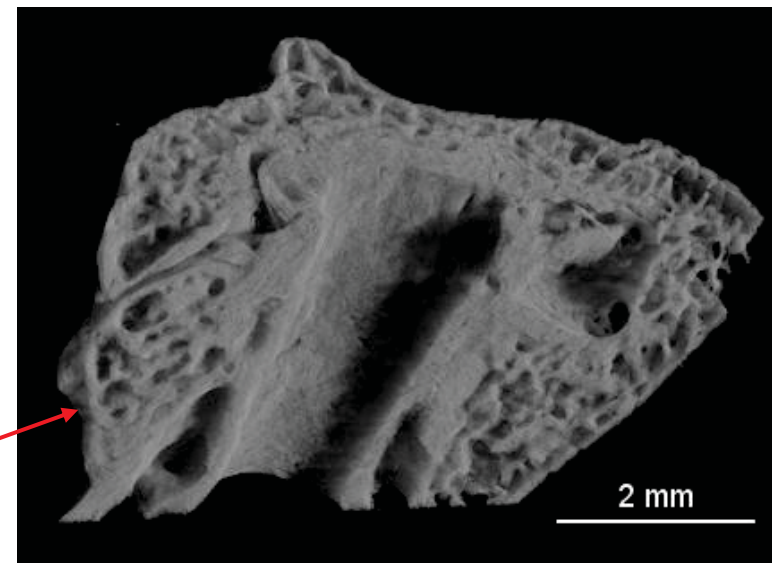
Two fused posterior trunk vertebrae. A section cuts the posteriorly situated vertebra through the anterior part of the neural arch and the right synapophyse. Pathologic development with thickened bony trabeculae is remarkable mainly at the right side of the vertebra.



Fossil snake vertebra – μCT at ELETTRA Trieste




There are several **stages of osteitis deformans** (Paget's disease): 1 – resorption phase (osteolytic phase); 2 - the mixed osteolytic and osteoblastic phase; **3 – osteosclerotic phase.**



LIBS - fossil snake vertebra



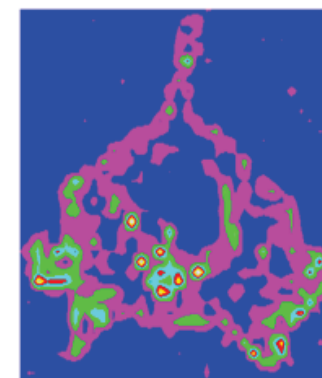
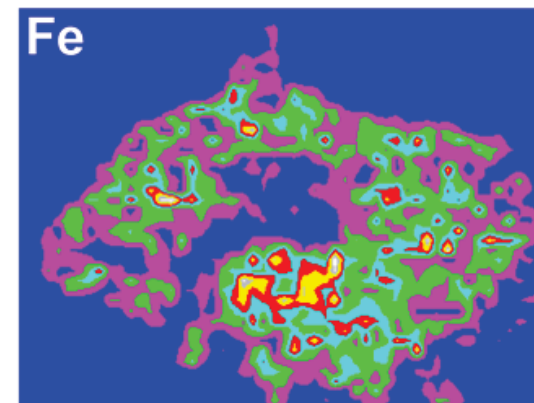
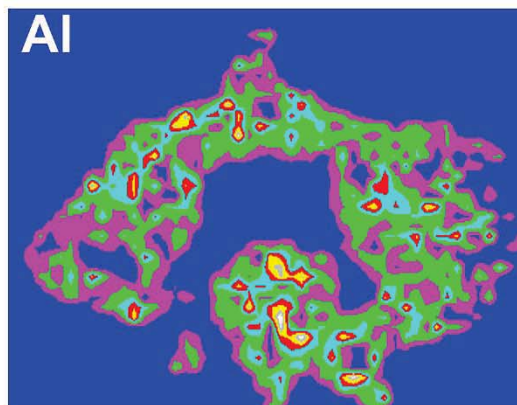
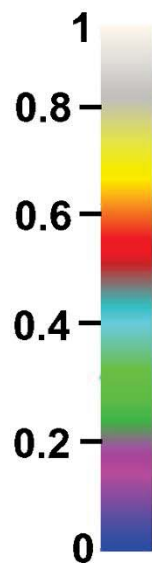
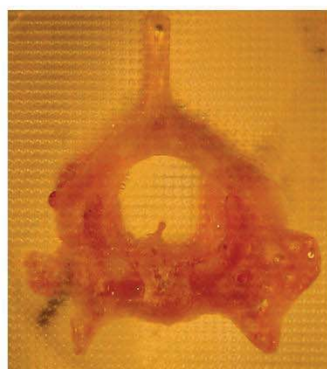
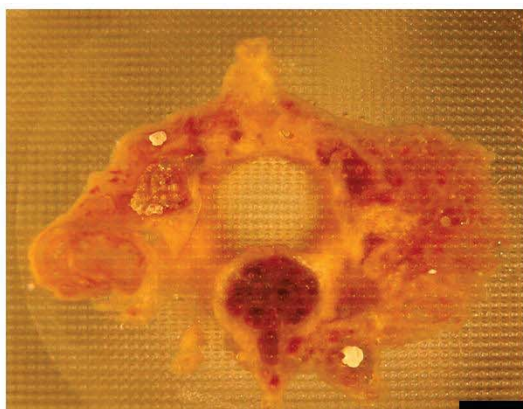
 **ICP-MS spectrometer** –
Agilent 7500 CE (Agilent,
Japan)

Content [mg/kg]	pathological	healthy
Mg	1226.71	1025.45
Al	3399.84	1798.90
Si	5287.27	1652.69
P	204503.11	209780.44
Ca	331288.82	338822.36
Fe	2812.89	1495.51
Zn	1177.80	1212.57
Sr	661.72	597.80
Ba	319.10	281.74

LIBS - fossil snake vertebra



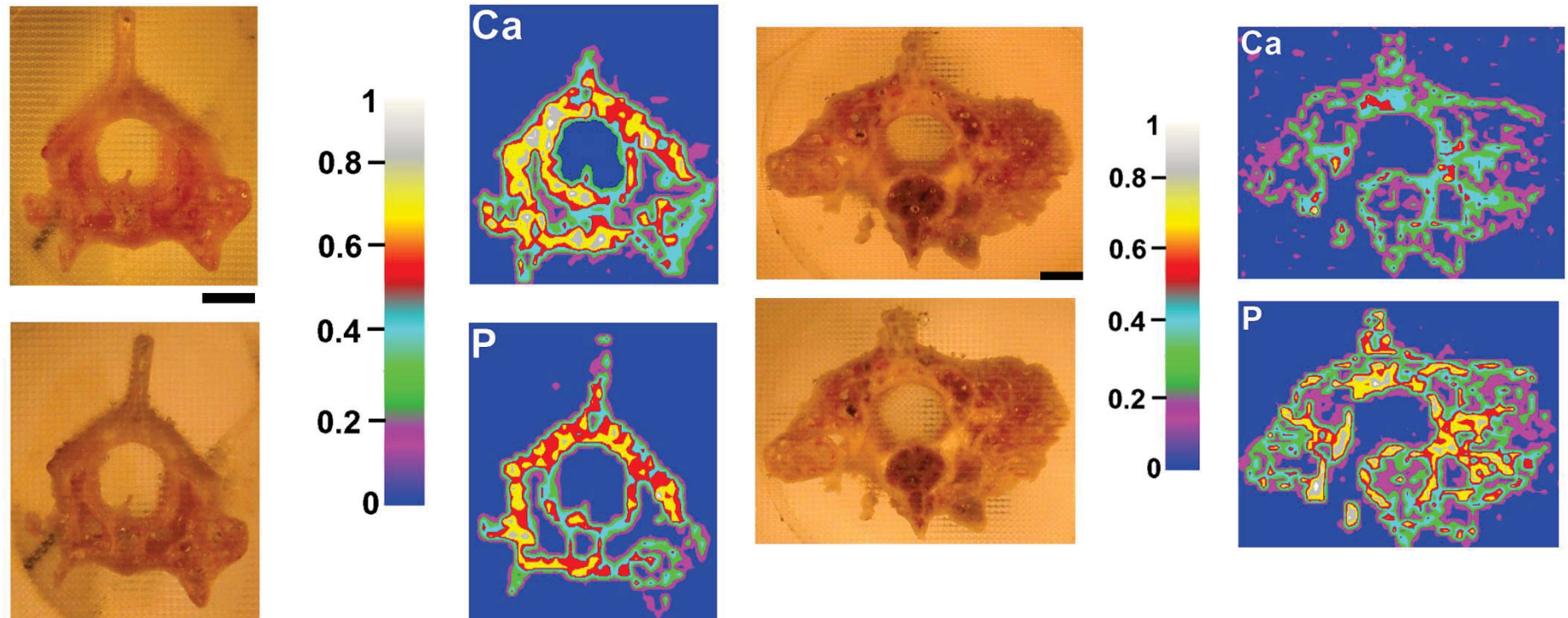
Pathological



Healthy

M. Galiová, J. Kaiser, K. Novotný, *et al.*: Investigation of the *osteitis deformans* phases in snake vertebrae by double-pulse laser induced breakdown spectroscopy. *Analytical Bioanalytical Chemistry*, 2010, 398, p. 1095-1107.

LIBS - fossil snake vertebra



1. New bony trabeculae in fossil vertebra show on the **highly increased representation of phosphorus $Ca/P < 1$ in pathological bony tissue** indicating the later stage of the *osteitis deformans* (Paget's disease).
2. Elemental mapping of pathologic bony tissue could be a powerful tool for **considering the *osteitis deformans* phases in fossil vertebrates.**

LIBS of artworks



LIBS mapping is used since 1990s for analysis or cleaning of the artworks. As an example, Klein *et al.** reported in 1999 on on-line control of laser cleaning of sandstone and stained glass. A combination of a KrF excimer laser and LIBS was used. The spectroscopic study of the plasma emission was used to determine the elemental composition of the crust and the underlying material. The on-line implementation of LIBS to the cleaning process provided important information about the optimal cleaning parameters of artworks from glass and stone in order to avoid over-cleaning.

*S. Klein, T. Stratoudaki, V. Zafiropulos, J. Hildenhagen, K. Dickmann, T. Lehmkuhl, *Appl. Phys. A-Mater. Sci. Process.* 69 (1999) 441-444.

LIBS of artworks



Most recently, a multi-technique (X-ray diffraction - XRD, Scanning electron microscopy - SEM, Fourier transform infrared spectroscopy - FT-IR, Differential scanning calorimetry - DSC, Thermogravimetry - TGA, and LIBS) approach was utilized by Şerifaki *et al.** for the characterization of materials used in the execution of historic oil paintings in the 19th century church in Ayvalık/Turkey.

LIBS spectral measurements indicated that the pigments used in wall paintings were red chrome, green earth and iron oxide.

*K. Serifaki, H. Boke, S. Yalcin, B. Ipekoglu, Mater. Charact. 60 (2009) 303-311.

Environmental applications

PLANT SAMPLES - Motivation



- Several transition metals (Cu, Fe, Zn etc.) are essential for plants just like for most other organisms.



- However, they can easily be toxic when present in excess.



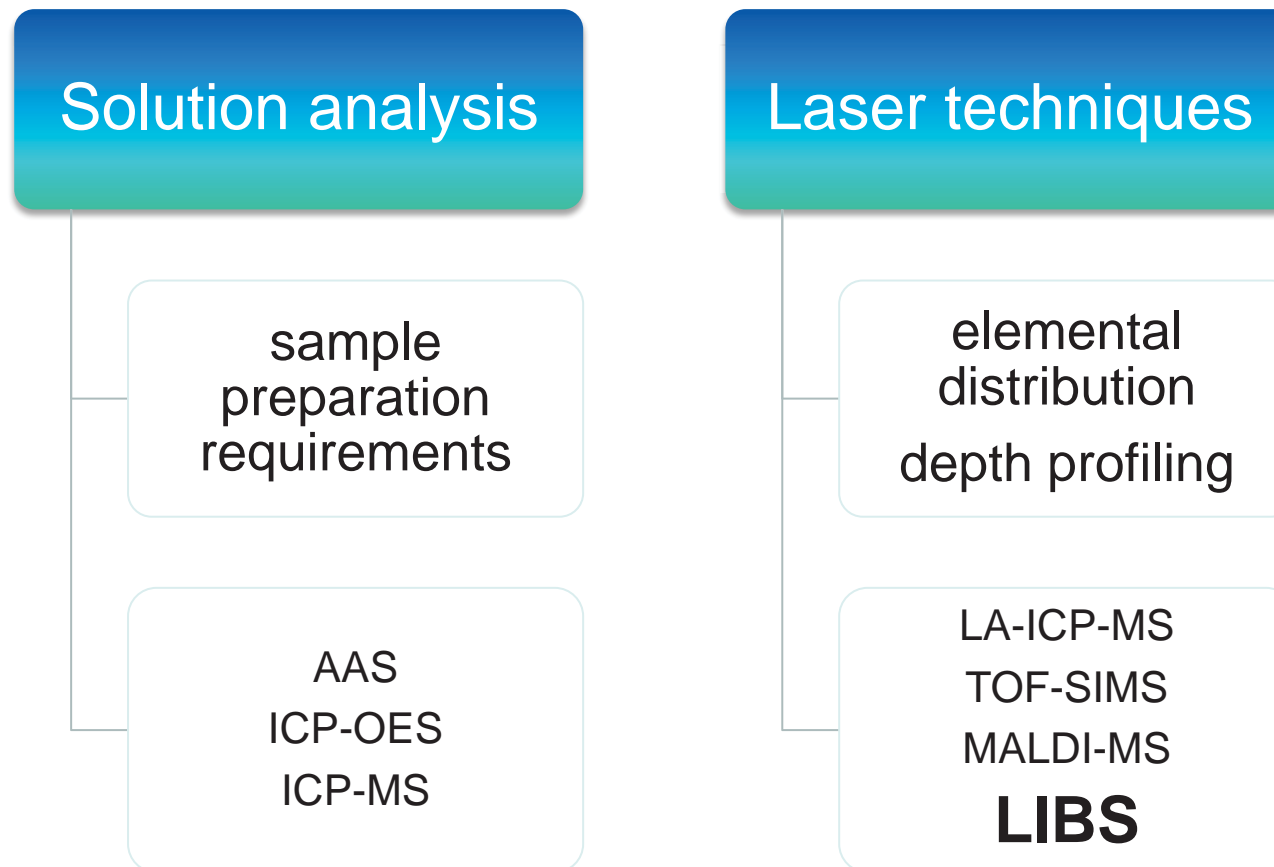
- In the course of industrialization emissions of metals have risen tremendously and significantly exceed those from natural sources for practically all metals.

PLANT SAMPLES - Motivation










- Beside the transition metals, also the circulation of toxic metals (e.g. Cd, Pb, Hg etc.) through soil, water and air has greatly increased.
- Investigation of influence of metals on an organism as well as of their transport and of maintaining of their level inside a cell is thus very topical.

Methods of plant elemental composition determination

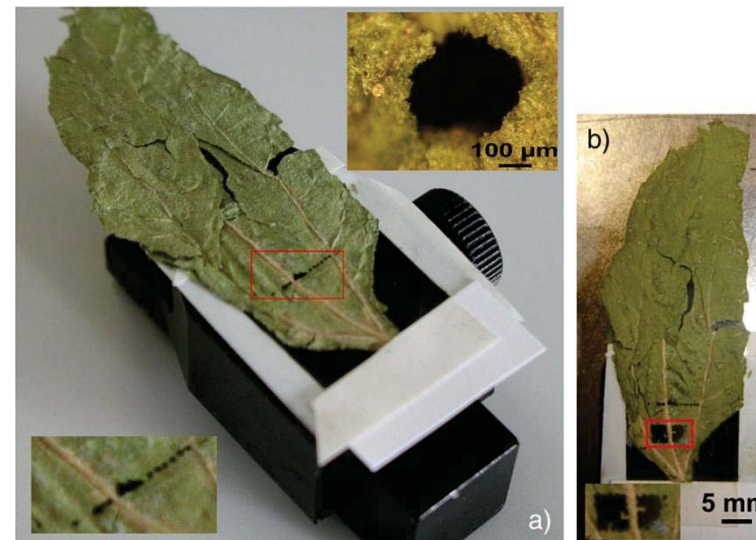
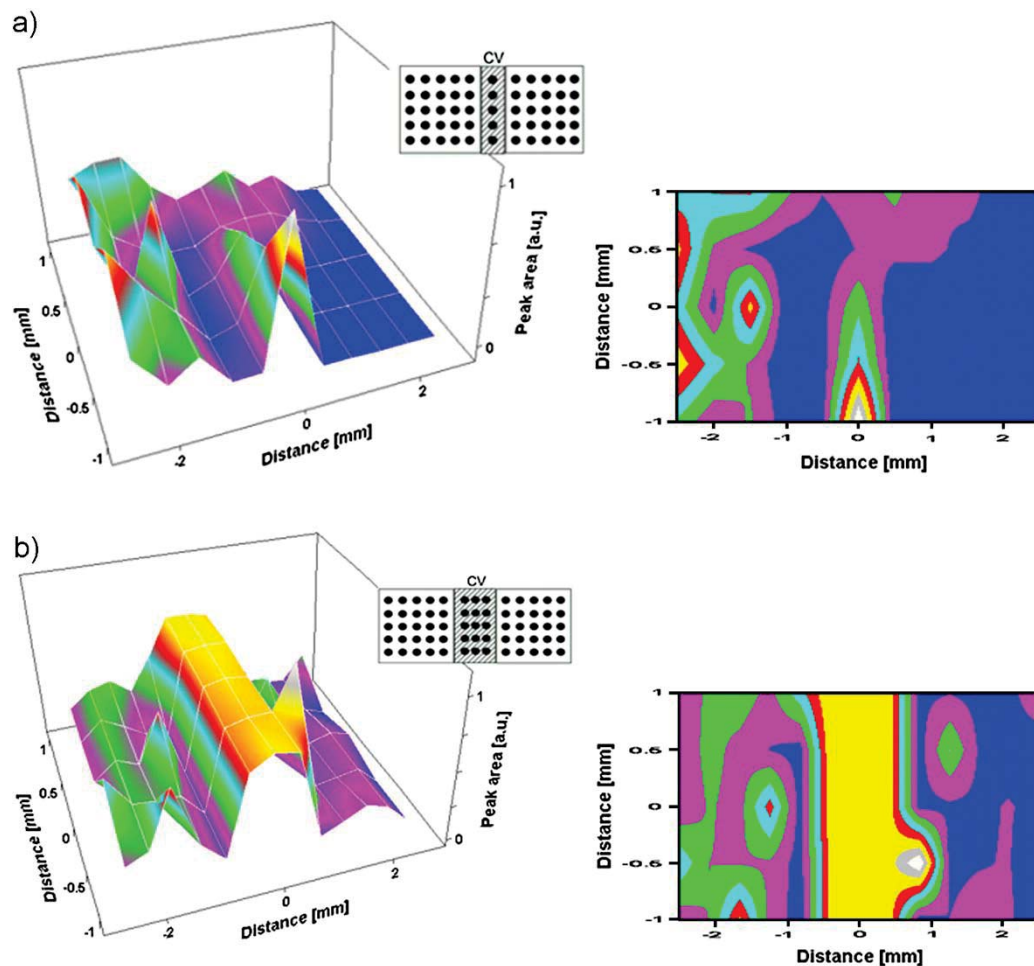


Investigated samples



Sample		Investigated part	Monitored elements	Methods			
				LIBS	LA-ICP-MS	(Dual-Energy) μ radiography	(Dual-Energy) μ tomography
<i>Helianthus Annuus</i>		leaves, roots, stems	Pb, Cd, Mg, K, Ag, Cu	X	X	X	X
<i>Zea mays</i>		leaves, roots, stems	Pb, S, Mg, Fe	X	X	X	X
<i>Cornus stolonifera</i>		leaves	Fe	X			
<i>Lactuca sativa L.</i>		leaves	Pb, Mg	X			
<i>Phaseolus Vulgaris</i>		leaves	Pb, Cd, Cu			X	
<i>Diplotaxis eruroides</i>		roots	Pb, Cd, Cu				X
<i>Pisum Sativum</i>		leaves	S			X	
<i>Hedera helix</i>		leaves	Mg			X	

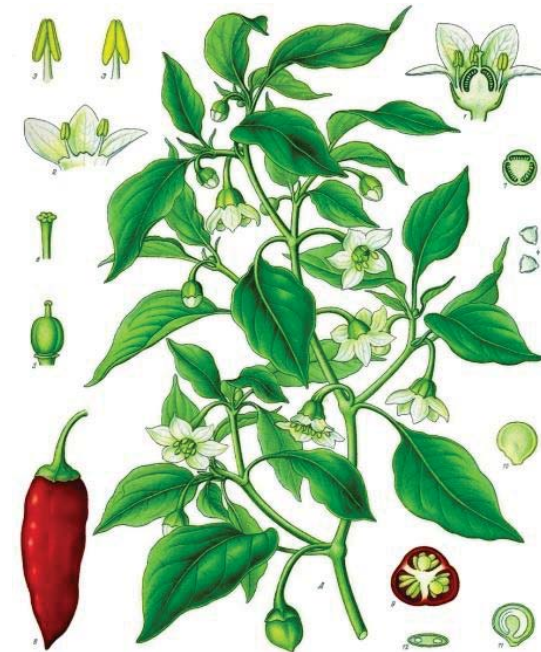
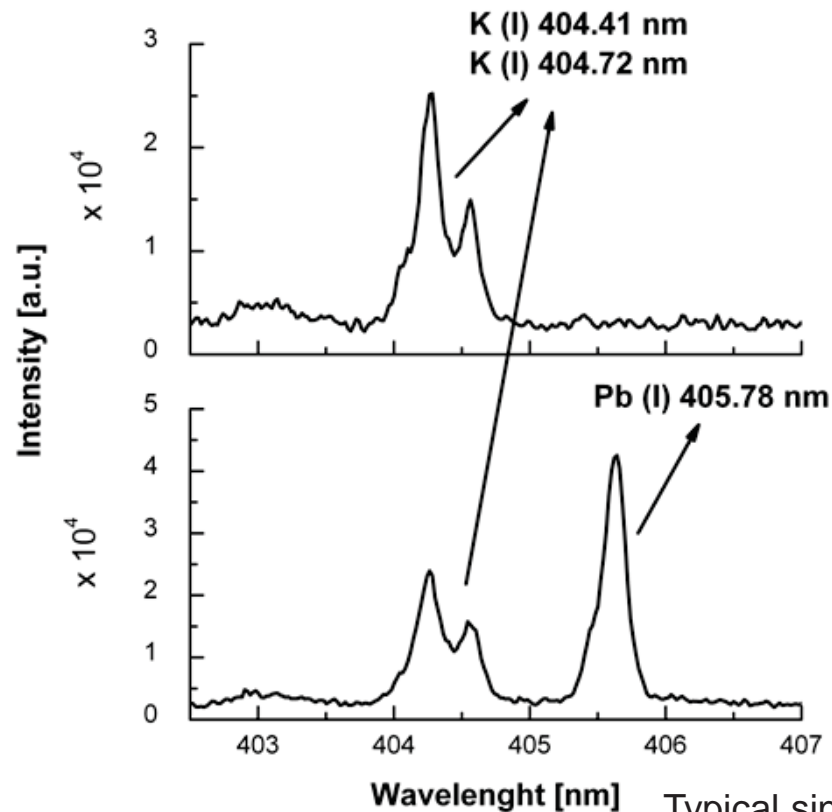
Helianthus annuus leaf



Map of the lead pollutant in a) 5 mM and b) 10 mM PbAc treated sample together with the schematics of the ablation craters distribution on the sample (CV— central vein of the leaf sample).

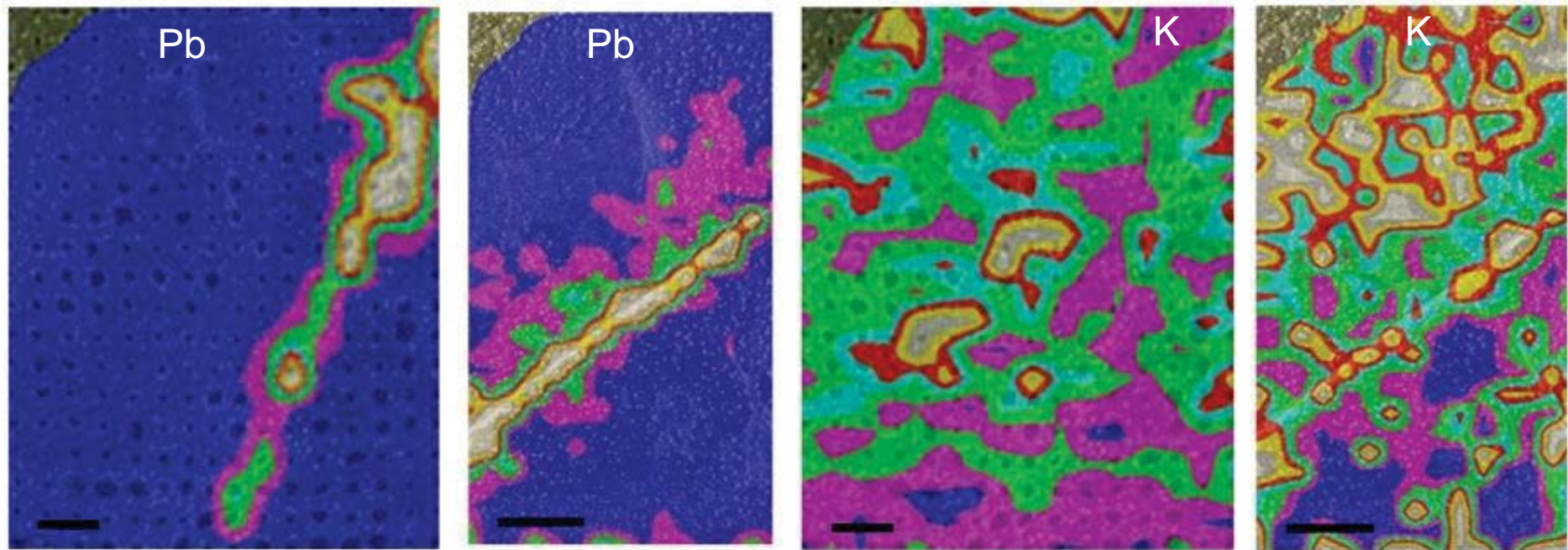
J. Kaiser, M. Galiová, K. Novotný, *et al.*: Mapping of the heavy-metal pollutants in plant tissues by Laser-Induced Breakdown Spectroscopy, *Spectrochimica Acta Part B* 62 71 (2007) 1597–1605.

Sample analysis



Typical single-shot LIBS spectra taken at two different position on the leaf of *Capsicum annuum* sample. The 405.78 nm Pb (I), and 404.41 nm, 404.72 K (I) lines used in the analysis are clearly visible. The spectra were obtained using the following experimental conditions: pulse energy (at the sample surface) 10 mJ, gating pulse for the ICCD detector – 1 μ s after the Q-switch signal and the integration time 10 μ s. For the mapping, the selected LIBS spectra were processed in the following way: background was subtracted (for each shot) and the area under the selected peak (for appropriate chemical element) was calculated.

Sample analysis

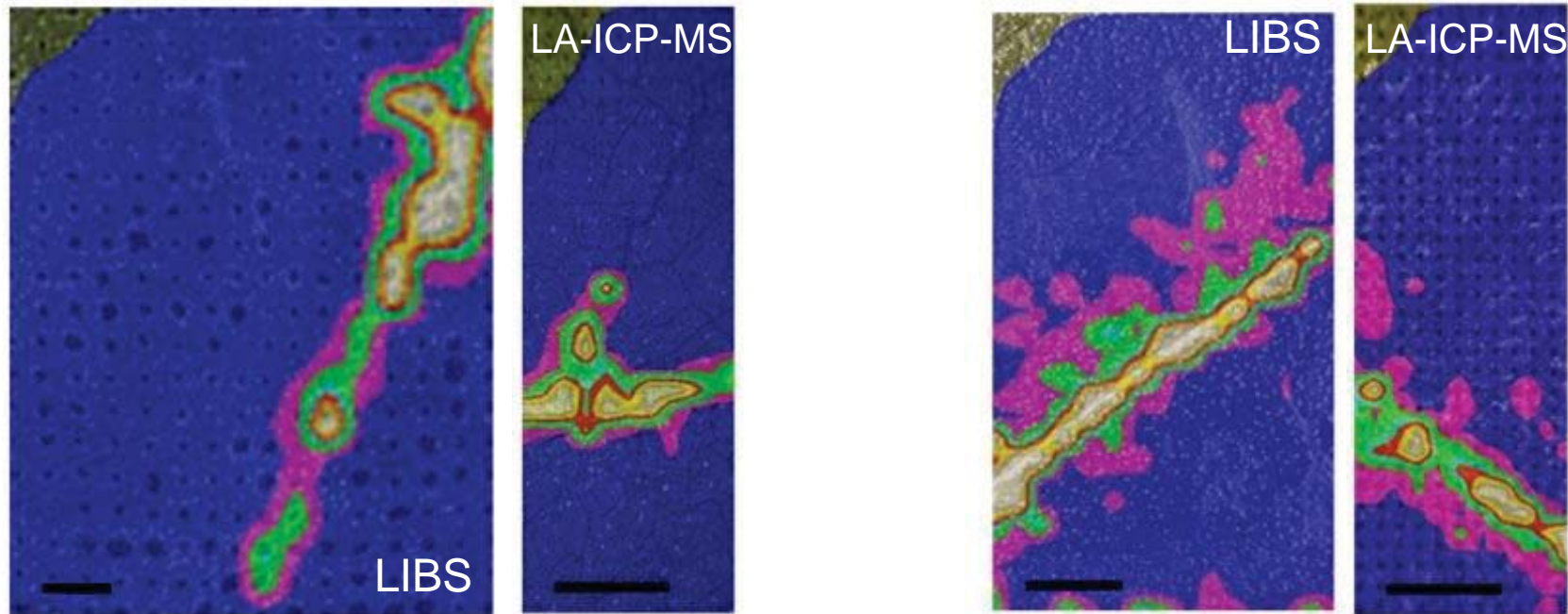


The maps of Pb and K obtained from the studied area of the 2 days 10 mM $\text{Pb}(\text{NO}_3)_2$ treated *Capsicum annum* leaf sample by LIBS analyses. The Pb distribution in fresh (frozen) and dried samples are visualized.

The maps are shown together with the photos of the samples. In the upper left corners, the part of the photograph is uncovered.

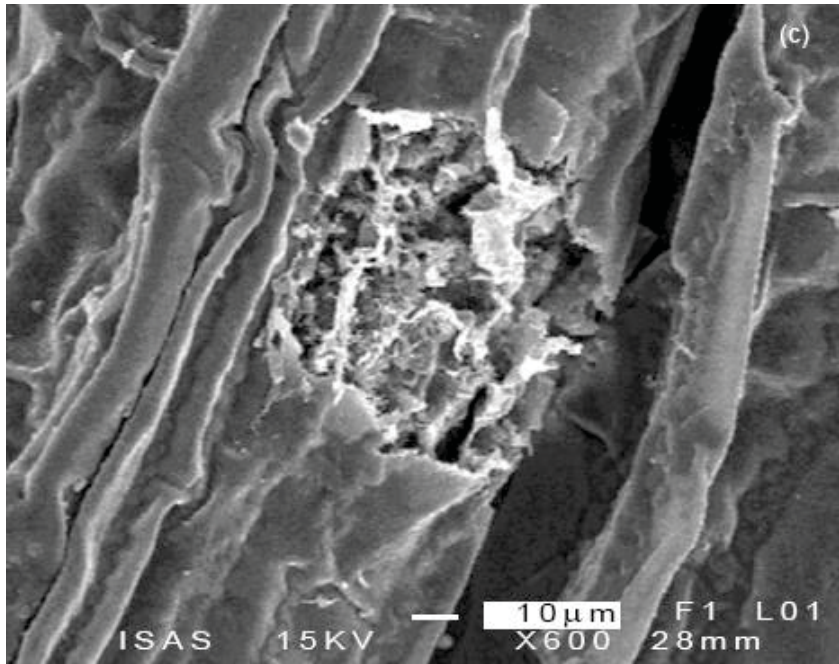
Lead is accumulated mainly in the central vein and the surrounding area of the leaf. The length of the bar is 1 mm.

LIBS versus LA-ICP-MS

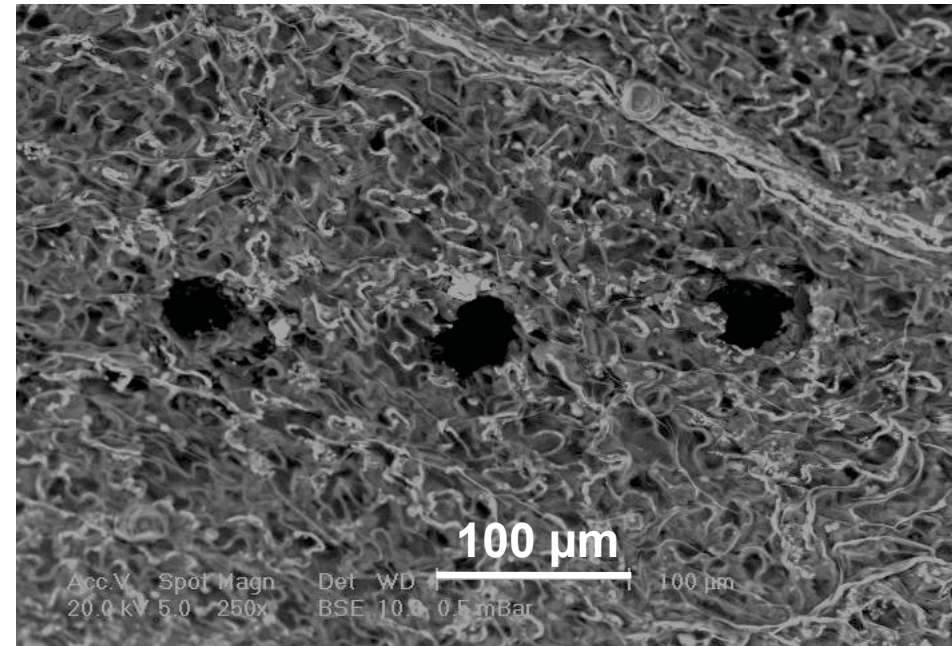


Comparison of the Pb maps obtained from the studied area of the 2 days 10 mM $\text{Pb}(\text{NO}_3)_2$ treated *Capsicum annuum* leaf sample by LIBS and LA-ICP-MS analyses. The LIBS and LA-ICP-MS ablation patterns had a spacing of 500 μm and 200 μm , respectively. The diameter of ablation craters was $\sim 200 \mu\text{m}$ for LIBS and $\sim 100 \mu\text{m}$ for LA-ICP-MS. The length of the bar is 1 mm.

fs- and short wavelength LIBS



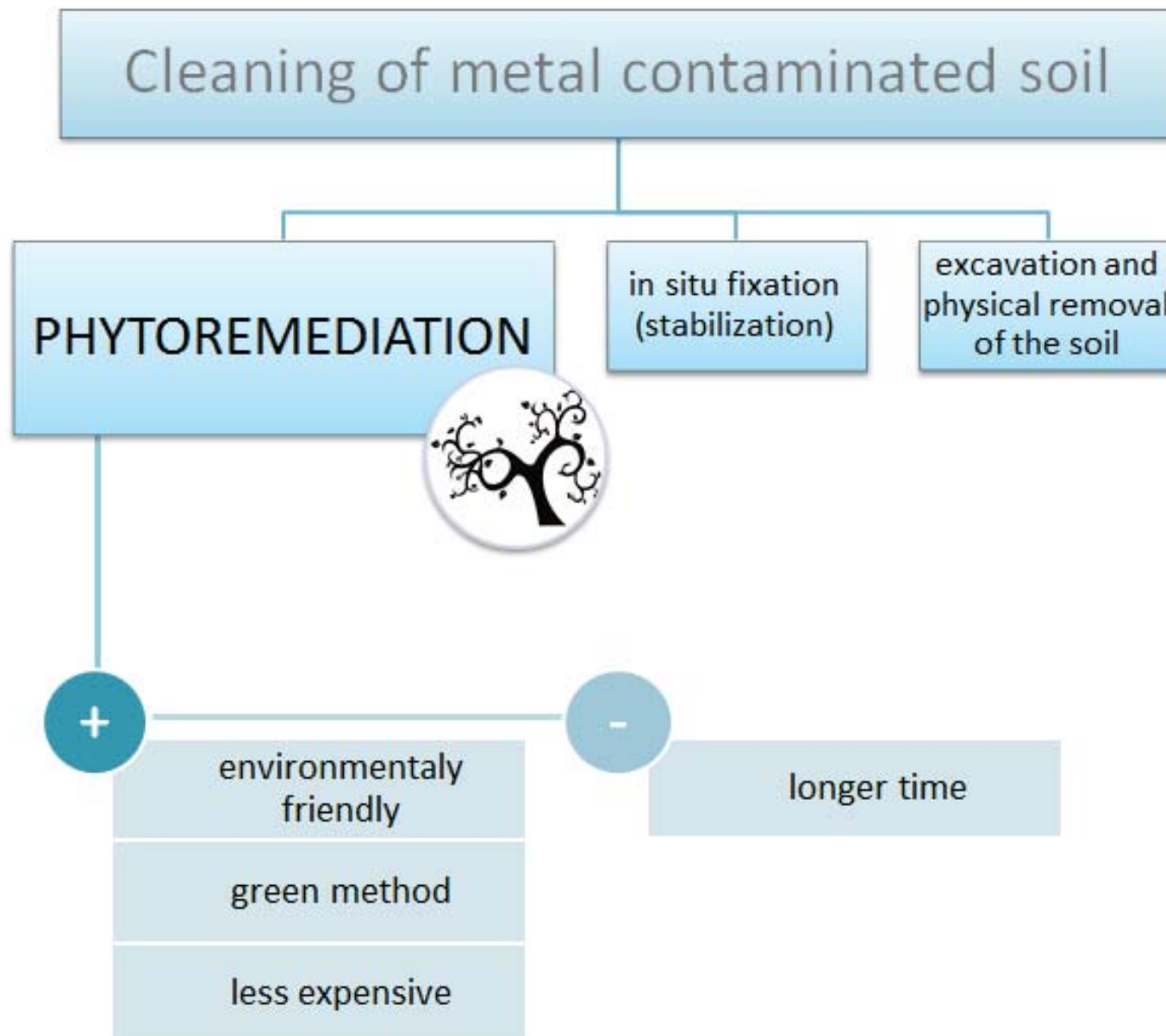
fs- LIBS: image of ablated spot obtained with an electron microscope*



Ablation laser: capillary-discharge based soft X-ray laser, wavelength: 46.9 nm, pulse duration ~2 ns, energy/pulse ~0.3 mJ. Image of ablated spot obtained with an electron microscope.

*SAMEK, O. *et al.*: Laser. Phys. Lett. 3, 21-26, (2006)

Phytoremediation



Plants useful for heavy-metal phytoremediation

resistant
strong tolerance
effective plant-transport mechanisms
high accumulation
high biomass
fast growth

- *Zea mays*
- *Helianthus annuus*
- *Viola lutea*
- *Thlaspi caerulescens*
- *Phaseolus vulgaris*

HERBS



- *Betula pendula*
- *Alnus glutinosa*
- *Salix viminalis*
- *Pinus contorta*
- *Populus tremula*

TREES



Trees in phytoremediation



- sufficient accumulation
- sufficient tolerance
- high shoot and aerial biomass
- stabilization - decrease a risk of air and water erosion
- in land where it is uneconomic to use other method
- where is no time pressure

Samples



Samples from naturally growing trees

Pinus sylvestris

Picea abies

Betula pendula

Populus tremula



Laboratory cultivated twigs

Picea abies

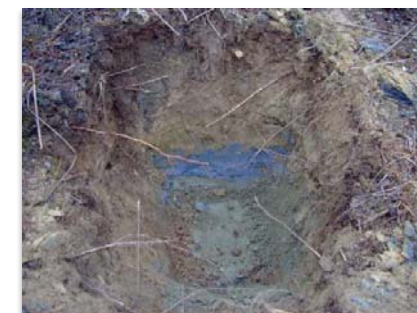
Phytoremediation



Samples from naturally growing trees

- recultivated sludge bed in locality **Smolník (Slovakia)**
- historical Cu-mining area
- exploited from the 14th century to 1990
- the mine was definitively closed in 1990-1994
- sludge bed remediation process was started in 1989
- overlapped by mould with sawdust and planted by birch and pine trees

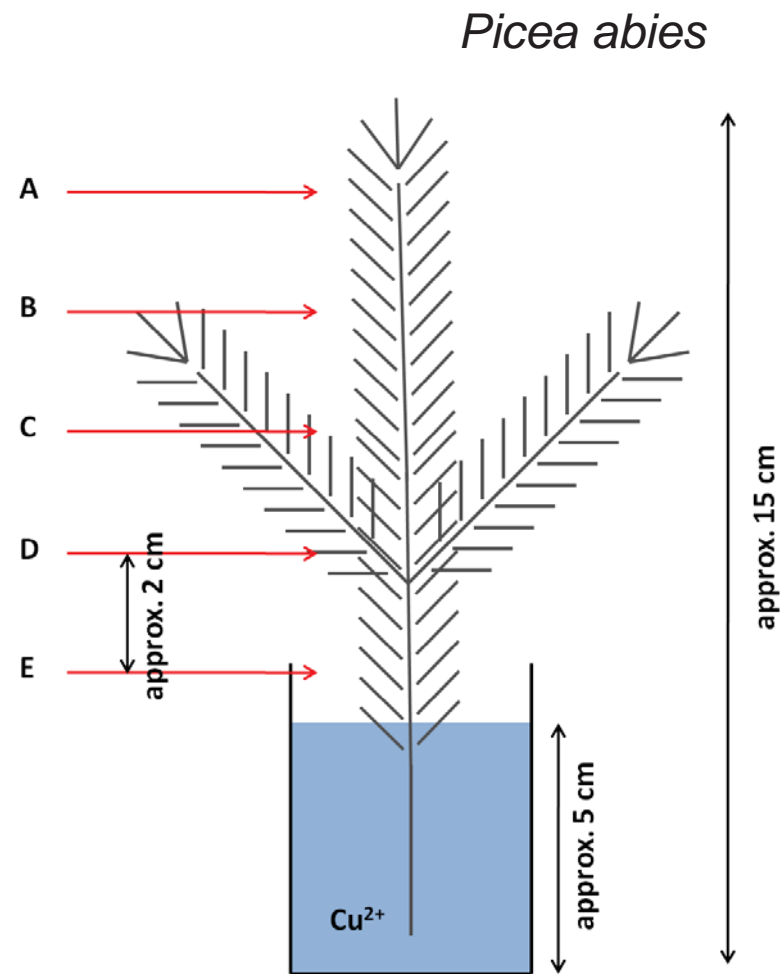
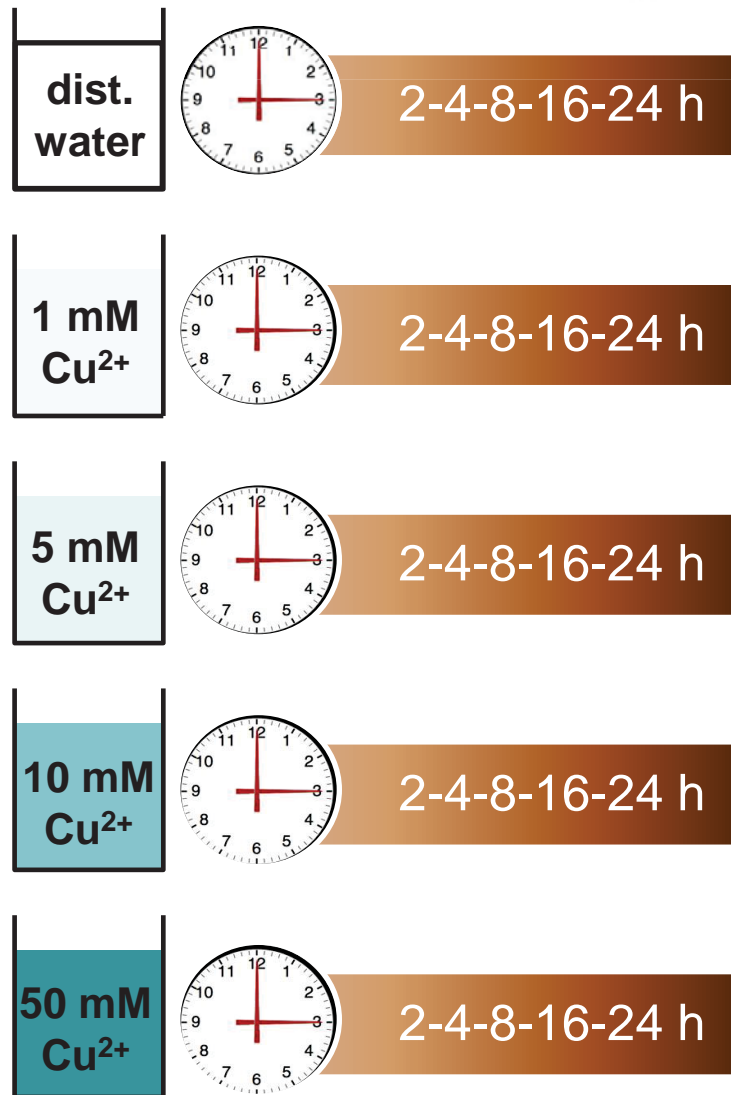
Cu, Ca



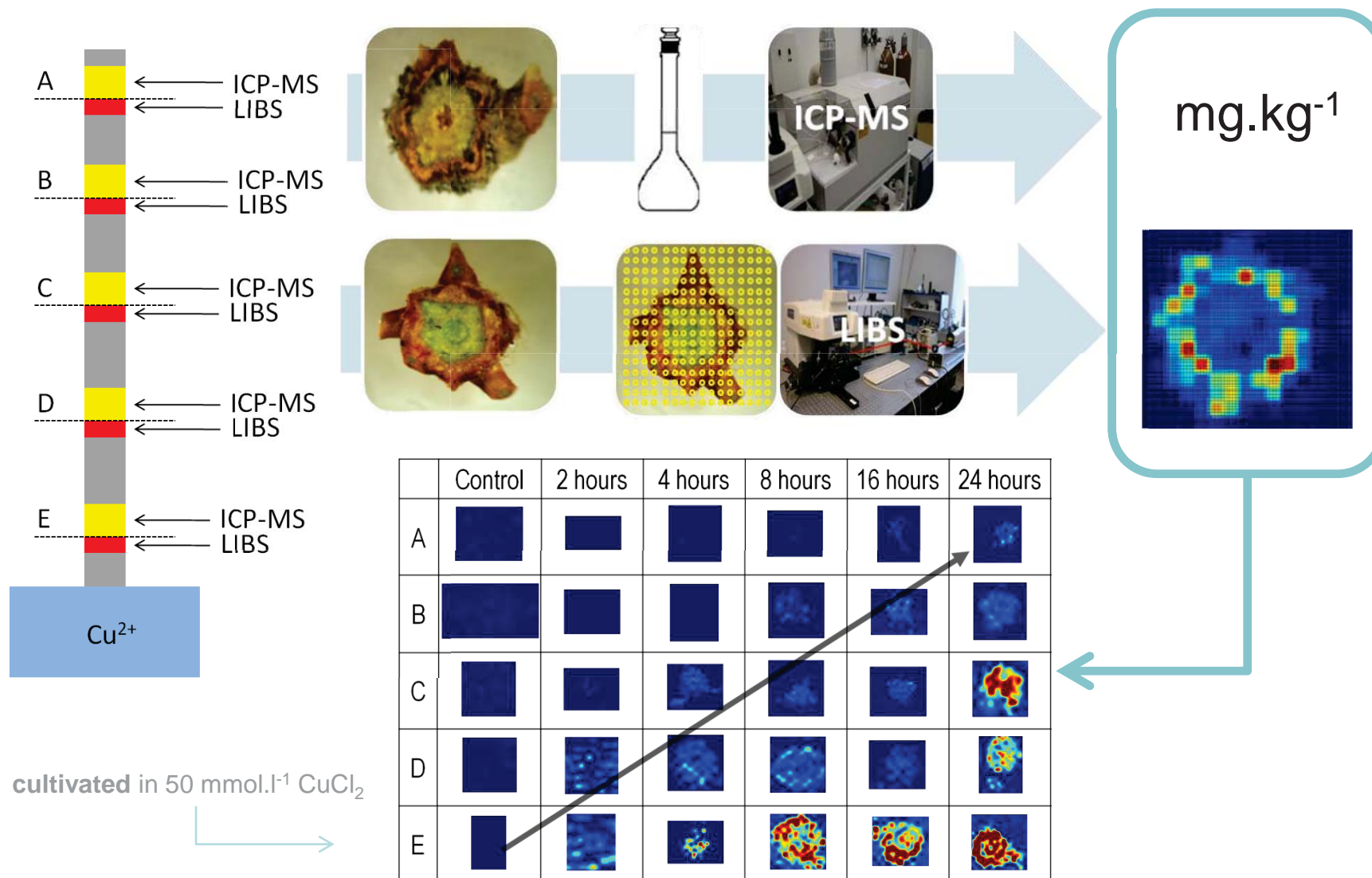
Phytoremediation



Laboratory cultivated twigs

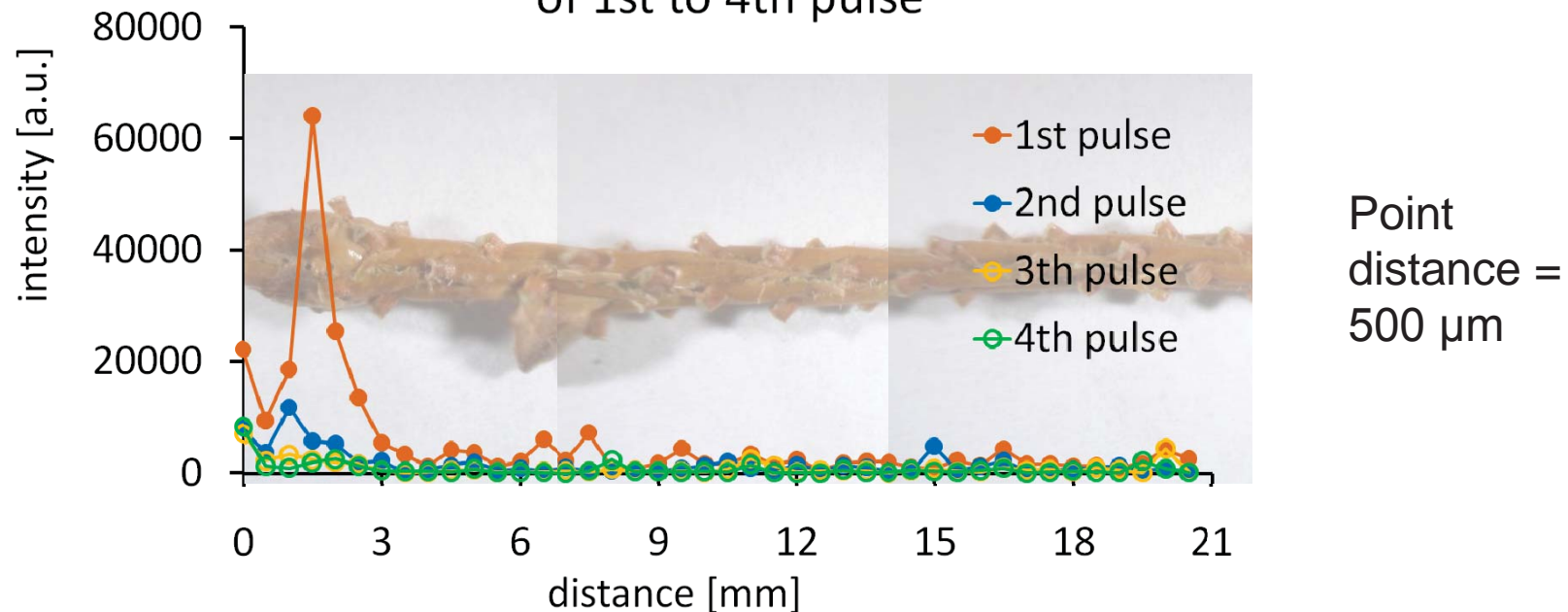


Phytoremediation



Smolník

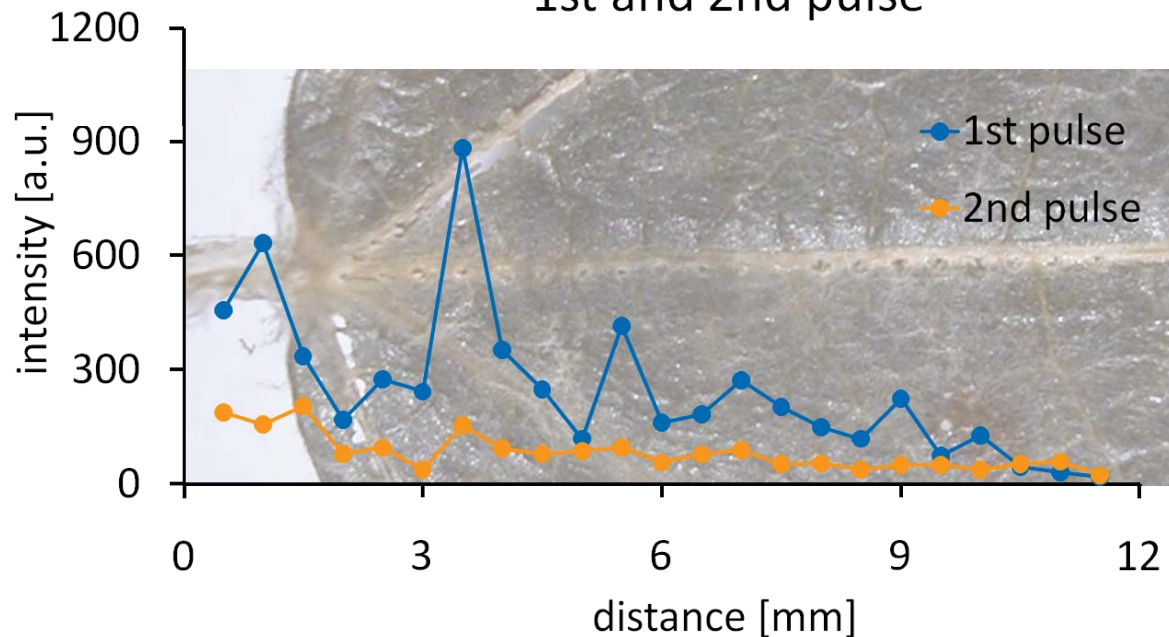
Ca (II) 317.933 - comparison of intensity signals of 1st to 4th pulse



Calcium longitudinal distribution on the spring and bud of spruce (*Pinus sylvestris*) obtained by LIBS **single pulse**, four laser pulses into each point were shot and signal intensities were compared.

Smolník

Cu(I) 324.754 - comparison of intensity signal of 1st and 2nd pulse

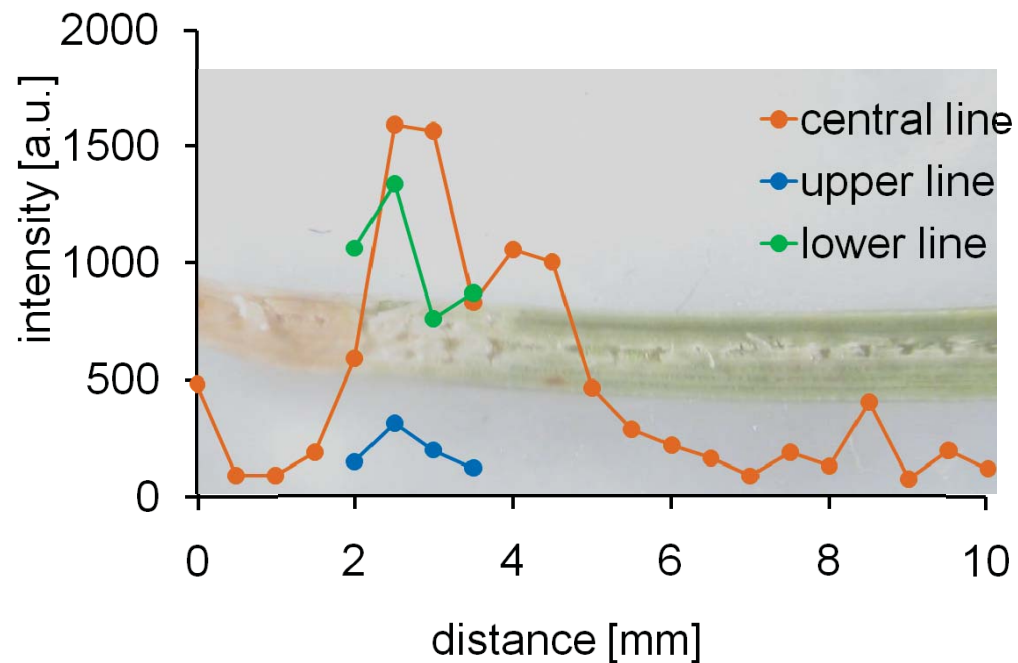


Point distance = 500 μm

Copper distribution in central vein of the aspen leaf (*Populus tremula*) obtained by LIBS **single pulse**; two laser pulses on each point.

Smolník

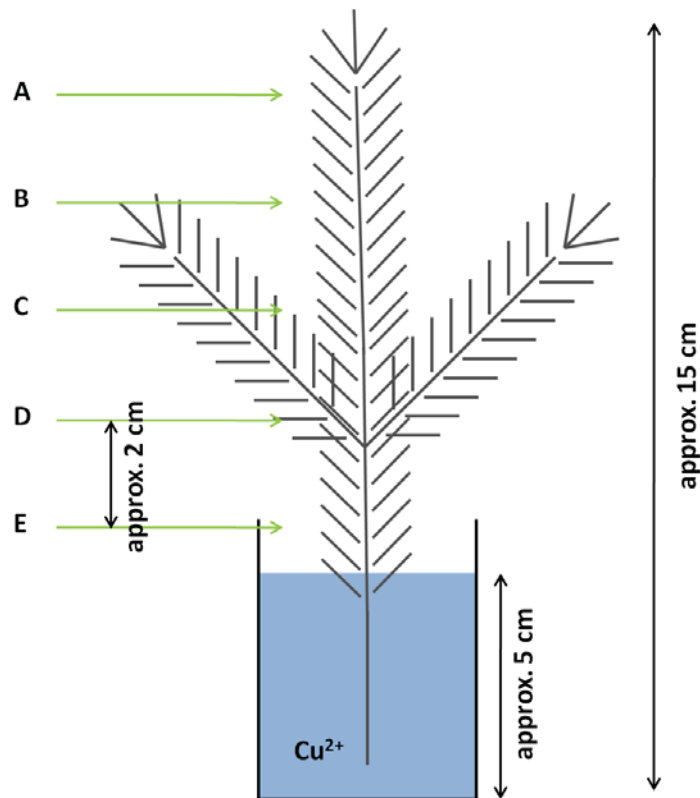
Cu(I) 324.754 - 1st pulse



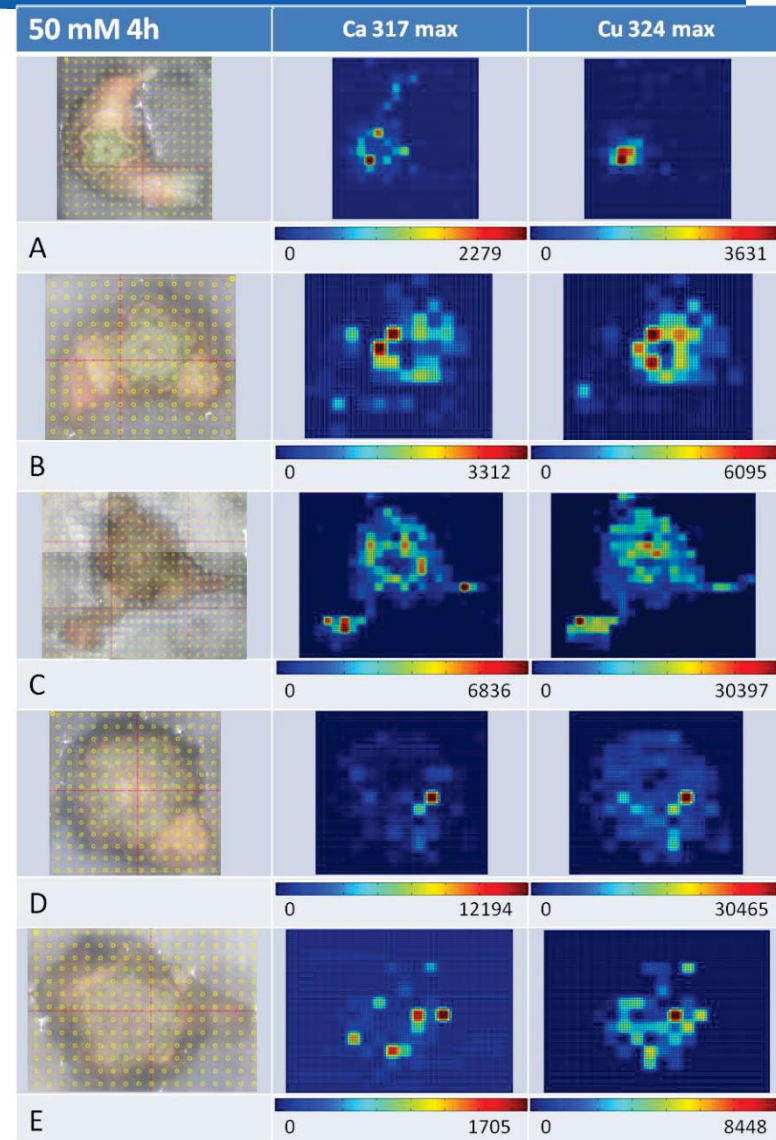
Point
distance =
500 μm

Copper distribution in the needle of pine tree (*Pinus sylvestris*) obtained by LIBS single pulse.

Phytoremediation

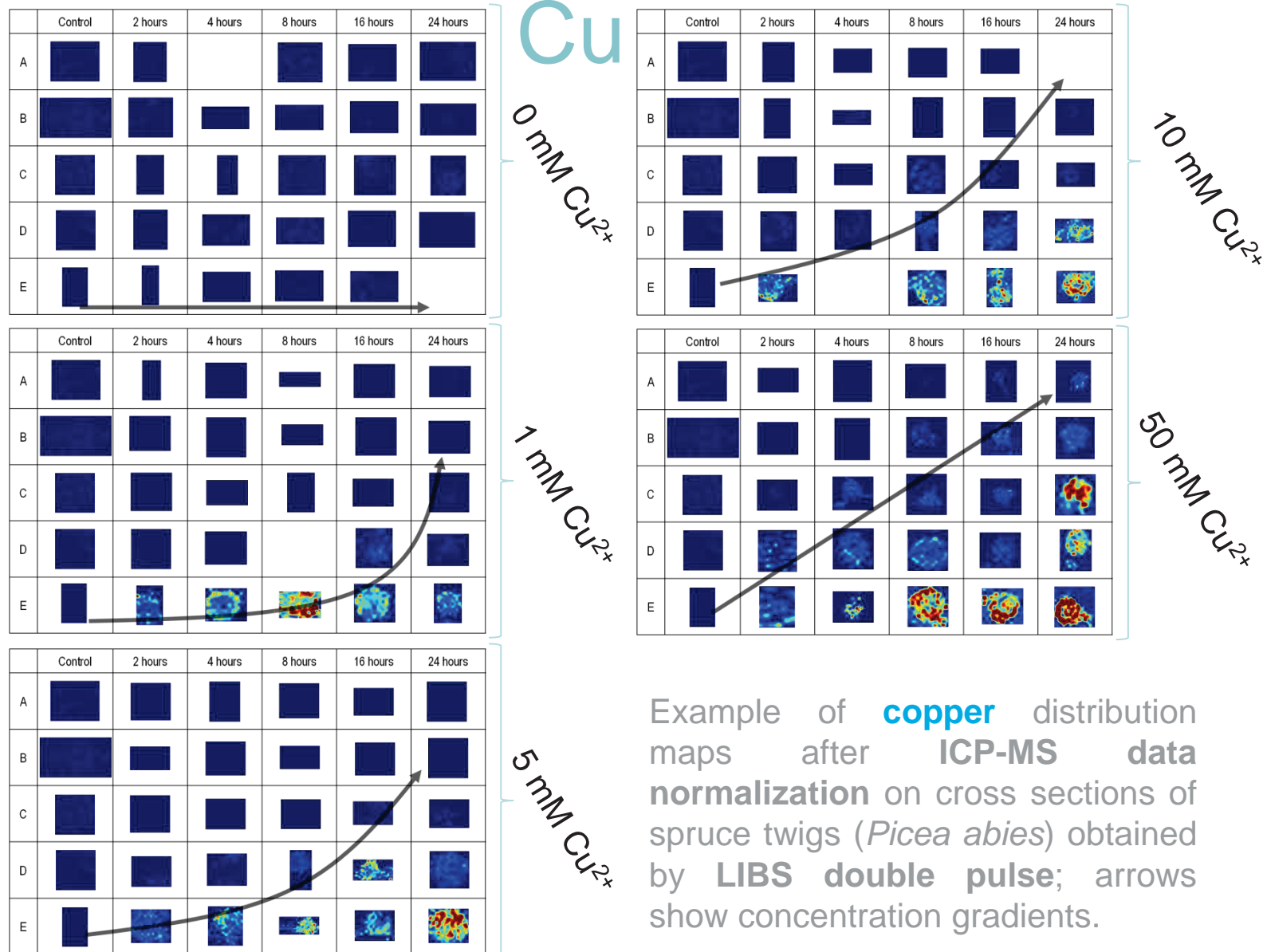


Example of **copper** and **calcium** distribution maps on cross sections of spruce twigs (*Picea abies*) cultivated in 50 mmol.l⁻¹ CuCl₂ obtained by LIBS double pulse.



Point distance = 150 μm

Phytoremediation



Example of **copper** distribution maps after **ICP-MS data normalization** on cross sections of spruce twigs (*Picea abies*) obtained by **LIBS double pulse**; arrows show concentration gradients.

Co-workers/Acknowledgements



R. Malina, M. Liška, J. Novotný, D. Procházka, P. Pořízka, M. Petrilak,
K. Procházková

*Institute of Physical Engineering, **Brno University of Technology**,
Technická 2, 616 69 Brno, Czech Republic*



K. Novotný, A. Hrdlička, L. Krajcarová, G. Vítková, V. Kanický, M. Holá, M.
Galiová, M. Ivanov,

*Dep. of Chemistry, **Masaryk University**, Kotlářská 2, 611 37 Brno, Czech
Republic,*



R. Kizek, P. Babula, K. Stejskal, V. Adam,
*Dep. of Chemistry and Biochemistry, **Mendel University of Agriculture and
Forestry**, Zemědělská 1, 613 00 Brno, Czech Republic*



M. Nývltová Fišáková
*Institute of Archaeology Brno, **Academy of Science**,
Královopolská 147, 612 00, Brno, Czech Republic*

This work was supported by the Ministry of Education, Czech Republic on the frame of grant ME10061, ME09015 and by the project “CEITEC - Central European Institute of Technology” (CZ.1.05/1.1.00/02.0068) from European Regional Development Fund.

Co-workers/Acknowledgements



Lanxiang Sun

Shenyang Institute of Automation, **Chinese Academy of Sciences**,
Shenyang City, 110016, China



Madhavi Z. Martin,

Plant Systems Biology Group, Environmental Sciences Division,
Oak Ridge National Laboratory, Oak Ridge, TN 37831-6038, USA



D.W. Hahn, P.K. Diwakar,

Department of Mechanical & Aerospace Engineering, **University of Florida**,
Gainesville, FL 32611, USA



L. Reale, A. Reale,

Faculty of Sciences, **University of L'Aquila**, Via Vetoio (Coppito 1), 67010
L'Aquila, Italy



L. Mancini, G. Tromba

Synchrotron Elettra, Strada Statale 14 - km 163,5, 34012 Basovizza, Trieste
Italy

THANK YOU FOR YOUR ATTENTION !

